DEPARTMENT OF BIOLOGICAL AND ECOLOGICAL SCIENCES (DEB)

XVI PhD COURSE IN GENETICS AND CELLULAR BIOLOGY

BIO/11

Proteomics and metabolomics in transfusion medicine: new technologies to improve red blood cell storage

PhD student

Valeria Pallotta

Tutor

Dott.ssa Sara Rinalducci

Coordinator

Prof. Giorgio Prantera

Index

Aim of the thesis

Despite decades of significant technological improvements, red blood cells can be stored under standard blood bank conditions for a limited span of life because RBC undergo a series of biochemical and physical changes, the so-called "storage lesions" that are related to the promotion of apoptosis-like phenomena. These anomalies compromise red cell survival upon transfusion and in turn transfusion efficacy in the recipient.

In the first section, this PhD thesis would evaluate new technologies to improve red cell storage quality, in term of safety and efficacy. To this end it was performed a biochemical and mass spectrometry-based analysis of:

(i) high-glycerol frozen RBCs (i.e., stored with a final concentration of 40% glycerol at -80°C for about 10 years);

(ii) RBCs stored under standard blood banking with the supplementation of antioxidants (N-acetyl-L-cysteine and ascorbic acid).

In the second section, the thesis would describe an innovative method to evaluate red cell storage quality through an extensive investigation of RBC cytosolic multi-protein complexes. In the light of this, it was performed a proteomic analysis in order to identify multimeric protein complexes that play a critical role in the maintenance of red blood cell functionality and survival *in vivo*.

Future investigations should expand the existing knowledge and determine whether and how these complexes might influence red cell ageing *in vivo* and *in vitro*, other than the insurgence of specific pathologies.

Chapter 1
Introduction

1.1 Structure, function and metabolism of erythrocytes

Blood is a connective tissue that is mainly involved in the transport of many substances such as nutrients, oxygen and metabolic waste products around the body. It also protects against deseases and helps to regulate pH and water balance.

In vertebrates, blood consists of two main components: plasma, which is a clear extracellular fluid, and cells, which are also called "corpuscles" or "formed elements". These last comprise erythrocytes or red blood cells (RBCs), leukocytes or white blood cells and thrombocytes or platelets.

Erythrocytes are the most abundant blood cells. By volume they constitute about 45% of whole blood in men and about 40% in women. This percentage is called Hematocrit (Hct).

Human erythrocytes are anucleated, disk-shaped and biconcave cells (7,5µm diameter x 2µm thickness) (**Figure 1**). This shape allows optimal flexibility while traveling through microcapillaries and permits maximal surface area for oxygen and carbon dioxide exchange [Barasa and Slijper, 2013]. Their red color is due to the spectral properties of the hemic iron ions in hemoglobin molecules (Hb). This metalloprotein, firstly described from Perutz in 1960 [Perutz, 1960], is the most abundant cytoplasmic protein in human erythrocytes (about 95% of total proteins). Each cell contains approximately 270 million of these biomolecules, each of which carry four heme goups. Thanks to heme groups of Hb erythrocytes can temporarily bind oxygen molecules (O_2) in the lungs and release them throughout the body. These cells also carry carbon dioxide (CO_2) back from the tissues.

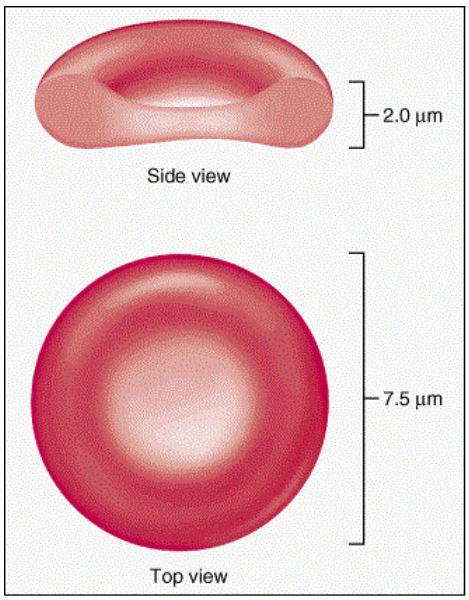

Figure 1. Structure of RBCs.

RBCs originate from hematopoietic stem cells (HSCs) residing in the bone marrow, which are capable of self-renewal via asymmetric cell division resulting in one identical HSC and one differentiating cell for each HSC. This differentiating cell matures during erythropoiesis through a series of proliferation and differentiation steps into a reticulocyte and eventually into an RBC [Barasa and Slijper, 2013]. By maturation, cells become

gradually specialized for their function. In the early stage organelles are present in erythrocytes, so cells can synthesize proteins such as haemoglobin. As the proteins accumulate, the number of organelles slowly diminishes. Complete differentiation of maturing erythrocytes needs of reorganization of membrane skeletal protein network and the loss of nuclei.

In healthy individuals, cells live in blood circulation for about 120 days. At the end of their lifespan they become senescent and are removed from circulation. The process of distruption of erythrocytes is called hemocatheresis and occurs mainly in the spleen, liver and bone marrow.

A balance between production and destruction keeps the erythrocyte number constant.

Since the cells lose intracellular organelles, they are uncapable of protein and lipid synthesis and oxidative phosphorylation [Bossi and Giardina, 1996]. This means that they can not replace damaged lipids or proteins and also produce ATP in oxidative phosphorylation. However, energy is required for the maintenance of osmotic balance through ATP-dependent pumps, of enzymes and membrane lipid protection from oxidative stress, and maintenance of Hb iron in reduced state (hemoglobin oxidation). So energy is needed for RBC integrity and deformability.

Erythrocytes must depend on two key metabolic pathways for production of high-energy compounds, as summarized in **Figure 2**. These are glycolysis or Embden-Meyerhoff pathway and hexose monophosphate shunt or pentose phosphate pathway (PPP).

Glycolysis generates 90-95% of energy needed by RBCs. In this pathway, glucose, i.e. the main red cell energy source, is metabolized with the production of 2 mol of ATP (adenosine triphosphate), NADH (nicotinamide adenine dinucleotide reduced form) and lactate as end products per mol of glucose [Bossi and Giardina, 1996]. ATP is the major high-energy phosphate nucleotide that powers the cation pump and NADH is a cofactor in the methemoglobin reductase reaction, which maintains heme iron in the reduced state to avoid the formation of methemoglobin.

Another end product of glycolysis is 2,3-disphosphoglycerate (2,3-DPG), necessary for the regulation of hemoglobin affinity to oxygen [Barasa and Slijper, 2013].

The final yield of ATP and 2,3-DPG varies depending on the activity of the Rapoport-Luebering shunt that allows the RBCs to regulate oxygen transport during conditions of hypoxia or acid-base imbalance.

Although to a lesser extent the PPP contributes to the energy status of the cell with the production of 2 mol of NADPH per mol of glucose entering the cycle [Bossi and Giardina, 1996]. In this pathway, glucose-6-phosphate undergoes oxidation followed by a series of reactions to yield fructose-6-phosphate and glyceraldehyde-3-phosphate, which are intermediates in the glycolytic pathway. The most important product is reduced nicotinamide-adenine dinucleotide phosphate (NADPH) which is required in the glutathione metabolism pathway to reduce oxidized glutathione (GSSG) in GSH by glutathione reductase. Reduced glutathione (GSH) is a tripeptide (glutamyl-cysteinyl-glycine) that reduces protein

sulfhydryl group. It is also involved in detoxifying the cellular peroxides [Barasa and Slijper, 2013] (see next paragraph).

The modulation of erythrocyte metabolism is driven by the oxygenation state of the cell (**Figure 3**).

During the high oxygenation state (HOS), the risk of oxidative stress should address erythrocyte metabolism toward the activation of those metabolic pathways that may lead to an increase of cell protection, namely the pentose phosphate shunt [Bossi and Giardina, 1996]. During the low oxygenation state (LOS), glucose is addressed towards glycolysis in order to increase ATP and 2,3-DPG production.

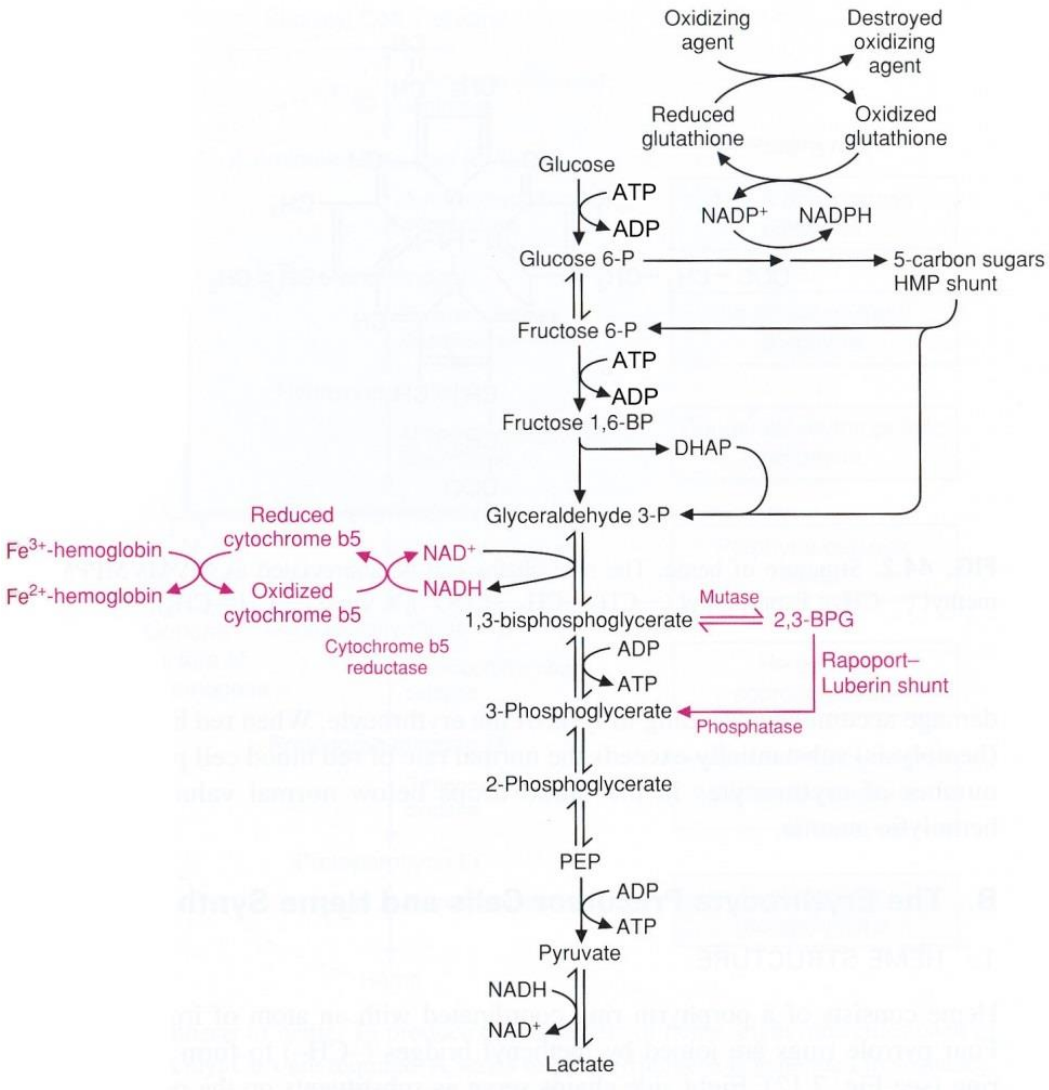

Figure 2. Overview of vital pathways in the red blood cells. In the Embden–Meyerhoff pathway glucose is anaerobically metabolized to pyruvate. Part of this pathway is the Rapoport–Luebering shunt, which is unique for the RBCs. For energy ATP is needed, which is generated through the Embden–Meyerhoff pathway. This pathway also provides reducing power (NADH) to keep hemoglobin in reduced state. NAD+ is produced by the pyruvate metabolism pathway. Other reducing power by NADPH originates from the pentose phosphate pathway, and is essential for keeping high glutathione (GSH) levels [Barasa and Slijper, 2013].

Castagnola et al. (2010) have reported the hypothesis that the glycolytic flux is modulated via a competition between glycolytic enzymes and deoxy-Hb for band 3, a transmembrane protein that accounts for about 25% of the total RBC membrane proteins. Band 3 is characterized by three distinct functional domains: the membrane spanning domain, which catalyzes the exchange of anions (mainly Cl^- and HCO_3^-) across the membrane; the short C-terminal cytoplasmatic domain that binds carbonic anhydrase II; and N-terminal cytoplasmatic domain (CDB3) that binds a variety of proteins by anchoring the RBC membrane to the underlying cytoskeleton via ankyrin and protein 4.2.

In HOS erythrocytes, the inibition of glycolytic enzymes, due to their binding to CDB3, should result in a reduced glucose flux through glycolysis. As a consequence, since glucose consumption is constant, more glucose is metabolized by the PPP (**Figure 3, left**). Conversely, in the LOS state the displacement of glycolitic enzymes from CDB3, induced by the binding of deoxy-Hb, results in an increased glucose flux throughout glycolysis (**Figure 3, right**) [Castagnola et al., 2010].

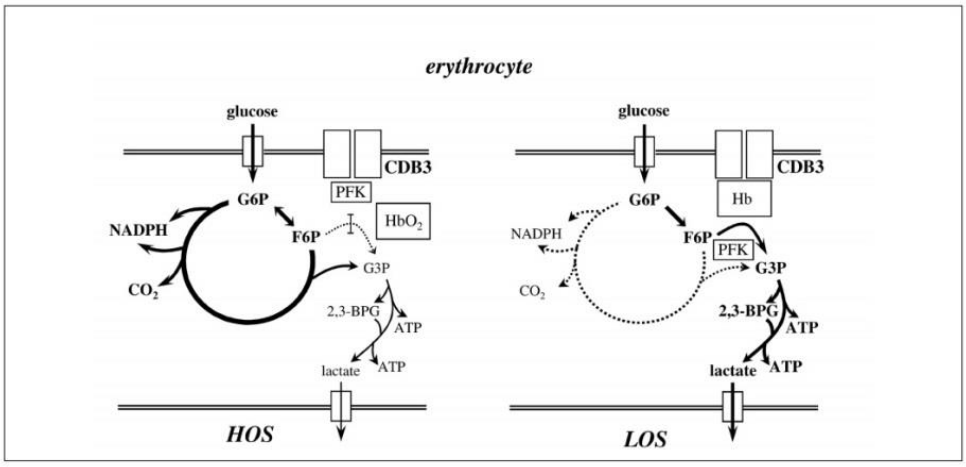

Figure 3. Simplified scheme representing the modulation of erythrocyte metabolism by the O_2 transition of Hb and its competition with glycolytic enzymes (mainly phosphofructokinase, PFK) for the cytoplasmic domain of band 3 (CDB3) [Castagnola et al., 2010].

1.2 Antioxidant defense system of Red Blood Cells (RBCs)

Reactive oxygen species (ROS) are formed and degraded by all aerobic organisms, leading to either physiological concentrations required for normal cell function, or excessive quantities, the state called oxidative stress. As the term ROS implies, intracellular production of those oxygen

intermediates threatens the integrity of various biomolecules including proteins, lipids and DNA [Nordberg and Arnèr, 2001].

To counteract oxidative stress, erythrocytes have a self-sustaining activity of antioxidant defense enzymes including superoxide dismutase (SOD), catalase (CAT), glutathione peroxidase (GPx), glutathione reductase (GR) and peroxiredoxins (Prxs), in addition to low-molecular-weight antioxidants, such as glutathione (GSH) and vitamin E and C [Silva et al., 2013].

In eukaryotic cells, superoxide ($O_2^{\bullet-}$) can be metabolized to hydrogen peroxide (H_2O_2) by the cytosolic 32-kDa dimeric Cu/Zn-SOD [Nordberg and Arnèr, 2001]. In this reaction two molecules of superoxide form hydrogen peroxide and molecular oxygen:

$$2\ O_2^{\bullet-} + 2\ H^+ \longrightarrow H_2O_2 + O_2$$

SOD is considered to be one of the major enzymes that protect cells from ROS.

Catalase, however, is a tetrameric heme-containing enzyme that catalyzes the dismutation of hydrogen peroxide to water and molecular oxygen:

$$2\ H_2O_2 \longrightarrow O_2 + 2\ H_2O$$

H_2O_2 is not a radical but it is still a harmful byproduct of many normal metabolic processes. Indeed it can be rapidly converted into hydroxyl radical ($^{\bullet}OH$) by Fenton reaction, in presence of Cu^+ and Fe^{2+}:

$$H_2O_2 + Cu^+/Fe^{2+} \longrightarrow {}^{\bullet}OH + OH^- + Cu^{2+}/Fe^{3+}$$

Thus CAT rapidly catalyzes the decomposition of a potential toxic compound into less-reactive molecules.

Glutathione peroxidase is a family of multiple isozymes involved in scavenging oxy- radicals [Lin et al., 2002]. The main reaction they catalyze is the reduction of H_2O_2 using glutathione (GSH) as substrate:

$$2\ GSH + H_2O_2 \longrightarrow GSSG + 2\ H_2O$$

Glutathione reductase (GR) then reduces the oxidised glutathione (GSSG) to complete the cycle:

$$GSSG + NADPH + H^+ \rightarrow 2\ GSH + NADP^+$$

Therefore GR is a key enzyme in the glutathione pathway for reduced glutathione (GSH) regeneration. This system is critical for the protection of hemoglobin and other proteins against peroxide damage in mammals [Hou et al., 2004].

GPx can also reduce other peroxides (for example lipid peroxides in cell membranes) to alcohols:

$$ROOH + 2\ GSH \rightarrow ROH + GSSG + H_2O$$

Peroxiredoxins [Chae et al., 1994a; Chae et al., 1994b] are a ubiquitous family of antioxidant enzymes that can be divided into three classes: typical 2-Cys Prxs; atypical 2-Cys Prxs; 1-Cys Prxs. All proteins share the same basic catalytic mechanism in which an active-site cysteine (the peroxidatic cysteine) is oxidized to a sulfenic acid by the peroxide substrate. The recycling of the sulfenic acid back to a thiol is what distinguishes the three enzyme classes [Wood et al., 2003].

Prxs exert their role in the cell through their peroxidatic activity so that hydrogen peroxide, peroxynitrite and a wide range of hydroperoxides (ROOH) are reduced and detoxified [Hofmann et al., 2002; Jacobson et al., 1999; Poole and Ellis, 1996; Bryk et al., 2000; Peshenko and Shichi, 2001]:

$$ROOH + 2\ e^- \rightarrow ROH + H_2O$$

The typical 2-Cys Prxs are the largest class of enzymes. They act as obligate homodimers containing two identical active site [Hofmann et al., 2002]. This class comprises PrxII, a most abundant protein in red cell.

A large number of low molecular weight compounds are considered to be antioxidants of biological importance, including ascorbic acid (vitamin C) and α-tocopherol (vitamin E).

Ascorbic acid is a water-soluble vitamin. Its antioxidant power depends on the high reducing potential of its carbon-carbon double bond (**Figure 4**) which readily donates one or two hydrogens and electrons to a variety of oxidants, including oxygen free radicals, peroxides, and superoxide.

Ascorbate acts protecting red cell membrane. However it does not directly affect membrane lipid peroxidation but it may perform this function indirectly by reducing the tocopheroxyl free radical

in the lipid bilayer. Thus intracellular ascorbate can regenerate α-tocopherol in the erythrocyte membrane and in turn α-tocopherol protects the cell membrane from lipid peroxidation.

α-tocopherol (α-TOH) is a lipid-soluble vitamin present in biological membranes (**Figure 4**). It acts as chain-breaking antioxidant thanks to hydroxyl group by which it reacts with unpaired electrons and can reduce [Nordberg and Arnèr, 2001]. The role of vitamin E is to protect polyunsaturated fatty acids in membranes against lipid peroxidation.

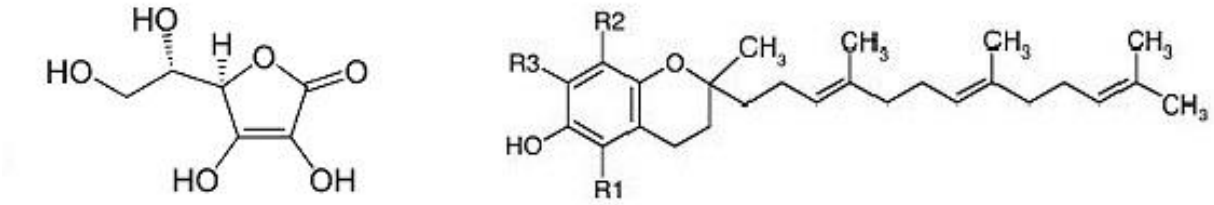

Figura 4. Left: structure of vitamin C (ascorbic acid); right: structure of vitamin E (α-tocopherol).

1.3 Red cell storage under standard blood bank conditions: historic evolution

The development of effective red blood cell biopreservation techniques that mantain ex vivo RBC viability and function represents the foundation of modern blood banking. The ability to preserve the integrity of RBCs outside their native environment for extended periods has not only separated blood donors and recipients in space and time, but also has made it possible for blood banks to provide safe, high-quality blood products in an efficient and effective manner [Scott et al., 2005].

The major force driving the field of red cell biopreservation is the enormous clinical need for RBC product. RBC transfusions are necessary for patients with low oxygen-carrying capacity due to traumatic/surgical hemorrhage, decreased bone marrow production (aplastic anemias), defective hemoglobin (hemaglobinopathies and thalassemia), and decrease RBC survival (hemolytic anemias).

Worldwide more than 80 million units of red cells are transfused each year, and in highly developed countries, about 1% of the population receives a transfusion annually. Red cells are the most commonly transfused blood component.

Blood storage begane in 1913 when Lee and Vincent demonstrate that citrate could prevent the coagulation of human blood [Stansbury et al., 2005]. Later Agote (1914) showed that citrate anticoagulation could facilitate human transfusion and in 1915 Lewisohn determined the critical amount of citrate required to anticoagulate a donor's blood without causing hypocalcemia in the recipient [Lewison, 1915]. In 1916 Rous and Turner firstly described the 4-week storage of rabbit red cells in citrate and glucose.

The introduction of citrate anticoagulant and glucose, used to support cellular metabolism, allowed the donor and recipient to be separated in time and in space respectively. This physical separation of donor and recipient is the basis of blood banking.

In 1917 Robertson worked out safe ways to store and transport blood, and transfused human blood stored for 26 days in the Rous-Turner citrate-glucose solutions [Rous and Turner, 1916; Robertson, 1918].

In subsequent decades, plastic blood bags were introduced and later, when the diethylhexyl phthalate (DHEP) was coupled with PVC classic bags, it has been shown a fourfold reduction of haemolysis and the time of storage increased twice. Nowadays it is known that DHEP enters the RBC membrane where it limits membrane loss by microvesiculation.

Around 1950 Gibson added phosphate to acid citrate glucose solution in order to offset the loss of phosphate from red cells [Walter and Murphy, 1952; Gibson et al., 1957]. The subsequent addition of adenine could help storage by cell shape, ATP and viability restoration, extending the storage time to 5 weeks (citrate, phosphate, dextrose, adenine: CPDA-1).

The first RBC additive solution, saline-adenine-glucose (SAG) was developed by European researchers in the late 1970's [Högman CF et al., 1978]. Soon after, in 1981, the same researchers added mannitol to help protect the RBC membrane and reduce hemolysis [Högman CF et al., 1981]. The addition of mannitol extended the storage time to 42 days, a period that is currently used today. The modified SAG formulation was named SAGM and to this day SAGM is the most widely used RBC additive solution (see next paragraph).

The exact formulation of SAG-M varies, so the term is usually restricted to the standard European formulation while U.S. varieties are designated by additive solution (AS) and a number as in AS-1 and AS-5 [Hess, 2010].

The subsequent development of filtration-leukoreduction has improved recovery and reduced hemolysis further, beacause it has been demonstrated that white blood cells break down in the cold and release proteases and lipases that cause damage to the RBCs during storage. So nowadays the practice of leukoreduction, by buffy coat removal or leukofiltration, became a fundamental strategy to increase RBC recovery and reduce haemolysis.

1.3.1 Blood collection and processing

Red cell concentrates are obtained starting from whole blood through a centrifugation that allows to separate erythrocytes from leuko-platelet layer (buffy coat) and plasma (**Figure 5, left**).

So a cellular separator instrument equipped with an optical sensor is used to physically separate blood components into different satellite bags. This multi bag system is composed by a "mother bag" containing CPD solution for the collection of whole blood (about 450 cc) which is connected with a first bag with SAG-M intended for red cell and a second one for the plasma. This procedure is called "top and bottom" collection.

After this step RBCs are ready for leukofiltration using filters that can remove 99,99% of White Blood Cells (**Figure 5, right**). So red cell concentrates are immediately ready for the use or to be stored for up to 42 days at 4°C.

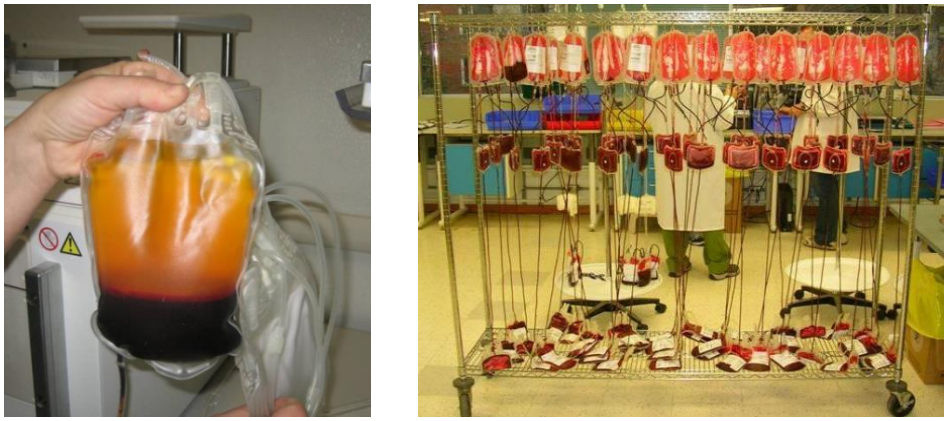

Figure 5. Left) Blood components after centrifugation. Right) Leukofiltration of RBCs.

1.3.2 Additive solutions

Nowadays SAGM (saline-adenine-glucose-mannitol) is the most widely used RBC additive solution. This is a modified SAG formulation (saline-adenine-glucose) developed by European researchers around 1981. Several countries apply a shorter 5 weeks shelf-life to their SAGM-RBC components despite the fact that SAGM is approved for 6-weeks storage. In **Table 1** a list of RBC additive solutions currently in routine use around the world is reported. SAGM has not been licensed by the Food and Drug Administration (FDA), so it is

not used in the USA, but only in Europe, UK, Australia, Canada and New Zealand. Other additive solutions, which are all essentially variations of SAG/SAGM, have been developed and commericalised in other countries, including AS-1, AS-3, AS-5, MAP and PAGGSM [Heaton et al., 1984; Simon et al., 1987; Cicha et al., 2000; Walker et al., 1990]. Specifically AS-1 and AS-5 are used in USA, AS-3 both in USA and Canada, MAP and PAGGSM only in Japan and in Germany respectively.

No new RBC additive solutions have been licensed for use for over 20 years.

	Licensed RBC additive solutions					
Constituents (mM)	**SAGM**	**AS-1** Adsol Baxter	**AS-3** Nutricel Pall Medical	**AS-5** Optisol Terumo	**MAP**	**PAGGSM** MacoPharma
NaCl	150	154	70	150	85	72
NaHCO3	-	-	-	-	-	-
Na2HPO4	-	-	-	-	-	16
NaH2PO4	-	-	23	-	6	8
Citric acid	-	-	2	-	1	-
Na-citrate	-	-	23	-	5	-
Adenine	1.25	2	2	2.2	1.5	1.4
Guanosine	-	-	-	-	-	1.4
Dextrose (glucose)	45	111	55	45	40	47
Mannitol	30	41	-	45.5	80	55
pH	5.7	5.5	5.8	5.5	5.7	5.7
Anti-coagulant	CPD	CPD	CP2D	CPD	ACD	CPD
FDA Licensed	No	Yes	Yes	Yes	No	No
Countries used	Europe UK Australia Canada New Zealand	USA	USA Canada	USA	Japan	Germany

Table 1 RBC additive solutions currently used around the world [Sparrow, 2012].

All of the currently licensed RBC additive solution have an acidic pH (~5.6-5.8), which is well below the normal physiological pH of 7.3 of venous blood. Acidic additive solutions (and anticoagulants) are used simply because at physiological and alkaline pH, glucose caramelises during heat-sterilization. Erythrocytes have sufficient buffering capacity to adjust the pH closer to physiological levels during the first week of storage. However the buffering capacity of RBCs is soon exhausted due to the generation of lactate (glycolytic pathway) [Sparrow, 2012].

Consequently the extracellular and intracellular pH of RBCs progressively becomes more acidic during storage, reaching a pH of ~6.5 at the end of storage [van der Meer et al., 2011]. An acidic intracellular environment alters the activity of certain enzymes and biochemical pathways. During storage the intracellular concentration of adenosine-5'-triphosphate (ATP) and 2,3-diphosphoglycerate (2,3-DPG) decline [van der Meer et al., 2011]. Over the past 15-20 years, research into the development of new additive solutions has focussed on ways to maintain higher the intracellular levels of ATP and 2,3-DPG during storage of red cells [Hess, 2006]. A significant driver for this research came from the military, who wanted to store RBCs for longer than 6 weeks. However longer storage time is not a key interest of civilian blood service and the medical community, whose desire is to support new technologies, including new RBC additive solutions that offer further improvement to the quality and efficacy of RBC components.

1.4 RBCs and storage lesions: "how long is too long?"

For several decades RBC components have been prepared as concentrates suspended in nutrient additive solution, which preserves and extends the shelf-life of the RBC component, allowing up to 6-7 weeks of refrigerated storage [Hess JR, 2006]. Nevertheless, during storage RBCs undergo a complex and progressive accumulation of physicochemical changes, collectively referred to as the RBC storage lesion [Högman CF and Meryman HT, 1999; Hess, 2010]. These time-dependent changes include metabolic, enzymatic, oxidative and physiologic lesions that reflect the deterioration of RBCs during conventional blood bank storage (**Table 2**).

Metabolic changes have been the best studied [Hess, 2010]. As previously reported, metabolism of RBCs is centered on glycolysis, the only source of energy for red cells. Protons produced by this process increase the acidity of cells and storage solutions as well. Acidosis inhibits in turn

the glycolysis pathway, in fact low pH have adverse effect on activity of hexose kinase (HK) and phosphofructokinase (PFK), so that less ATP and NADH is produced as storage progresses. The inhibition of HK leads to a poor production of NADPH and glutathione, since it is reduced the amount of glucose 6-phosphate going through the exose-monophosphate shunt.

Moreover, at any storage pH less than 7.2, the breakdown of 2,3-DPG is favored, and this in turn leads to an initial burst of ATP production.

As a result of these activities, red cell ATP concentrations initially rise as 2,3-DPG is broken down, stay above their initial concentrations for 2–3 weeks, and then decline steadily. The pH typically declines from 7.0 to 6.5, and the rate of glucose consumption decreases by more than 50%. As it was mentioned before, the slowing of glycolysis also leads to reduced production of NADH leading to reduced activity of methaemoglobin reductase, and thus the methaemoglobin concentration of stored red cells increases over 6 weeks of storage, typically from about 1–2%.

Low temperature profoundly reduces the activity of the major membrane sodium-for- potassium pump, which is ATP-dependent. As a result, the potassium that slowly leaks out of RBCs is not returned, and the concentration of extracellular potassium in the suspending fluid in the red cell bag typically rises at a rate of about 1 mEq/L/day [Hess, 2010].

Metabolic
1. Acidosis
2. Lower ATP, DPG
3. Lower glutathione, NADH, NADPH

Enzymatic (Reduced with leukoreduction)
1. Loss of surface glycands
2. Lysolipids
3. Protein damage

Oxidative
1. Damage to proteins e.g. Band III
2. Decoration of proteins
a. Benign – glycation of Hb
b. Inflammatory – e-lysines (AGEs)
3. Oxidized lipids – micro-vesicles
4. Lysolipids – TRALI

Physiologic
1. Shape change
2. Membrane loss
3. Apoptosis

Table 2 Components of the red cell storage lesion [Hess, 2010]**.**

Enzymatic lesions were related to the presence of white blood cell (WBC) during blood storage. As previously reported, leukoreduction step has also been shown to improve red cell storage. Removal of metabolically active WBC from RBC concentrates minimizes glucose consumption, waste product accumulation and damage from leukocyte enzymes, resulting in a significant decrease in hemolysis during hypotermic storage [Högman, 1998].

Physical changes include membrane loss and the associated changes in RBC shape and rheology. During storage red cells evolve from smooth biconcave discs to subtly bumpy discs (echinocytes) to grossly bumpy spheres called spheroechinocytes (**Figure 6**) [Hess, 2010].

It has been demonstrated that this process is associated with decreased pH and ATP concentration and increased intracellular concentration of calcium. The return toward the normal red cell shape occurs in parallel with increasing ATP concentration, regeneration of 2,3-DPG and the restoration of normal sodium, potassium and calcium gradients. However, beyond the early spheroechinocyte stage, red cells lose their membrane through a blebbing mechanism involving cytoskeleton remodeling and membrane asymmetry disruption, with the exposure of phosphatidylserine at the outlet of the plasma membrane. Thus, small corpuscles of less than 1 μm, named microvesicles, bud from the tips of erythrocyte spines (**Figure 7**). This process is irreversible, since the cells have no mechanisms to replace lost membrane. At the end of the storage, the densest cells have lost all extra membrane and have become rigid spheres [Hess, 2010].

Last but not least, oxidative damage to lipids and proteins also contributes to red cell injury during storage [Sharifi et al., 2000]. RBCs are continuously exposed to oxygen and are also rich in polyunsaturated lipids, target of free radicals, and iron (hemoglobin molecules), a powerful catalyzer of free radical through Fenton reaction. Red cells are normally supplied with superoxide dismutase and methemoglobin reductase, so that the dangerous products are quickly removed.

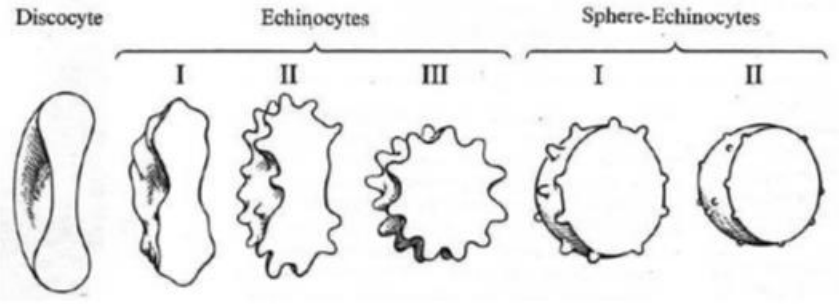

Figure 6. Evolution of erythrocyte morphology during blood bank storage.

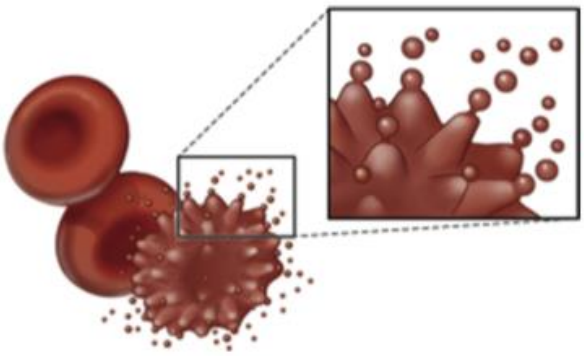

Figure 7. Blebbing mechanism of red blood cells

.

However, as red cell storage progresses and the flux through the glycolytic pathway is slowed, NADH concentration falls and methemoglobin concentration rises [Dumaswala et al., 2000]. This molecule is less stable than ferrous hemoglobin, increasing the chance that the heme will come free from the globin heme pocket and the iron will then also come out of the heme. Under these circumstances, the chanches that superoxide radicals and water will meet in the presence of a free iron or heme to undergo Fenton transformation into hydroxyl radical increase and hydroxyl radical readily damages lipids and proteins [Hess, 2010].

1.5 Alternative methods in red cell storage

While increased research effort is being directed to better understand the effects of storage on RBCs and the potential impact on transfusion outcomes [Glynn, 2010], slower progress is being made in finding ways to deter the detrimental effects of the RBC storage lesion.

Current research suggest that the RBC hypothermic storage lesion still significantly influences the efficacy of transfusion as it is responsible for the association of blood transfusion with an increased lenght stay in the hospital [Martin et al., 1994], impaired tissue oxygen use [Marik and Sibbald, 1993], proinflammatory and immunomodulatory effects [Blajchman, 2002], increased infections [Leal-Noval et al., 2003], multiple organ system failure [Zallen et al., 1999], and ultimately, increased morbidity and mortality [Vamvakas and Taswell, 1994; Whyte, 1998; Purdy et al., 1997; Ho et al., 2003].

The currently accepted biological marker of RBC viability, which is minimal 24-hour post-transfusional survival of 75% od RBCs, does not reflect the clinical effects of transfusion [Ho et al., 2003]. In addition, *in vivo* assessment of RBC viability by measurement of RBC recovery using radioactive labeling with chromium 51 has many disadvantages, including practical limits and source of error [Hess and Greenwalt, 2002].

Improvement of current red cell hypothermic storage would have an enormous effect on RBC availability, safety and quality.

For the last two decades, the focus of red blood cell biopreservation research has been on lengthening the RBC hypothermic storage period over 42 days by modification of additive solution, blood collection protocol and devices. As a result, solutions allowing 7-week hypothermic storage, such as ErythroSol, MAP and PAGGS-S/M, have been developed for clinical use [Högman, 1999; Walker et al., 1990]. In addition, several rejuvenation solutions have been proposed, of which Rejuvesol is currently the only solution approved by the Food and Drug Administration (FDA).

According to Valeri [2002], for optimum survival and function, liquid preserved RBCs should be hypothermically stored in the currenlty licensed additive solution for no more than 2 weeks.

The continuously increasing need for a safe, high-.quality RBC product will ensure future advances in red blood cell biopreservation.

1.5.1 Cryopreservation of erythrocyte concentrates

Cryopreservation is the process of preserving the biological structure and/or function of living systems by freezing to and storage at ultralow temperature. This method uses the beneficial effect of decreased temperature to suppress molecular motion and arrest metabolic and biochemical reactions.

Cryopreservation is the only current technology that maintains *ex-vivo* biologic functions and provides long-term RBC storage.

The idea of storing RBC at ultralow subzero temperatures has been around for at least 150 years [Rowe, 1994]. Sinche 1950s, cryopreservation has been used in transfusion medicine for long-term storage of RBCs from donors with rare or unusual phenotypes [Rowe, 1994; Valeri and Ragno, 2006] and for military deployment [Kakaiya et al., 2008; Lelkens et al., 2006]. Moreover stockpiling of frozen red cells can be beneficial in emergency or clinical situations, where demand exceeds the supply of RBCs.

At the moment, the shelf life of high-glycerol frozen RBCs (i.e., stored with a final concentration of 40% glycerol at -80°C) has been approved for up to 10 years [Kakaiya et al., 2008].

Glycerol is used as cryoprotective agent, in order to protect red cells from low-temperature injury. This molecule is an attractive cryoprotectant for RBCs because it is relatively non-toxic at high concentrations and readily permeates the cell at 37°C. Over the years, two different protocols have been utilized for cryostorage of red cells in presence of glycerol. These differ in glycerol concentration (either 15-20% or 40% w/v), in the cooling rate (rapid or slow) and in the storage temperature (-196°C or -80°C). [Rowe et al., 1968; Meryman and Hornblower, 1972].

Although glycerol has slow toxicity, a post-thaw deglycerolization washing procedure is necessary to avoid hemolytic transfusion reactions and renal failure after infusion [Bechdolt et al., 1986; Cregan et al., 1991; Klein and Anstree, 2005]. The removal of glycerol is achieved by washing RBC units in a continuous flow centrifuge. This procedure results in a loss of about 15% of the cells [Valeri, 2004]. Thawed/deglycerolized units are expected to meet the minimum standards for transfusion (hemolysis below the 0.8% threshold in Europe and <1% in the USA, and *in-vivo* recovery at 24 h post transfusion >75%).

Henkelman and colleagues [2010] have recently reported that RBC processing steps have the largest effect on cryostored RBC quality, while storage duration itself has minimal effects on red cells. In order to standardize cell processing steps, Haemonetics Corporation (Braintree, Mass) have developed an automated closed system (ACP 215) for the glycerolization and deglycerolization of RBC units. The system uses sterile connectors, inline filters and a disposable polycarbonate bowl with an external seal that allows sequential processing of 2 RBC units (**Figure 8**).

A body of evidence has been accumulated which indicates that cryostored RBCs apparently do not show any classical "storage lesion", in contrast to that observed in red cells stored at 1-6°C [Hess et al., 2010].

On the other hand, it has been reported that thawed RBCs are more fragile than fresh units, as they display higher osmotic fragility [Henkelman et al., 2010]. In addition, intra-cellular calcium content has been shown to increase in the presence of glycerol and upon freeze/thawing of RBCs, probably due to the blockade Ca^{2+} pumps or activation of nonspecific cation channels [Kofanova et a., 2008]. Freeze-thawing and deglycerolization of red blood cells have been thus suggested to compromise ion permeability of the plasma membrane [Kofanova et a., 2008].

Figure 8. ACP 215, Haemonetics Corporation (Braintree, Mass).

The current direction of RBC cryopreservation research involves the development of novel methods to eliminate common problems associated with glycerol-preserved erythrocytes. These research areas involve ice-free cryostorage or vitrification, the use of extracellular cryoprotectant agents and the use of intracellular sugar as cryoprotectant. The first method is used in order to bypass ice formation and the detrimental effects of this step. The second alternative approach is cryopreservation with cryoprotective extracellular macromolecules that are biodegradable and well tolerated by the patients (such as some sugars and polymers); because these molecules do not penetrate the RBC membrane, the osmotic fragility and other problems associated with the use of glycerol would be avoided. The last approach involves the use of low concentrations of intracellular sugars such as trehalose and sucrose. This is an emerging area of interest thanks to the properties of these molecules that can protect critical biological structures during freezing and thawing through the formation of a stable glassy matrix.

1.5.2 Formulation of rejuvenation solutions

Red blood cell storage under blood bank conditions is associated with a sequence of biochemical, metabolic and mechanical changes leading to the progressive loss of cell viability.

In particular, the storage-dependent accumulation of reactive oxygen species (ROS) is mainly related to the progressive loss of metabolic modulation [D'Alessandro et al., 2012;Messana et

al., 2000], resulting in the impairment of antioxidant defences [Jozwik et al., 1997]. Indeed, in humans, each day about 3% of the body's hemoglobin undergoes spontaneous autoxidation to methemoglobin because of the high concentrations of iron in red cells. As prevoiusly reported, Fenton reaction ultimately promotes the accumulation of superoxyl and hydroxyl radicals, the latter being considered as the primary mechanism of injury in stored RBCs [Jozwik et al., 1997].

In this view, preventing the accumulation of oxidative stress has been regarded as a viable strategy to improve the quality of stored RBCs. Over the years, several approaches have been proposed to achieve this aim:

(i) Supplementation of metal chelators, such as deferoxamine, diethylenetriaminepentaacetic acid or ethylenediaminetetraacetic acid, which bind iron released from ageing erythrocytes [Knight et al., 1992];

(ii) Oxygen depletion [Yoshida and Shevkoplyas, 2010], to remove the main substrate of ROS-generating reactions;

(iii) Supplementation of anti-oxidants in the additive solutions, using compounds containing thiol groups and vitamins (expecially C in the form of ascorbate/dehydroascorbate and vitamin E) [Knight et al., 1993; Dawson et al., 1981; Dawson et al., 1980; Magnusardottir and Skuladottir, 2006; Ma et al., 2002].

The last strategy has attracted a great deal of interest during recent decades, expecially in the light of the central role of glutathione (GSH) in intracellular antioxidant system. Indeed, glutathione is the substrate of three key RBC antioxidant enzymes: glutathione peroxidase, glutathione reductase and glutathione S-transferase. Glutathione peroxidase catalyses the decomposition of H_2O_2 and the reduction of lipid hydroperoxides to stable hydroxy-acids. Therefore, ROS are not generated in glutathione reactions, as is the case for superoxide dismutase (SOD)-catalysed reactions, from which it can be inferred that glutathione-related enzymatic mechanisms are primarly committed to protection against the auto-oxidation of erythrocytes [Raftos et al., 2010].

Oxidized glutathione is constantly reduced by glutathione reductase through its utilization of NADPH, which is mainly generated via the pentose phosphate pathway (PPP). However, it has been recently confirmed that the progressive loss of metabolic modulation over storage proportionally impairs the capacity of RBC to replensih NADPH reservoirs via the PPP, expecially after the second week of storage [Gevi et al., 2012; Messana et al., 2000].

In the light of this, two alternative strategies could be pursued:

- to preserve GSH levels by promoting *de novo* synthesis of this tripeptide by fuelling a key limiting substrate precursor, L-cysteine, in the form of N-acetyl-L-cysteine (NAC) [Whillier et al., 2009];
- to reduce GSSG back to GSH, via reactions involving dehydroascorbate/ascorbate (vitamin C) [May, 1998; Rizvi et al., 2009].

N-acetyl-L-cysteine molecule is an acetylated cysteine residue, as illustrated in **Figure 9**. It has long been used therapeutically for the teatment of acetaminophen (paracetamol) overdose, acting as a precursor for the substrate (L-cysteine) in synthesis of hepatic glutathione. Other therapeutic uses of this drug have also emerged, including alleviation of clinical symptoms of cystic fibrosis, nephropathy and thrombosis [Rushworth and Megson, 2013].

NAC has a double biological effect. It can act as a direct antioxidant thanks to the thiolic group –SH (glutathione-independent way) or perform a glutathione-dependent antioxidant activity through the supply of L-cysteine (Cys). Indeed, GSH is synthesized through the conjugation of Cys with L-glutamate (glutamate-cysteine ligase) and subsequently addition of L-glycine thanks to GSH synthase (**Figure 10**).

The glutathione-dependent antioxidant activity is performed through different mechanisms (**Figure 11**). It has been reported that N-acetylcysteine can be extracellularly deacetylated and that Cys is taken into cells via amino acid transporters. Moreover intact NAC can penetrate the cell membrane prior to hydrolysis to Cys in the intracellular environment. Whitin red cell, Cys residue partecipates in GSH biosynthesis, as previously reported.

In its reduced form, GSH have a wide variety of functions, from antioxidant protection to protein thiolation and drug detoxification, often supported by specific enzymes (**Figue 11**). Glutathione is a critical intracellular antioxidant that helps to limit the impact of oxidative stress and to protect vital cellular components (lipids and proteins) against harmful peroxidation.

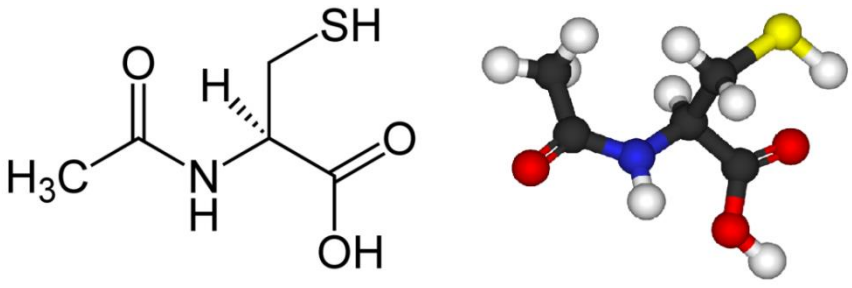

Figure 9. N-acetyl-L-cysteine molecule.

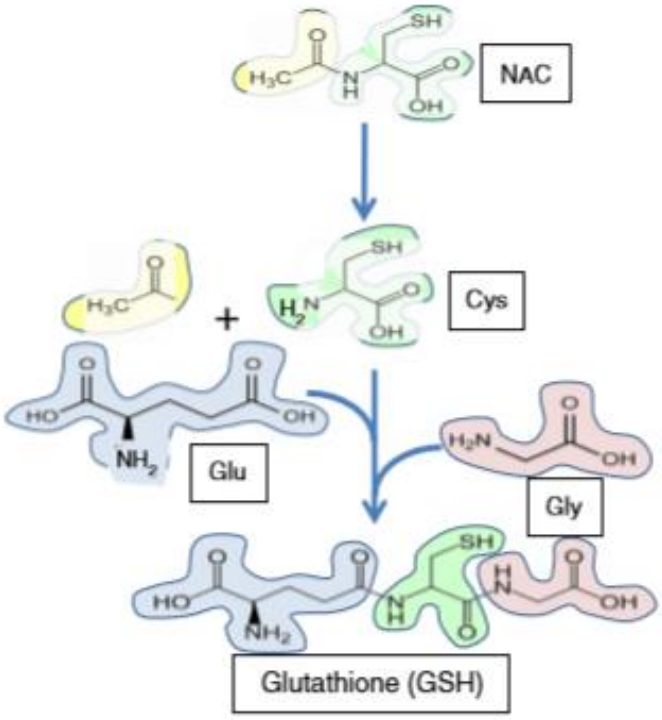

Figure 10. N-acetyl-L-cysteine: a cysteine pro-drug.

While thiol compound like GSH are known to protect directly against oxidative stress, ascorbate helps to preserve α-tocopherol from oxidation, a compound that is found in lipoproteins and in the RBC membrane [May et al., 1998].

Uptake of ascorbic acid by erythrocytes is very slow and occurs by simple diffusion [Horning et al., 1971; Hughes et al., 1968; Wagner et al., 1987; Okamura, 1979]. However, dehydroascorbic acid (DHA), the two-electron oxidized form of ascorbate, is taken up by human red cells by facilitated diffusion on the glucose transporter (GLUT1). Once it has entered the cell, DHA is rapidly converted to ascorbate.

The mechanism by which erythrocytes reduce intracellular DHA to ascorbate was initially considered to be NADH-dependent [Orringer et al., 1979]. More recent studies have suggested that it is primarly GSH-dependent [Rose et al., 1993] (**Figure 11)**.

Vitamin C may perform its antioxidant function indirectly by reducing the tocopheroxyl free radical ($E^{\bullet}$) in the lipid bilayer [Packer et al., 1979; Leung et al., 1981].

The ability of erythrocytes to recycle ascorbate, coupled with the ability of ascorbate to protect vitamin E in the cell membrane, provides a powerful mechanism for preventing lipid peroxidative damage.

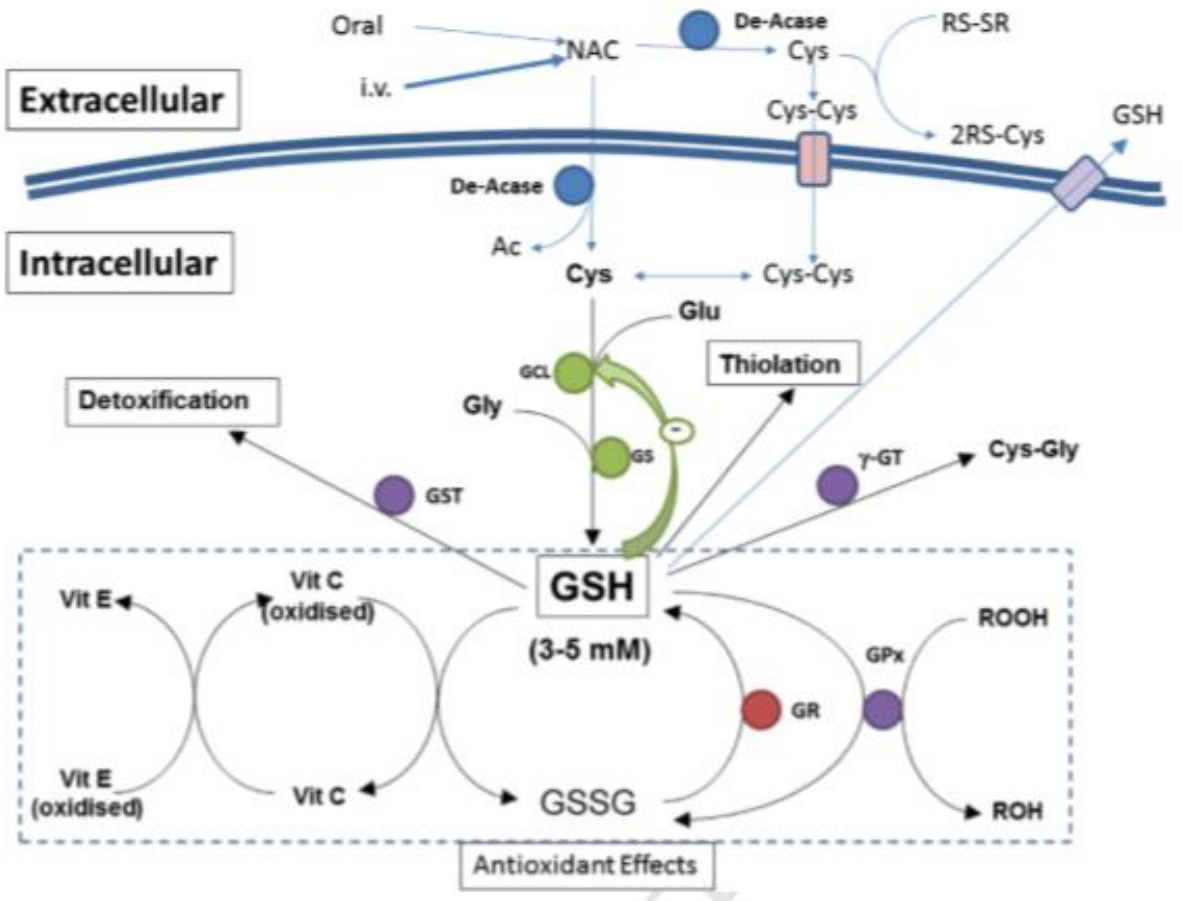

Figure 11 . Impact of NAC on synthesis and utilization pathways for glutathione (GSH).

1.6 Proteomics and its application in transfusion medicine

Despite the mapping of human genome has allowed the identification of over 30,000 genes, continuous efforts have been made to associate the data acquired with DNA functions. So, new tools of investigation and also new disciplines of study have been developed in order to explore the potential applications of genome-related information. These new fields of study are: (i) genomics, the comprehensive analysis of DNA structure and function; (ii) transcriptomics, the study of the mRNA pool found within a cell and correlated to gene expression; (iii) proteomics, the study of the structure, function and location of all proteins expressed in a biological system.

The latter is the field of the "proteome". The term proteome was coined by Wilkins and colleagues in 1996 to indicate the "PROTeins expressed by a genOME" [Wilkins et al., 1996], that are dynamic and changing based on the type and functional state of a cell.

Proteomics exploits several technologies such as two-dimensional polyacrylamide gel electrophoresis (IEF/SDS-PAGE) and other non-gel based separation techniques, such as High-Performance Liquid Chromatography (HPLC) coupled with mass spectrometry.

This discipline has been used for the analysis of blood components since the mid-1970s and at the moment it seems to be the most promising tool in transfusion medicine, for global quality assessment of the production process of blood components and blood derivates.

In particular, proteomics was successfully employed to study RBCs. The first proteomic study of RBCs dates back to 1981 and was conducted by Rosemblum to analyze red cell membrane proteins in normal, adults, neonates and patients with erythrocyte membrane disorders [Rosemblum, 1981]. A lot of studies were successfully performed on RBCs, such as those regarding the analysis of the changes that red cells undergo during storage, also known as storage lesions.

The proteomic approoach is a valuable way to do a global screening of storage-related changes in order to evaluate protective factors against oxidative stress and also to improve the quality of the shelf-life of RBC units.

References

Barasa B, Slijper M. Challenges for red blood cell biomarker discovery through proteomics. Biochim Biophys Acta. (2013) doi:pii: S1570-9639(13)00360-9.

Bechdolt S, Schroeder LK, Samia C, Schmidt PJ. In vivo hemolysis of deglycerolized red blood cells. Arch Pathol Lab Med. 1986;110:344-5.

Blajchman MA. Immunomodulation and blood transfusion. Am J Ther 2002;9:389-395.

Bossi D, Giardina B. Red cell physiology. Mol Aspects Med. (1996);17(2):117-28.

Bryk R, Griffin P, Nathan C. Peroxynitrite reductase activity of bacterial peroxiredoxins. Nature. (2000);407(6801):211-5.

Castagnola M, Messana I, Sanna MT, Giardina B. Oxygen-linked modulation of erythrocyte metabolism: state of the art. Blood Transfus. (2010);8 Suppl 3:s53-8. doi: 10.2450/2010.009S. Review.

Chae HZ, Robison K, Poole LB, Church G, Storz G, Rhee SG. Cloning and sequencing of thiol- specific antioxidant from mammalian brain: alkyl hydroperoxide reductase and thiol-specific antioxidant define a large family of antioxidant enzymes. Proc Natl Acad Sci. USA (1994);91:7017– 21.

Chae HZ, Chung SJ, Rhee SG. Thioredoxin-dependent peroxide reductase from yeast. J Biol Chem. (1994);269:27670-8.

Cicha J, Suzuki Y, Tateishi N et al. Gamma-ray-irradiated red blood cells stored in mannitol-adenine.-phosphate medium: rheological evaluaton and susceptibility to oxidative stress. Vos Sang 2000;79:75-82.

Cregan P, Donegan E, Gotelli G. Hemolytic trabsfusion reaction following transfusion of frozen and washed autologous red cells. Transfusion 1991;31:172-5.

Dawson RB, Hershey RT, Myers CS, Eaton JW. Blood preservation XLIV. 2,3-DPG maintenance by dehydroascorbate better than D-ascorbic acid. Transfusion 1980;20:321-3.

Dawson RB, Hershey RT, Myers CS, Miller RM. Blood presevration 35. Red cell 2,3-DPG and ATP mantained by DHA-ascorbate-phosphate. Transfusion 1981;21:219-23.

D'Alessandro A, D'Amici, Vaglio S, Zolla L. Time-course investigation of SAGM-stored erythrocyte concentrates: from metabolism to proteomics. Haematologica 2012;97:107-15.

Dumaswala UJ, Wilson MJ, Wu YL, Wykle J, Zhuo L, Douglass LM et al. Glutathione loading prevents free radical injury in red blood cells after storage. Free Radic Res. 2000; 33:517-29.

Gevi F, D'Alessandro A, Rinlducci S, Zolla L. Akterations of red blood cell metabolome during cold liquid storage of erythrocyte concentrates in CPD-SAGM. J Proteomics. 2012;76:10-27.

Gibson TG, Rees SB, McManus TJ, Scheitlin II WA. A citrate phosphate dextrose solution for the preservation of human blood. Am J Clin Pathol. (1957);28:569-78.

Glynn SA. The red cell storage lesion: a method to the madness. Transfusion 2010; 50:1164-9.

Heaton A, Miripol J, Aster R et al. Use of Adsol® preservation solution for prolonged storage of low viscosity AS-1 red blood cells. Br J Haematol 1984;57:467-78.

Henkelman S, Lagerberg JW, Graaff R et al. The effects of cryopreservation on red blood cell rheologic properties. Transfusion 2010;50(11):2393-2401.

Hess JR. An update on solutions for red cell storage. Vox Sang 2006; 91: 13-9.

Hess JR. Red cell storage. J Proteomics (2010);73:368-73.

Hess JR. Red cell changes during storage. Transfus Apher Sci 2010; 43: 51-9.

Hess JR, Greenwalt TJ. Storage of red blood cells: new approaches. Transfus Med Rev. (2002);16:283–95.

Ho J, Sibbald WJ, Chin-Yee IH. Effects of storage on efficacy of red cell transfusion: When is it not safe? Crit Care Med.2003;31:S687-S697.

Hofmann B, Hecht HJ, Flohé L. Peroxiredoxins. Biol Chem. (2002);383:347-64.

Högman CF, Hedland K, Zetterstroem H. Clinical usefulness of red cells preserved in protein-poor mediums. N Engl J Med. (1978);299:1377-82.

Högman CF, Hedlund K, Sahleström Y. Red cell preservation in protein-poor media. III. Protection against in vitro hemolysis. Vox Sang. 1981; 41: 274-81.

Högman CF. Preparation and preservation of red cells. Vox Sang. 1998;74:177-178.

Högman CF. Liquid-stored red blood cells for transfusion:a status report. Vox Sang. 1999;76:67-77.

Högman CF, Meryman HT. Storage parameters affecting red blood cell survival and function after transfusion. Transfus Med Rev 1999; 13: 275-96.

Horning D, Weber F, Wiss O. Uptake and release of [1-^{14}C]ascorbic acid and [1-^{14}C]dehydroascorbic acid by erythrocytes of guinea pigs. Clin Chim Acta 1971;31:25-35.

Hou WC, Liang HJ, Wang CC, Liu DZ. Detection of glutathione reductase after electrophoresis on native or sodium dodecyl sulfate polyacrylamide gels. Electrophoresis. (2004);25(17):2926-31.

Huges R and Maton SC. The passage of vitamin C across the erythrocyte membrane. Brit J Haematol. 1968;14:247-53.

Jacobson FS, Morgan RW, Christman MF, Ames BN. An alkyl hydroperoxide reductase from Salmonella typhimurium involved in the defense of DNA against oxidative damage. Purification and properties. J Biol Chem. (1989);264:1488–96.

Jòzwik M, Jòzwik M, Jòzwik M et al. Antioxidant defence of red blood cells and plasma in stored human blood. Clin Chim Acta 1997;267:129-42.

Kakaiya R, Aronson CA, Julleis J. Whole blood collection and component processing. AABB technical manual. 16th ed. Bethesda (MD):AABB Press;2008. P.201-11.

Klein HG, Anstee D. Mollison's blood transfusion in clinical medicine. 11th ed. Massachussets:Blackwell Publishing 2005.

Knight A, Voorhees RP, Martin L. The effect of metal chelators on lipid peroxidation in stored erythrocytes. Ann Clin Lab Sci 1992;22:207-13.

Knight A, Blaylock RC, Searles DA. The effect of vitamins C and E on lipid peroxidation in stored erythrocytes. Ann Clin Lab Sci. 1993;23:51-6.

Kofanova OA, Zemlyanskikh NG, Ivanova L et al. Changes in the intracellular Ca2+ content in human red blood cells in the presence of glycerol. Bioelectrochemistry 2008;73(2):151-154.

Leal-Noval SR, Jara-Lopez I, Garcia-Garmndia JL et al. Influence of erythrocyte concentrate storage time on post-surgical morbidity in cardiac surgery patients. Anesthesiology 2003;98:815-822.

Lelkens CC, Koning JG, de Korte D, Floot IB, Noorman F. Experieces with frozen blood products in the Netherlands military. Transfus Apher Sci. 2006;34:289-98.

Leung HW, Vang MJ, Mavis RD. The cooperative interaction between vitamin E and vitamin C in suppression of peroxidation of membrane phospholipids. Biochim Biophys Acta 1981;664:266-72.

Lewison R. A new and greatly simplified method of blood transfusion. Med Rec. (1915);87:141-2.

Lin CL, Chen HJ, Hou WC. Activity staining of glutathione peroxidase after electrophoresis on native and sodium dodecyl sulfate polyacrylamide gels. Electrophoresis. (2002);23(4):513-6.

Ma EP, Liu XZ, Han Y et al. New tactics of human red blood cells stored at 4 degrees C-protective effect of antioxidant solution on red blood cells damage. Zhongguo Shi Yan Xue Ye Xue Za Zhi 2002;10:153-5. Abstract.

Magnusardottir AR, Skuladottir GV. Effects of storage time and added antioxidant on fatty acid composition of red blood cells at -20 degrees C. Lipids 2006;41:401-4.

Marik PE, Sibbald WJ. Effect of stored-blood transfusion on oxygen delivery in patients with sepsis. JAMA 1993;269:3024-3029.

Martin CM, Sibbald WJ, Lu X et al. Age of transfused red blood cells is associated with ICU lenght of stay. Clin Invest Med 1994; 17:B21.

May JM. Ascorbate function and metabolism in the human erythrocyte. Front Biosci. 1998;3:d1-10.

May JM, Qu ZC, Mendiratta S. Protection and recycling of alpha-tocopherol in human erythrocytes by intracellular ascorbic acid. Arch Biochem Biophys. 1998;349:281-9.

Meryman HT, Hornblowr M. A method for freezing and washing red blood cells using a high glycerol concentration. Transfusion 1972;12:145-156.

Messana I, Ferroni L, Misiti F et al. Blood bank conditions and RBCs: the progressive loss of metabolic modulation. Transfusion 2000;40:353-60.

Nordberg J, Arnér ES. Reactive oxygen species, antioxidants, and the mammalian thioredoxin system. Free Radic Biol Med. (2001);31(11):1287-312. Review.

Okamura M. Uptake of L-ascorbic acid and L-dehydroascorbic acid by human erythrocytes and HeLa cells. J Nutr Sci Vitaminol. 1979;25:269-79.

Orringer EP and Roer ME. An ascorbate-mediated transmemebrane-reducing system of the human erythrocyte. J Clin Invest. 1979;63:53-8.

Packer JE, Slater TF, Willson RL. Direct observation of a free radical interaction between vitamin E and vitamin C. Nature 1979;278:737-8.

Purdy FR, Tweeddale MG, Marrick PM. Association of mortality with age of blood transfused in septic ICU patients.Can J Anaesth.1997;44:1256-1261.

Raftos JE, Whilliert S, Kuchel PW. Glutathione synthesis and turnover in human erythrocyte: alignment of a model based on detailed enzyme kinetics with experimental data. J Biol Chem. 2010;285:23557-67.

Rizvi SI, Pandey KB, Jha R, Maurya PK. Ascorbate recycling by erythrocytes during aging in humans. Rejuvenation Res 2009;12:3-6.

Robertson OH. Transfusion with preserved red blood cells. Br Med J. (1918);1:691-5.

Rose RC and Bode AM. Biology of free radical scavangers: an evaluation of ascorbate. FASEB J 1993;7:1135-42.

Rosenblum BB. Two-dimensional gel electrophoresis of erythrocyte membrane proteins. Prog Clin Biol Res. 1981;56:251-68.

Rous P., Turner JR. The preservation of living red blood cells in vitro. J Exp Med. (1916);23:219-48.

Rowe AW. Cryopreservation of red blood cells. Vox Sang. 1994;67:201-6.

Rowe AW, Eyster E, Kellner A. Liquid nitrogen preservation of red blood cells for transfusion: a low glycero- rapid freeze procedure. Cryobiology 1968;5:119-128.

Rushworth GF, Megson IL. Existing and potential therapeutic uses for N-acetylcysteine: the need for conversion to intracellular glutathione for antioxidant benefits. Pharmacol Ther. 2014;141(2):150-9.

Scott KL, Lecak J, Acker JP. Biopreservation of red blood cells: past, present, and future. Transfus Med Rev. (2005);19(2):127-42. Review.

Sharifi S, Dzik WH, Sadrazadeh SM. Human plasma and tirilazad mesylate protect stored human erythrocytes against the oxidative damage of gamma-irradiation. Transfus Med 2000; 10:125-30.

Silva DG, Belini Junior E, de Almeida EA, Bonini-Domingos CR. Oxidative stress in sickle cell disease: An overview of erythrocyte redox metabolism and current antioxidant therapeutic strategies. Free Radic Biol Med. (2013);65C:1101-1109.

Simon TL, Marcus CS, Myhre BA, Nelson EJ. Effects of AS-3 nutrient-additive solution on 42 and 49 days of storage of red cells. Transfus.1987;27:1778-82.

Sparrow RL. Time to rivisit red blood cell additive solutions and storage conditions: a role for "omics" analysis. Blood Transfus. 2012;19Suppl2:s7-11.

Stansbury LG, Hess JR, Roger I. Lee: the right man at the right time. Transuf Med Rev. (2005);19:81-4.

Valeri CR. Status report on the quality of liquid and frozen red blood cells. Vox Sang. 2002;83:193-196.

Valeri CR. Red cell freezing and its impact on the supply chain. Transfuss. Med 2004;14:387-388.

Valeri CR and Ragno G. cryopreservation of human blood products. Transf Apher Sci. 2006;34:271-87.

Vamvakas EC, Taswell HF. Long-term survival alter blood transfusion. Transfusion 1994;34:471-477.

Wagner ES, White W, Jennings M, Bennett K. The entrapment of [^{14}C]ascorbic acid in human erythrocytes. Biochim Biophys Acta 1987;902:133-6.

Walker WH, Netz M, Ganshirt KH. 49 day storage of erythrocyte concentrates in blood bags with the PAGGS-mannitol solution. Beitr Infusionsther 1990;26:55-9.

Walter CW, Murphy Jr WP. A closed gravity technique for the preservation of whole blood in ACD solution utilizing plastic equipment. Surg Gynecol Obset. (1952);94:687-92.

Whillier S, Raftos JE, Chapman B, Kuchel PW. Role of N-acetylcysteine and cysteine in glutathione synthesis in human erythrocytes. Redox Rep. 2009;14:115-24.

Whyte GS. The transfused population of Canterbury, New Zeland and its mortality. Vox Sang 1988;54:65-70.

Wilkins MR, Sanchez JC, Gooley AA et al. Progress with proteome projects:why all proteins expressed by a genome should be identified and how to do it. Biotechnol Genet Eng Rev. 1996;13:19-50.

Wood ZA, Schröder E, Robin Harris J, Poole LB. Structure, mechanism and regulation of peroxiredoxins. Trends Biochem Sci. (2003);28(1):32-40. Review.

Yoshida T, Shevkoplyas SS. Anaerobic storage of red blood cells. Blood Transfus. 2010;8:220-36.

Zallen G, Offner PJ, Moore EE et al. Age of transfused red blood cells is an independent risk factor for postinjury multiple organ failure. Am J Surg 1999;178:570-572.

Chapter 2

A better RBC storage rather than a longer one

2.1 Monitoring of red blood cells during processing for cryopreservation: from fresh blood to thaw-washing

Cryostorage of red blood cells (RBCs) represents a valid alternative to liquid storage, since units can be preserved safely for at least a decade while conserving RBC viability. While cryostorage has attracted a great deal of attention clinically, little is known about the biochemistry and physiology of cryostored erythrocyte concentrates.

In the present study, we investigated cryostorage of RBCs through monitoring of cell processing steps (from fresh blood, to glycerolization, thawing and deglycerolization/washing) through repeated assays of standard parameters (MCV, RDW-SD) and scanning electron microscopy.

Cell processing for cryostorage resulted in increased RBC volumes. Shape alterations caused an increase in osmotic fragility and permeability to ions. A significant pH drop was observed which could not to be attributed to a higher metabolic rate, since the levels of lactate did not show substantial fluctuation during the cell processing steps tested in this study. Membrane anomalies are likely related to the hemolysis observed which preferentially affected the densest and oldest cell sub-populations, as confirmed by means of discontinuous density gradients.

Our results indicate that cryostorage itself in presence of glycerol does not significantly affect RBCs. Most of the alterations observed were related to cell processing and, in particular, to the increase of cytosolic glycerol as a consequence of the glycerolyzation step.

Further studies might profitably investigate replacing glycerol with non-penetrating cryoprotectants.

2.1.1 Materials and methods

Sample collection

Whole blood (450 mL±10%) was collected at the “Celio” Military Hospital in Rome (Italy) from 10 healthy donor volunteers into CPD anticoagulant (63 mL) and leukodepleted. After separation of plasma by centrifugation, RBCs were suspended in 100 mL of Saline, Adenine,

Glucose, Mannitol (SAG-M) solution. Ten leukoreduced RBC units were then prepared and cryopreserved, according to the high-glycerol freezing method [Lagerberg et al., 2007].

Briefly, RBC units with a Hct of approximately 60% and fewer than 106 white blood cells were obtained from the blood bank and stored at 2 to 6 °C for 2 h, after which glycerolization and freezing was performed. Glycerolization to a final concentration of 40% glycerol (wt/vol) was accomplished using the Haemonetics ACP 215 device. All glycerolized RBC units were frozen and stored at −80±10 °C in a mechanical freezer for at least 12 months. Frozen RBC units were thawed in a temperature-controlled water bath at 40 °C, until the units reached a temperature between 25 and 30 °C. Thawed RBCs were deglycerolized using the Haemonetics ACP 215 device and resuspended in SAGM.

Thawed deglycerolized RBCs were stored in polypropylene tubes at 2 to 6 °C. The supernatant osmolarity of all the thawed deglycerolized units was below 400 mOsm/kg H_2O, indicating an efficient removal of glycerol.

Samples were collected at four sequential stages: (i) fresh blood, within 2 h from collection; (ii) after glycerolization; (iii) after thawing; and, within 2 h after thawing, (iv) after deglycerolization through repeated washing cycles.

RBC analysis

The RBC mean cell volume (MCV), red cell distribution width-standard deviation (RDW-SD), the mean cell hemoglobin concentration (MCHC), and the hematocrit (Hct) were determined with a hematology analyzer (CA 530-Oden, Medonic, Stockholm, Sweden).

Determination of intracellular pH, lactate and glycerol

Red cell pellets obtained by centrifuging 600 µL of suspension in a nylon tube at 30,000×g for 10 min, were frozen, thawed during 5 min and then refrozen. Triplicate measurements of pH were then made with a Radiometer pH glass capillary electrode maintained at 20 °C and linked to a Radiometer PHM acid–base analyzer. To prevent the acid shift seen when samples are kept unfrozen these pH measurements were made immediately after a second thawing of each lysate.

Lactate and glycerol determinations was performed upon methanol/chloroform/water sample extraction through rapid-resolution, reversed phase, high performance liquid chromatography and mass spectrometry, according to the method of D'Alessandro et al. [D'Alessandro et al., 2011]. Results were plotted as mass spectra counts, which are proportional to the metabolite concentrations within the linearity range of the instrument, or fold-change variations upon

normalization to the results obtained through testing of fresh RBCs. Rapid resolution, reversed phase, high performance liquid chromatography (RR-RP-HPLC) was performed to separate low-molecular weight compounds, as previously reported [D'Alessandro et al., 2011]. The RR-RP-HPLC directly eluted into an ion trap Rapid resolution, reversed phase, high performance liquid chromatography (RR-RP-HPLC) was performed to separate low-molecular weight compounds, as previously reported [D'Alessandro et al., 2011]. The RR-RP-HPLC directly eluted into an ion trap mass spectrometer (HCT Bruker, Bruker Daltonics, Bremen, Germany), where the compounds were monitored through Multiple Reaction Monitoring (MRM). Mass to charge ratio for precursor and fragment ions to be selected, monitored and quantified were determined as previously reported [D'Alessandro et al., 2011], in agreement with international online available databases (Metlin, Scripps Center for Biotechnology - available at http://metlin.scripps.edu/metabo_info.php?molid=105 – Last accessed on January 30, 2012).

Hemolysis

Hemolysis was calculated according to Harboe [Harboe, 1959]. Samples were diluted in distilled water and incubated at room temperature for 30 min to lyse RBCs. Samples from lysed RBCs were diluted 1⁄300 while supernatants were diluted 1⁄10 in distilled water. After a 30 min stabilization and vortex mixing (Titramax 100, Heidolph Elektro, Kelheim, Germany), the absorbance of hemoglobin was measured at 380, 415 and 450 nm (PowerWave 200 Spectrophotometer, Bio-Tek Instruments, Winooski, Vermont, USA). The mean blank was subtracted and the corrected OD (OD*) was calculated as follows: $2\times OD_{415}-OD_{380}-OD_{450}$.

Osmotic fragility

The osmotic fragility of RBCs reflects the ability of the membrane to maintain structural integrity. Osmotic fragility was determined by stepwise dilution through PBS solutions ranging from 0.90% to 0.35%.

RBCs with a Hct of 30% to 40% were diluited 1:100 in each PBS solution, mixed and incubated for 30 min at 4°C, followed by centrifugation for 12 min at 1100×g. The free Hb in the supernatant was measured using a spectrophotometer. The concentration of PBS necessary to induce 50% hemolysis defined the osmotic fragility index of the RBCs [Gyongyossy-Issa et al., 2005]. With this method, a larger osmotic fragility index corresponds to more fragile cells.

Density gradients

Density-fractionated RBCs werre prepared using Percoll (Sigm-Aldrich, St. Louis, MO, USA) discontinuous gradients, as described by Bosch et al. [Bosch et al., 1992]. Briefly, the gradient was built up in five layers of 2 mL containing 80% (1.096 g/mL), 71% (1.087 g/mL), 67% (1.083 g/mL), 64% (1.080 g/mL) Percoll, respectively, in buffer A [26.3 g/L bovine serum albumin, 132 mmol/L NaCl, 4.6 mmol/L KCl, and 10 mmol/L HEPES pH 7.1]. RBCs were washed with buffer B [9 mmol/L Na2HPO4, 1.3 mmol/L NaH2PO4, 140 mmol/L NaCl, 5.5 mmol/L glucose, and 0.8 g/L bovine serum albumin] and diluted with 1 vol of buffer A. One-half milliliter of this suspension was layered on the Percoll gradient and separation was achieved after 15 min of centrifugation at 3000rpm at room temperature. Fractions were collected by careful pipetting and extensively rinsed with buffer B to remove residual Percoll.

Scanning electron microscope (SEM)

Scanning electron microscopic studies of RBC were performed with a JEOL JSM 5200 electron microscope. Blood samples from each one of the ten subjects were collected (i) soon after withdrawal and separation of RBCs through centrifugation, as specified above (fresh blood); or (ii) upon cryostorage, after thawing, deglycerolization and washing steps. Packed RBCs were then fixed in phosphate-buffered (pH 7.2–7.4) 2.5% glutaraldehyde for 1 h, washed two times in 0.1 M phosphate buffer (pH 7.2–7.4), and mounted on poly-L-lysine-coated glass slides. The glass slides were kept in a moist atmosphere for 1 h, washed in phosphate buffer, postfixed in 1% osmium tetroxide for 1 h, rinsed in distillated water, and dehydrated in graded ethanol (50–70–90–100%). After critical-point drying with liquid CO2 in a vacuum apparatus and covering with a gold-palladium layer, the samples underwent scanning electron microscopic analysis. The different cell shapes were identified using Bessis' classification [Bessis, 1972], as previously reported [D'Alessandro et al., 2012]. The percentage of discocytes, echinocytes, spheroechinocytes, stomatocytes, spherostomatocytes, and spherocytes were evaluated by counting 1000 to 1500 cells in randomly chosen fields.

2.1.2 Results and discussion

Metabolism was unaffected by cell processing steps

In comparison to fresh blood (7.01 $\pm$ 0.14 pH units), supernatant pH moderatelky increased after glycerolization and thawing (7.32 $\pm$ 0.34 and 7.46 $\pm$ 0.43, respectively). After

deglycerolization through repeated washing cycles, supernatant pH returned to below the starting level (6.91 ± 0.11) (**Figure 12.A**).

Cytosolic pH did not show major fluctuations during the various cell processing steps (approximately 6.95 units, remaining constant from fresh blood to thawed RBCs), while it significantly decreased after deglycerolization/washing (6.39 ± 0.13 units) (**Figure 12.B**).

However, internal pH drop after deglycerolization/washing was not related to lactate accumulation, since no significant fluctuations of lactate levels were observed among samples collected at each cell processing step (**Figure 12.C**).

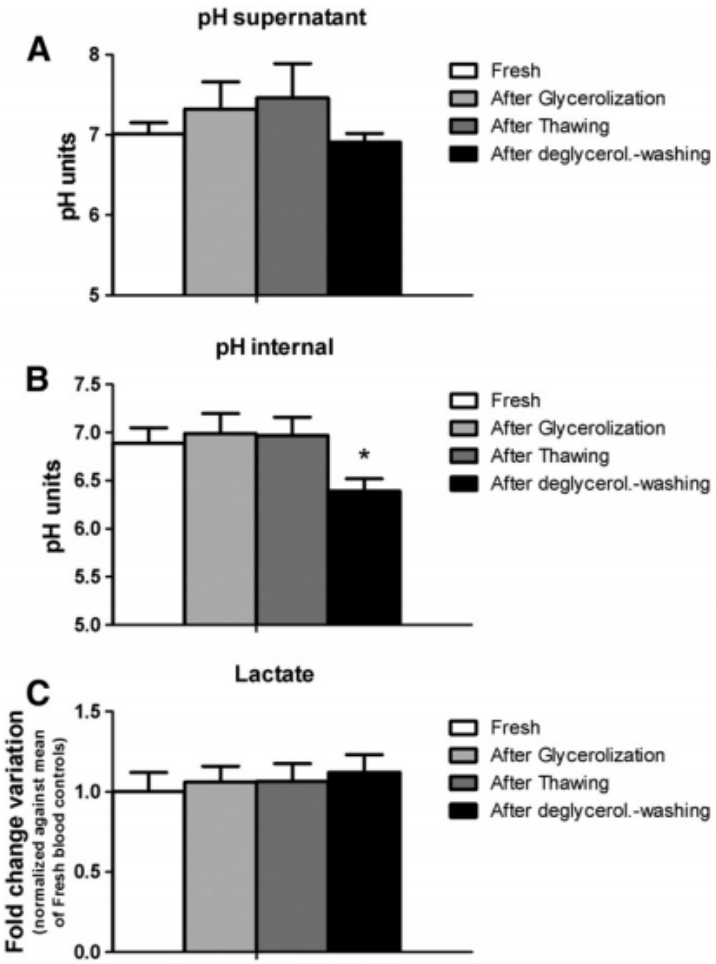

Figure 12. Graphs illustrating trends for supernatant pH (A), internal pH (B) and lactate (C) during each one of the tested cell processing steps: fresh red blood cell controls (white column), after glycerolization (light gray), after storage and thawing (dark gray), and after deglycerolization through washing (black).
*indicates statistical significanca (p-value < 0.05 ANOVA) between groups (columns).

All these metabolic parameters indicate that cryostorage did not significantly affect metabolic activities, since pH was not altered prior to deglycerolization/washing of RBCs and lactate

concentration did not vary significantly during celol processing. These observations are in agreement with previous reports from the literature which indicated that no substantial ATP nor 2,3-DPG losses are observed after cryostorage [Henkelman et al., 2010; Holovati et al., 2008]. This is consistent with the assumption that enzymatic activity should be halted at a storage temperature of -80°C.

While lactate and supernatant pH did not vary significantly during cell processing, internal cellular pH decreased after the multiple washing steps accompanying the deglycerolization process (**Figure 12**). A tentative explanation might involve alteration of action homeostasis. Indeed, changes affecting the RBC membrane might dysregulate cation pumps, as previously proposed by Kofanova and colleagues [Kofanova et al., 2008].

Alterations to cell morphology and fragility triggered by the glycerolization step were only partially reversible

Cytoplasmic glycerol was undetectable (baseline mass spectra counts) in fresh blood controls, while it significantly increase upon glycerolization (p-value < 0.01 ANOVA). After cryostorage, thawing and deglycerolization, cytoplasmic glycerol levels significantly decreased again, although glycerol was still detectable through mass spectrometry (**Figure 13).**

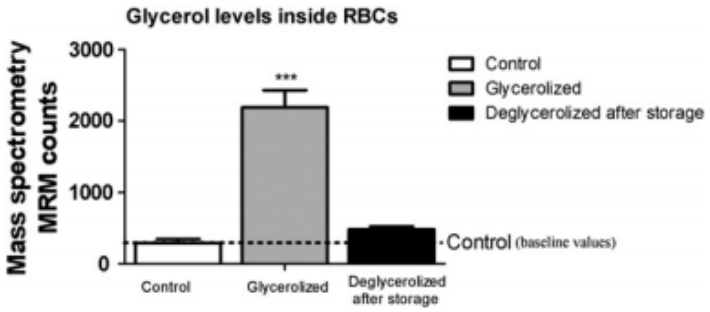

Figure 13. Cytoplasmic glycerol levels in freshly drawn (white column), glycerolized (gray column), cryostored/thawed, and deglycerolized (black column) RBCs. Results are reported as mass spectra counts through multiple reaction monitoring (MRM), a mass spectrometric approach which allows detecting, isolating and fragmenting a specific molecular mass to charge ratio (m/z). Glycerol was quantified as 91.04 m/z $(M\text{-}H)^-$ in negative ion mode, in agreement with international database (METLIN, Scripps Centre for Biotechnology – availabloe at http://metlin.scripps.edu/metabo_info.php?molid=105 last accessed on January 30, 2012).

In **Figure 14** we report variations of several RBC parameters during each one of the cell processing steps, including Mean Cell Volume (MCV), red cell distibution width-standard

deviation (RDW-SD), mean cell hemoglobin content (MCHC), hematocrit (Hct), osmotic fragility and hemolysis percentage

MCV increased significantly upon glycerolization (from 89.4 ± 4.5 of fresh RBCs to 126.04 ± 2.3 of glycerolized RBCs), while it remained constant upon cryostorage even after thawing (129.6 ± 3.3). Deglycerolization and washing restored lower MCV values (93.7 ± 5.9), though stioll higher than controls (**Figure 14.A**).

Red cell distribution width-standard deviation (RDW-SD) followed a similar trend to MCV, since glycerolized RBCs were characterized by higher values (73.92 ± 0.45) than fresh RBC controls (43.15 ± 2.39), even after thawing (73.22 ± 0.56). On the other hand, deglycerolization through multiple washing cycles resulted in a decrease in RDW-SD (48.6 ± 4.71), though final RDW-SD values were still higher than the average reference range (**Figure 14.B**).

The mean corpuscolar hemoglobin concentration (MCHC) is a measure of the concentration of hemoglobin in an average red blood cell. It is calculated by dividing the hemoglobin by the hematocrit [Europena Directorate for the Quality of Medicine & Heklathcare, 2011]. MCJC values were significantly influenced by glycerolization (23.4 ± 1.62 against 33.1 ± 0.57 for fresh RBC controls), while they remained almost identical upon storage and after thawing (23.1 ± 2.32). However, normal values were restored after deglycerolization and thawing (28.1 ± 5.46) (**Figure 14.C**).

Hematocrit (Hct) was increased by glycerolization (71.45 ± 2.82) when compared to fresh RBC concentrates (61.34 ± 3.29). However, the Hct dropped below control values at the end of cryostorage (57.45 ± 4.19%) (**Figure 14.D**).

Analogously, osmotic fragility increased after glycerolization (0.78 ± 0.39) and storage/thawing (0.73 ± 0.45) in comparison to fresh RBC controls (0.48 ± 0.1%). After RBCs had been deglycerolized and washe, osmotic fragility was highe than in fresh RBC controls (0.69 ± 0.22) (**Figure 14.E**).

Finally, hemolysiis increased significantly from the 0.23 ± 0.03% value for fresh RBCs to 2.67 ± 1.95 and 4.73 ± 3.65 in glycerolized and stored/thawed RBCs, respectively. However, after the deglycerolization/washing step, final hemolysis values decreased substantially (0.33 ± 0.05%) and were thus lower than 0.8%, the maximum threshold for hemolysis allowed by the Europena Council guidelines (**Figure 14.F**).

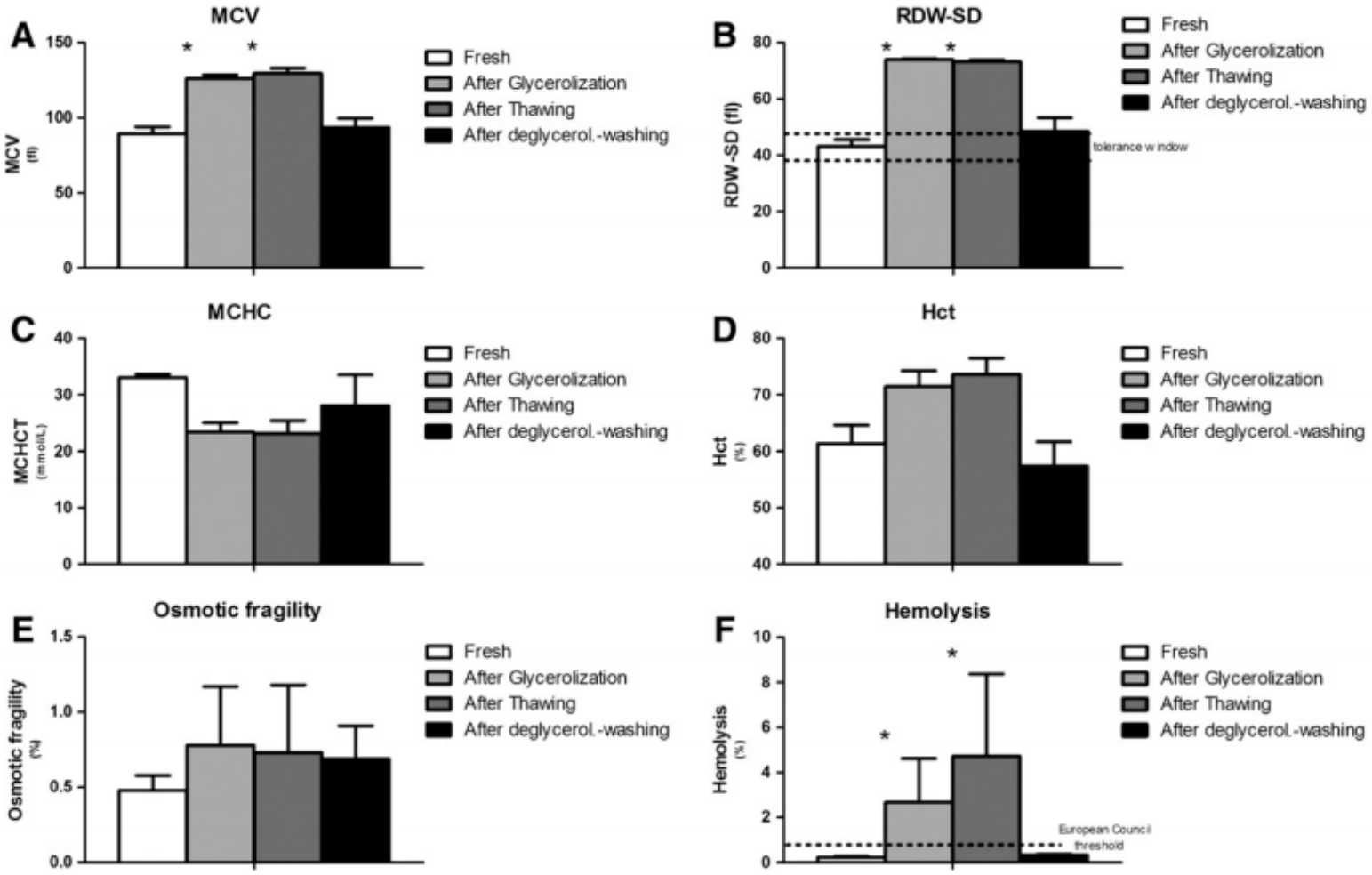

Figure 14. Graphs illustrating variations for several parameters including mean cell volume (MCV— A), red cell distribution width-standard deviation (RDW-SD — B), mean cell hemoglobin content (MCHC — C), hematocrit (Hct — D), osmotic fragility (E) and hemolysis percentage (F) during each one of the tested cell processing steps: fresh control red blood cells (white column), after glycerolization (light gray), after storage and thawing (dark gray), and after deglycerolization and washing (black).
* indicates statistical significance (p-valueb0.05 NOVA) between groups (columns).

Scanning Electron Microscpe (SEM) micrographs were made on fresh blood samples (a picture of day 0 discocytes is provided in **Figure 15.A**) and RBCs after cryostorage (**Figure 15.B**). After cryostorage, RBCs showed membrane anomalies (i.e. non –discocyte shape) in almost half of the RBCs (47.3 $\pm$ 3.4%), including small echinocyte (**Figure 15.C**) and spheroechinocyte sub-population (5.6 $\pm$ 1.2%) (**Figure 15.E**). In contrast, at the end of the shelf life of hypothermically stored RBCs (42 days at 1-6°C), approximately 76.3 + 6.7% of RBCs showed membrane shape alterations.Furthermore, at 42 days of liquid storage a much higher percentage of RBCs were spheroechinocytes or spherocytes (approximately 25%) (**Figure 15.D**).

RBC shape appeared to be significantly altered after glycerolization step, which was accompained by a significant increase in the MCV and the RDW-SD. This is likely due to glycerol entering the cell (**Figure 13**) resulting in inreased cell volumes.

While cryostorage and the thawing step did not affect these parameters at all, we expected that the washing step would have removed glycerol and thus return the MCV and RDW-Sd values back to the normal range.

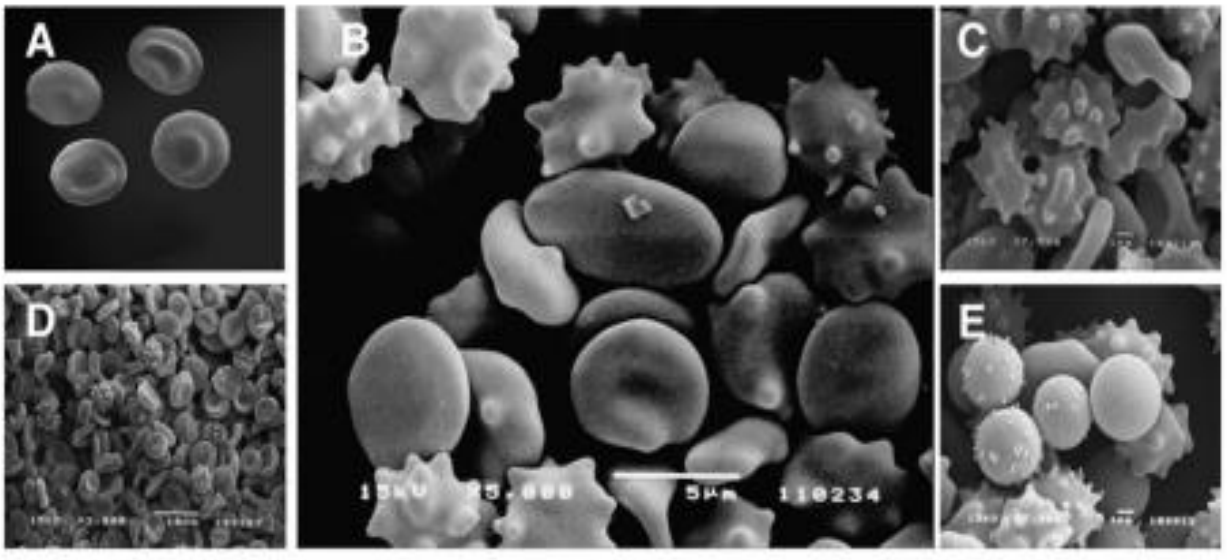

Figure 15. Scanning electron micrographs of red blood cells. In (A), a detail is provided of discocytes from fresh blood (detail re-elaborated through Photoshop CS5, Adobe, CA, USA). In (B), a detail of thawed/deglycerolized/washed red blood cells upon cryostorage. In (C) and (E), a detail is provided of red blood cells showing membrane abnormalities upon cryostorage and, in particular, of echinocytes and spheroechinocytes, respectively. In (D), the micrograph shows red blood cells upon 42 days of liquid (CPD-SAGM) storage under refrigeration (1–6 °C). The figure has been composed through Adobe Photoshop CS5.

However, despite the washing step, both MCV and RDW-SD were still higher than in fresh blood controls. This was most marker in the RDW-SD which was 11.21% higher than controls (**Figure 14)**. These observation are in line with the results reported by Henkelman et al. [Henkelman et al., 2010] and may be related to the increased cytoplasmic glycerol that was measured at the end of the washing steps (**Figure 13**).

RBCs osmotic fragility increased following the glycerolization step and remained higher than in fresh blood controls thrroughout processing. The RBC morphological alterations documented by SEM analysis are consistent with and likely contributory to this increased osmotic fragility (**Figure 15**).

Hemolysis mainly involved older cell populations

Erythrocyte fractions of varying density were isolated by discontinuous density gradient centrifugation of fresh erythrocytes after withdrawal (**Figure 16.A**) and after cryostorage (**Figure 16.B**). In fresh blood, five different density fractions could be observed (**Figure 16.A**). At the end of cryostorage (after thawing and deglycerolization throughwashing steps) only 3 bands were still visible, since the 2 densest fractions has disappeared (band 4 and 5 in **Figure 16**).

A decrease in MHCH and Hct is consistent with previous reports indicating that not all RBCs presenta t the start of processing survive to the end of cryostorage [Henkelman et al., 2010; Holovati et al., 2008]. We measured this loss at approximately 5%. This is confirmed by our measured hemolysis. Although the final washing steps restored free hemoglobin levels to below the 0.8% threshold tolerated by the Europena Council guidelines the starting free hemoglobin levels were consistent with a 4.73 $\pm$ 3.65% hemolysis at the end of cryostorage and thawing. However, it is worthwhile noting that free hemoglobin levels were significantly higher than fresh control RBCs right after the initial glycerolization step (2.67 $\pm$ 1.95).

Discontinuous cell density gradients were used to determine if the hemolyzed cells might be coming from a RBC-sub-population that might be unusually susceptible to the stresses of cell processing of cryostorage. According to the literature [Bosch et al., 1992; Pierpont et al., 1988], the density of RBCs increases as the cells age. This is probably due to the loss of both water and hemoglobin during senescence, though the fomer at a higher rate, which could results in a increase in cell density [Pierpont at al., 1988]. During the various processing steps involved in cryostorage and deglycerolization, the denset RBC sub-populations (band 4 and 5 in **Figure 16**) disappeared from the density gradient. We therefore propose that older sub-populations are more susceptible to hemolysis.

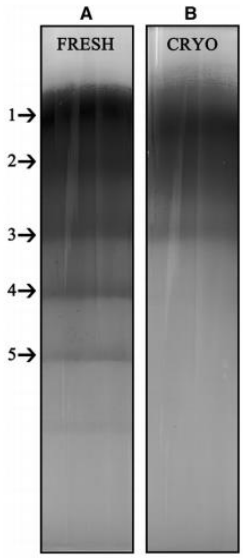

Figure 16. Discontinuous density gradients of fresh blood (A-left column) and deglycerolized/washed cryostored blood (B-right column). Band 1 represents the least dense and youngest population, while band 5 the densest and oldest one.

2.1.3 Conclusion

Cryopreservation of living cells and tissues has become a routine technique in biological and medical laboratories, although cryostorage of RBC concentrates is not as widely utilized. The mechanism of cryoprotection promoted by penetrating agents has been well characterized during the last fifty years, since Lovelock's first analysis [Lovelock, 1953]. In brief, the initial concentration and viscosity of protective polymer solutions reduce the extent and rate of cell water loss to extracellular ice and limit the injurious osmotic stress, which cells face during freezing at moderate rates to -20°C. Below -20°C, glass formation n (vitrification) prevents further osmotic stress by isolating cells from extracellular ice crystals, virtually eliminating continuing cell water loss [Takahashi et al., 1988]. Cryoprotectants reduce the amount of ice formed at any given temperature, as they increase the total concentration of all solutes in the system. Cryoprotectants must thus be able to penetrate into the cells and have low toxicity. Many compounds have such properties, including glycerol, dimethyl sulfoxide, ethanediol, and propanediol [Pegg, 2007].

Cryoprotectants have been divided into two categories, namely those which penetrate cell membranes and those which do not. The cryoprotectant glycerol provides a unique window

on the mechanism of action of cryoprotectants, since it is a penetrating agent if added at physiological temperatures but it is essentially impermeant if added at 0 °C [Pegg, 2007].

In the present study, we observed that glycerolization of RBCs resulted in increased cell volumes which were not completely returned to normal values, even after deglycerolization. Shape alterations also occurred and these appeared to be closely related to an increased permeability to ions and to an increase in osmotic fragility. The observed pH drop could not be attributed to metabolism, since lactate did not accumulate during the cell processing steps. Membrane alterations were assessed indirectly through RBC parameters (MCV, RDW-SD) and directly, through electron microscopy. Membrane anomalies probably liea t the basis of the hemolytic phenomena. Our discontinuous density gradient data suggest that these preferentially target older cell sub-populations.

To conclude, our results indicate that cryostorage itself in presence of glycerol does not substantially affect RBCs; most of the alterations observed were related to the RBC processing steps and, in particular, to the penetration of glycerol inside RBCs as confirmed by mass spectrometry and in agreement with the literature [Rowe et al., 1968; Meryman and Hornblower, 1972].

RBC membrane permeability to glycerol has been shown to depend mainly on the presence of aquaporin channels [Wang et al., 2005]. When glycerol penetrates the cell, on the one hand it protects the erythrocyte from much of the freezing damage, while on the other hand it seems likely that it triggers and alters protein-protein interactions in the cytosol and cytoskeleton. Glycerol is a polar molecule which, at high concentrations, is known to alter the ionic strength and the dielectric constant of aqueous solutions [Sedgwick et al., 2007; Farnum, and Zukoski, 1999]. The effects of glycerol penetration inside RBCs might thus result in alterations compromising the cell structure.

Looking to the future it should be worthwhile to test the effects of non-penetrating cryoprotectants (such as large molecular-weight polymers – eg, polyvinylpyrrolidone or polyethylene glycol – or the less toxic sucrose and trehalose) [Sedgwick et al., 2007; Farnum, and Zukoski, 1999]. Trehalose, in particular, is naturally used by plants when facing abiotic stresses such as cold stress [Iordachescu and Imai, 2008], and might represent an experiment-of-nature meeting the challenges posed by cryopreservation.

2.2 Red blood cell storage with vitamin C and N-acetylcysteine prevents oxidative stress-related lesions: a metabolomics overview

Mass spectrometry-based metabolomics has recently proven its worth, as an innovative and highly sensitive tool to dissect red blood cell metabolism and enable a wide series of translational applications in the field of erythrocyte biology and transfusion medicine.
In the present study, we exploited a validated HPLC-MS analytical workflow to determine the effects of vitamin C and NAC supplementation (antioxidants) on the metabolome of CPD-SAGM erythrocyte concentrates stored under blood bank conditions.
As a result, we could observe decreased energy metabolism fluxes (glycolysis and PPP), depressed by the competitive uptake of ascorbate and glucose.
Supplementation of anti-oxidants was indeed effective in positively modulating the redox poise, through the promotion of glutathione homeostasis, which resulted in decreased haemolysis, lower accumulation of malondialdehyde and oxidation byproduct metabolites (including GSSG and prostaglandins).
Antioxidants did not help preserving erythrocyte morphology, as gleaned through scanning electron microscopy. Through these results, we could confirm a central role for energy metabolism, rather than oxidative stress, in the accumulation of the most evident RBC storage lesions (such as those targeting the erythrocyte phenotype).

2.2.1 Materials and methods

Sample collection

Red blood cell units were drawn from healthy donor volunteers according to the policy of the Italian National Blood Centre guidelines (Blood Transfusion Service for donated blood) and upon informed consent in conformity with the declaration of Helsinki. We studied RBC units collected from 10 healthy donor volunteers [age 39.4 ± 7.5(mean ± S.D.)]. Units were stored either under standard conditions at 4° for up to 42 days (i) in presence of CDP-SAGM, or (ii) in CPD-SAGM with the addition of ascorbic acid (0.23 mM -SIGMA Aldrich, Milan, Italy) and N-acetyl cysteine (0.5 mM -SIGMA Aldrich, Milan, Italy). Sterility was assessed throughout the whole storage period.

Samples were removed aseptically for the analysis on a weekly basis. Samples for metabolomics analyses were collected at 0, 7, 21, 28 and 42 days of storage.

Determination of haemolysis, intracellular pH and malondialdehyde

Hemolysis was calculated following the method by Harboe [Harboe, 1959]. Samples were diluted in distilled water and incubated at room temperature for 30 min to lyse red blood cells. Samples from lysed RBCs were diluted 1⁄300 while supernatants were diluted 1 ⁄ 10 in distilled water. After stabilizing during 30 min and vortex mixing (Titramax 100, Heidolph Elektro, Kelheim, Germany), the absorbance of the hemoglobin was measured at 380, 415 and 450 nm (PowerWave 200 Spectrophotometer, Bio-Tek Instruments, Winooski, Vermont, USA). The mean blank was subtracted and the corrected OD (OD*) was calculated as follows: $2 \times OD_{415} - OD_{380} - OD_{450}$.

Red cell pellets obtained by centrifuging 600 µl of suspension in a nylon tube at 30,000×g for 10 min, were frozen, thawed during 5 min and then refrozen. To prevent an acid shift observed when samples are kept unfrozen, triplicate measurements of pH were made immediately after a second thawing of each lysate with a Radiometer pH glass capillary electrode maintained at 20°C and linked to a Radiometer PHM acid-base analyzer.

Malondialdehyde (MDA) levels were estimated in RBCs following the Stocks and Dormandy's method with some modifications [Stocks and Dormandy, 1971]. Briefly, 0.2 mL of RBCs was suspended in 3.0 mL of Krebs's Ringer phosphate buffer solution (pH 7.4), and 1 mL of the cell suspension was treated with 1 mL of 10% trichloroacetic acid and centrifuged at 1000 x g for 5 minutes. One milliliter of supernatant was then mixed with 1 mL of 0.67% thiobarbituric acid and heated over a water bath for 20 minutes at 85 to 90°C. The solution was cooled and read against a complementary blank at 532 nm (optical density [OD]1) and 600 nm (OD2). A blank was prepared separately without RBCs. The net OD was calculated after subtracting absorbance at OD2 from that at OD1. The MDA level was determined from the standard plot and expressed as nmol/mL RBCs.

Metabolite extraction

Metabolite extractions and metabolomics analyses were performed as previously reported [D'Alessandro et al., 2011]. For each sample, 0.5mL from the pooled erythrocyte stock was transferred into a microcentrifuge tube (Eppendorf ® Germany). Erythrocyte samples were then centrifuged at 1000g for 2 minutes at 4°C. Tubes were then placed on ice while supernatants were carefully aspirated, paying attention not to remove any erythrocyte at the interface. Samples were extracted following the protocol by D'Alessandro et al. [D'Alessandro et al., 2011]. The erythrocytes were resuspended in 0.15 mL of ice cold

ultra-pure water (18 MΩ) to lyse cell, then the tubes were plunged into a water bath at 37°C for 0.5 min. Samples were mixed with 0.6 mL of -20°C methanol and then with 0.45 mL chloroform. Subsequently, 0.15ml of ice cold ultra-pure water were added to each tube and they were transferred to -20°C freezer for 2-8 h. An equivalent volume of acetonitrile was added to the tube and transferred to refrigerator (4°C) for 20 min. Samples with precipitated proteins were thus centrifuged for 10000 x g for 10 min at 4 °C .

Finally, samples were dried in a rotational vacuum concentrator (RVC 2-18 - Christ Gmbh; Osterode am Harz, Germany) and re-suspended in 200 µl of water, 5% formic acid and transferred to glass auto-sampler vials for LC/MS analysis.

Untargeted Metabolomics analyses

An Ultimate 3000 Rapid Resolution HPLC system (LC Packings, DIONEX, Sunnyvale, USA) was used to perform metabolite separation. The system featured a binary pump and vacuum degasser, well-plate autosampler with a six-port micro-switching valve, a thermostated column compartment. Samples were loaded onto a Reprosil C18 column (2.0mm×150mm, 2.5 µm - Dr Maisch, Germany) for metabolite separation.

Chromatographic separations were achieved at a column temperature of 30°C; and flow rate of 0.2 mL/min. For downstream negative ion mode (-) MS analyses, A 0–100% linear gradient of solvent A (10mM tributylamine aqueous solution adjusted with 15mM acetic acid, pH 4.95) to B (methanol mixed with 10 mM TBA and with 15 mM acetic acid, pH 4.95) was employed over 30 min, returning to 100% A in 2 minutes and a 6-min post-time solvent A hold. For downstream positive ion mode (+) MS analyses, a 0–100% linear gradient of solvent A (ddH_2O, 0.1% formic acid) to B (acetonitrile, 0.1% formic acid) was employed over 30 min, returning to 100% A in 2 minutes and a 6-min post-time solvent A hold.

Due to the use of linear ion counting for direct comparisons against naturally expected isotopic ratios, time-of-flight instruments are most often the best choice for molecular formula determination. Thus, mass spectrometry analysis was carried out on an electrospray hybrid quadrupole time-of flight mass spectrometer MicroTOF-Q (Bruker-Daltonik, Bremen, Germany) equipped with an ESI-ion source. Mass spectra for metabolite extracted samples were acquired both in positive and in negative ion mode. ESI capillary voltage was set at 4500V (+) (-) ion mode. The liquid nebulizer was set to 27 psi and the nitrogen drying gas was set to a flow rate of 6 L/min. Dry gas temperature was maintained at 200°C. Data were stored in centroid mode. Data were acquired with a stored mass range of m/z 50–1200.

Automatic isolation and fragmentation (AutoMS^n mode) was performed on the 4 most intense ions simultaneously throughout the whole scanning period (30 min per run).

Calibration of the mass analyzer is essential in order to maintain an high level of mass accuracy. Instrument calibration was performed externally every day with a sodium formate solution consisting of 10 mM sodium hydroxide in 50% isopropanol: water, 0.1 % formic acid. Automated internal mass scale calibration was performed through direct automated injection of the calibration solution at the beginning and at the end of each run by a 6-port divert-valve.

Data elaboration and statistical analysis

In order to reduce the number of possible hits in molecular formula generation, we exploited the SmartFormula3D software (MAVEN, Princeton, USA), which directly calculates molecular formulae based upon the MS spectrum (isotopic patterns) and transition fingerprints (fragmentation patterns). This software generates a confidence-based list of chemical formulae on the basis of the precursor ions and all fragment ions, and the significance of their deviations to the predicted intact mass and fragmentation pattern (within a predefined window range of 5 ppm). Triplicate runs for each one of the 10 biological replicates over storage duration were exported as mzXML files and processed through MAVEN data analysis software MAVEN [Melamud and Vastag, 2010]. Mass spectrometry chromatograms were elaborated for peak alignment, matching and comparison of parent and fragment ions, and tentative metabolite identification (within a 20 ppm mass-deviation range between observed and expected results against the internal database – KEGG database) [Kanehisa and Goto, 2000]. MAVEN is an open-source software that could be freely downloaded from their websites (http://metlin.scripps.edu/download/ and http://genomics-pubs.princeton.edu/mzroll/index.php?show=download). Metabolite assignment was further elaborated in the light of the hydrophobicity/hydrophilicity of the compound and its relative retention time in the RP-HPLC run (as gleaned through database information and, for a subset of metabolites). Relative quantitative variations of intact mass peak areas for each metabolite assigned through MS/MS were determined against day 0 controls and only statistically significant results were considered (ANOVA *p-values* < 0.01). Data were further refined and plotted as fold change variation against the respective day 0 control with GraphPad Prism 5.0 (GraphPad Software Inc.).

Acetonitrile, formic acid, and HPLC-grade water, purchased from Sigma Aldrich (Milano, Italy). Standards (equal or greater than 98% chemical purity) ATP, L-lactic acid,

phosphogluconic acid, NADH, D-fructose 1,6-biphosphate, D-fructose 6-phosphate, glyceraldehydes phosphate, phosphoenolpyruvic acid, L-malic acid, L-glutamic acid, oxidized glutathione, a-ketoglutarate were purchased from Sigma Aldrich (Milan).

Scanning Electron Microscopy (SEM)

SEM studies of RBC were performed at day 0, 28 and 42 for control and (vitamin C + NAC) supplemented erythrocyte concentrates by means of an JEOL JSM 5200 electron microscope. Blood samples were fixed in phosphate-buffered (pH 7.2–7.4) 2.5% glutaraldehyde for 1 h, washed two times in 0.1 M phosphate buffer (pH 7.2–7.4), and mounted on poly-L-lysine-coated glass slides. The glass slides were kept in a moist atmosphere for 1 h, washed in phosphate buffer, postfixed in 1% osmium tetroxide for 1 h, rinsed in distillated water, and dehydrated in graded ethanol (50–70–90–100%). After critical-point drying with liquid CO_2 in a vacuum apparatus and covering with a gold-palladium layer, the samples underwent scanning electron microscopic analysis. SEM image panels were assembled with Photoshop CS 5.1 (Adobe 18 Systems–Mountain View, CA, USA).

The percentages of discocytes, echinocytes, spheroechinocytes, stomatocytes, spherostomatocytes, and spherocytes were evaluated by counting 1000 to 1500 cells in randomly chosen fields. Classification was indeed performed as previously reported [D'Alessandro et al., 2012; Blasi et al., 2012], since RBCs manifesting echinocyte and stomatocyte shapes are capable of returning to the discocyte shape under certain conditions. Thus, these RBC shape changes are considered potentially reversible transformations. In contrast, RBCs assuming spheroechinocyte, spherostomatocyte, spherocyte, ovalocyte, and degenerated shapes are irreversibly changed cells.

2.2.2 Results and discussion

The addition of ascorbic acid and NAC influenced pH by demodulating glycolysis

The addition of ascorbic acid and N-acetylcysteine (NAC) did not provoke major fluctuation of additive solution (CPD-SAGM) pH, which was decreased by 0.2 immediately upon addition, but did not show any major deviation from the control upon introduction of packed RBCs (**Figure 17.A-B**). In particular, pH (both internal – **Figure 17.A** and external – **Figure 17.B**) were consistently higher (especially the latter) throughout the whole storage duration,

while the former showed higher levels than control counterparts starting from storage day 21 onwards.

The supplementation of vitamin C and NAC had measurable positive effects on haemolysis (**Figure 17.C**), especially within storage day 28 and, in particular, in between storage day 0 and 21.

Malondialdehyde showed a progressive increment both in control and supplemented erythrocyte concentrates, although control units showed constantly higher levels than the supplemented counterparts (**Figure 17.D**).

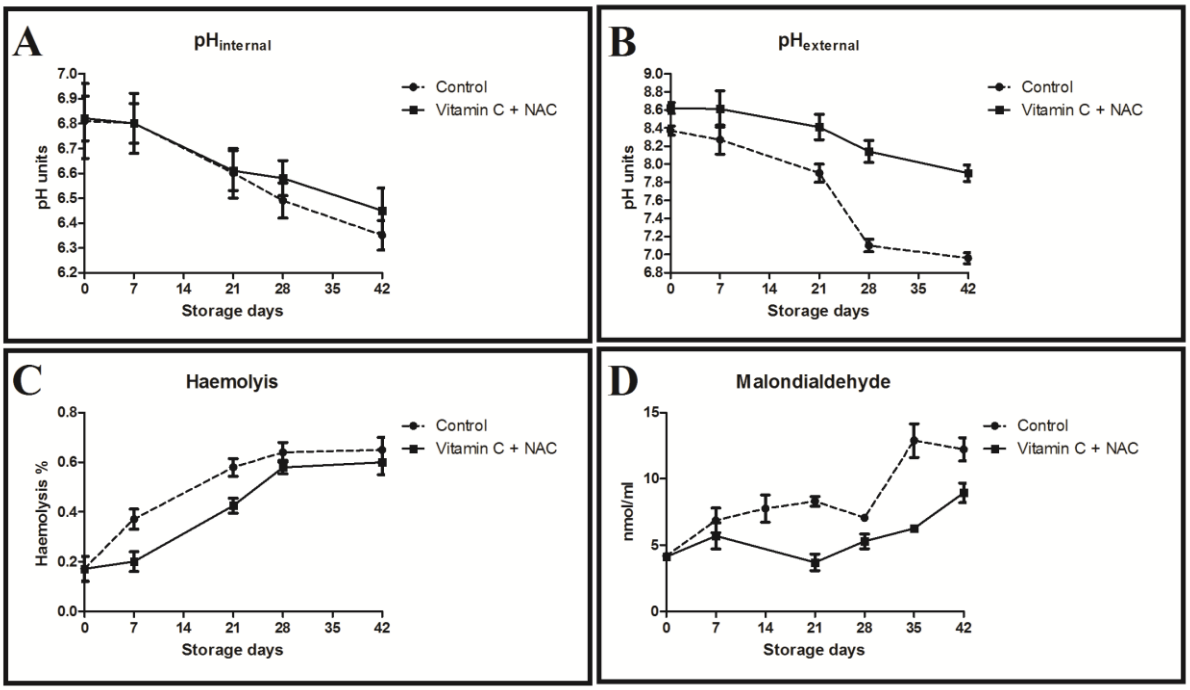

Figure 17. A time course overview of internal pH, external pH, haemolysis and malondialdehyde accumulation for control (gaped line) and vitamin C + NAC-supplemented (continuous line) CPD-SAGM erythrocyte concentrates stored at 4°C for up to 42 days.

Upon three hours from the supplementation of vitamin C and NAC (day 0), we could observe the intracellular accumulation of NAC (1.5 $\pm$ 0.04 fold-change variation against controls), ascorbate (1.67 $\pm$ 0.24), dehydroascorbate (35.00 $\pm$ 2.14), GSH (2.24 $\pm$ 0.41) and α-tocopherol (205.48 $\pm$ 4.73), apparently unaltered levels of oxidized glutathione (GSSG - 1.02 $\pm$ 0.09), while intracellular glucose levels were apparently decreased (0.62 $\pm$ 0.11), as reported in **Figure 18**. The decreased levels of glucose are consistent with the documented

competition between ascorbate and D-glucose for GLUT transporters for membrane transport (internalization) in human RBCs [May, 1998]. Immediate benefits on the levels of GSH and α-tocopherol were expected as well, on the basis of the NAC-promoted biosynthesis of the former [Mazor et al., 1996], and the antioxidant and protective action of ascorbic acid on the latter [May ey al., 1998]. Slower internalization of glucose in supplemented erythrocyte concentrates (**Figure 18**) might also justify the influence on the slope of the pH decrease curves (**Figure 17.A-B**), as described above. Indeed, a slower glycolytic rate might result in lower lactate accumulation and reduced pH decrease. In order to underpin this hypothesis, MS-based metabolomics analyses were performed to assay metabolic fluxes for glucose consumption.

HPLC-MS runs were performed in triplicate on samples extracted from each donated unit at 0, 7, 21, 28, and 42 days of storage. In order to report the main results in a more readable layout, metabolites accounting for the most relevant catabolic pathways in RBCs were grouped and plotted as fold-change variation of time course measurements in each group, normalized against day 0 controls (in this view, it is worthwhile stressing that the day 0 levels of specific metabolites already differed upon 3 hours from supplementation, as also reported in **Figure 18** for a subset of redox poise-related metabolites).

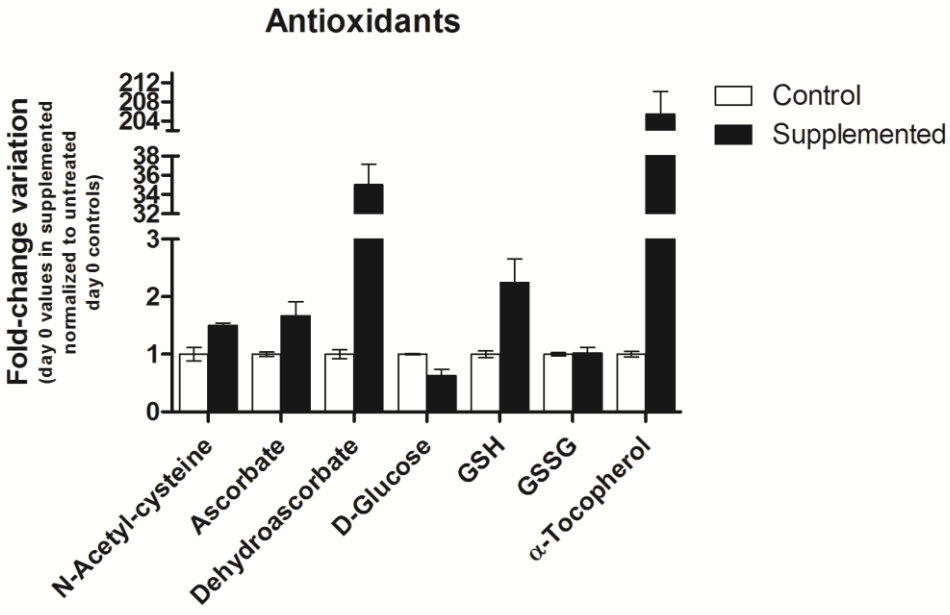

Figure 18. An overview of relative quantities for a subset of metabolites involved in redox metabolism poise at day 0, after three hours from supplementation with vitamin C and NAC. Results are plotted as fold-change variations (mean ± SD) against untreated controls.

The analysed pathways could be enlisted as follows: (i) glycolysis (**Figure 19**), (ii) PPP (**Figure 20**), (iii) glutathione homeostasis (**Figure 21**); (iv) lipid peroxidation (**Figure 22**), (v) purine metabolism (**Figure 23**).

In **Figure 19**, we report how glycolytic intermediates, including glucose 6-phosphate (G6P), fructose 6-phosphate (F6P), glyceraldehyde 3-phosphate (G3P), pyruvate, and byproducts of lactic fermentation (lactate), consistently decreased upon supplementation of vitamin C and NAC. On the other hand, DPG levels followed a peculiar trend, with a rapid decrease in supplemented units within the first week of storage, while day 21 levels in supplemented units were higher than in controls (**Figure 19)**, suggesting a long-term positive effect of NAC-vitamin C supplementation to RBCs, in agreement with previous studies on ascorbate [Dawson et al., 1980a; Dawson et al., 1980b; Dawson et al., 1981].

Higher levels of NADH in vitamin C + NAC-supplemented erythrocyte concentrates might be explained in the light of two considerations: (i) a reduced glycolytic rate and slower lactate production rate is accompanied by a slower oxidation rate of NADH back to NAD^+; (ii) NADH is also an essential cofactor for the cytochrome b5 reductase – methemoglobin reductase, which is responsible for the reduction of oxidized iron in methemoglobin back to ferrous state. Therefore, higher NADH levels might represent an indirect proof of a lower necessity of RBCs to cope with hemoglobin oxidation in vitamin C + NAC-supplemented units.

ATP higher levels in supplemented units are consistent with the positive effect on ATP preservation observed during whole blood storage in presence of ascorbic acid [Zan et a. 2005], and with early blood preservation studies on the effects of ascorbic acid and dehydroascorbate [Dawson et al., 1980a; Dawson et al., 1980b; Dawson et al., 1981].

A tentative explanation to this phenomenon is tied to the relative concentrations of cyclic AMP (cAMP – **Figure 19**), which constantly increases in control RBCs (and deoxygenated units, as we observed in our recent study) [D'Alessandro et al., 2013] over storage duration, while it remains constant and slowly decreases in vitamin C-NAC supplemented units.

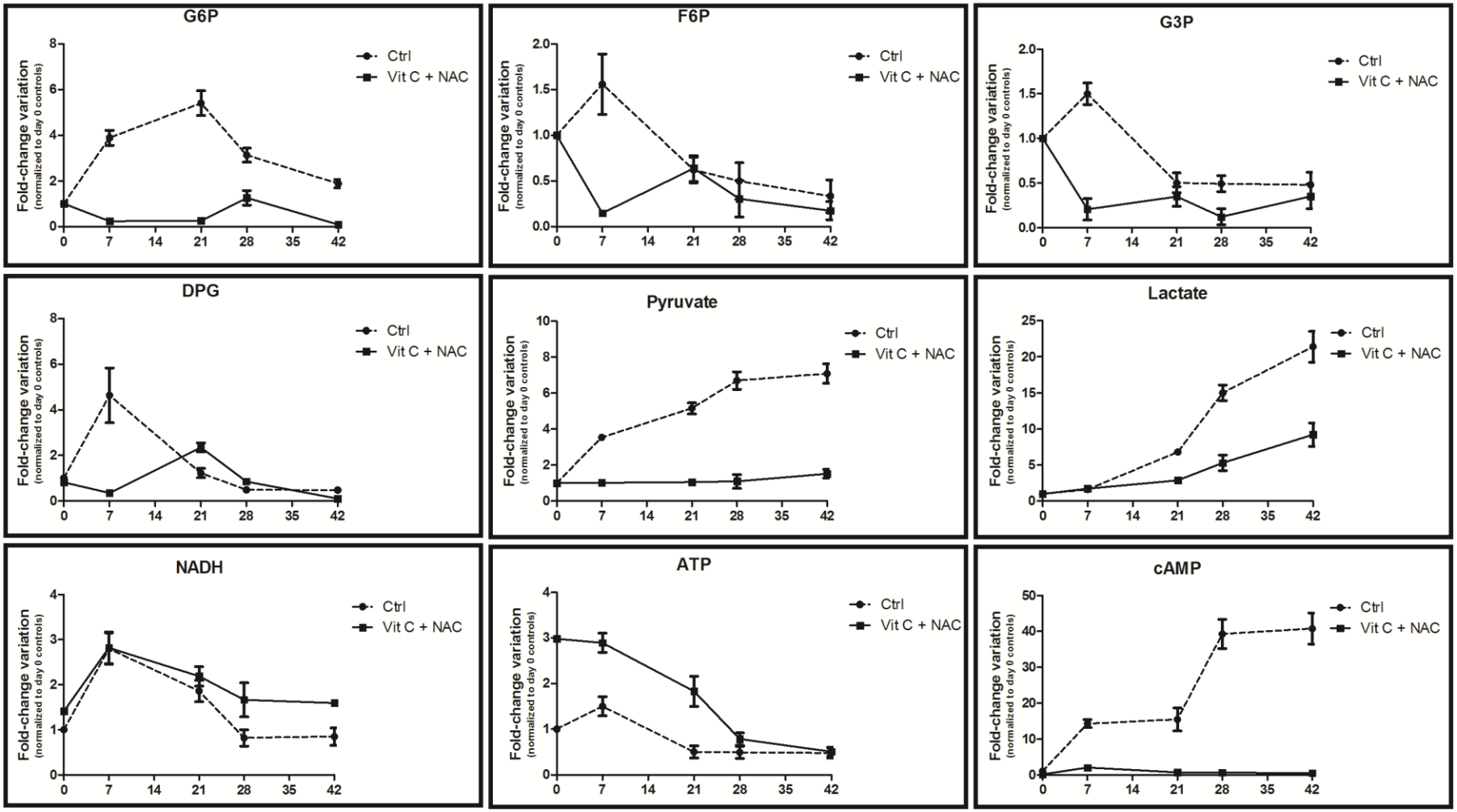

Figure 19. Time course metabolomic analysis of glycolysis in RBCs stored under control conditions (gaped line) or in CPD-SAGM supplemented with vitamin C and NAC (continuous line) at 4°C for up to 42 days. Results are plotted on a weekly basis (storage day 0, 7, 21, 28 and 42), as fold-change variations (means ± SD) upon normalization against day 0 controls.

Abbreviations: G6P: glucose 6-phosphate; F6P: fructose 6-phosphate; G3P: glyceraldehyde 3-phosphate; DPG: diphosphoglycerate; cAMP: cyclic AMP.

Indeed, while it has been reported that long term anaerobiosis promoted glycolytic metabolism in RBCs and prolonging the conservation of high energy phosphate reservoirs and purine homeostasis [Yoshida et al., 2007], it is nonetheless true that ATP decreases (though slowly than in "oxygenated" controls) despite glycolysis being sustained throughout the whole anaerobic storage duration (glycolytic intermediates and lactate accumulate constantly until storage day 42) [D'Alessandro et al., 2013]. In our previous research, we could thus hypothesized that progressive decrease of high energy phosphate compounds in deoxygenated units might not only reflect ATP and DPG sequestering by deoxy-Hb, which should occur early upon deoxygenation, but it might rather reflect cAMP-mediated ATP release by RBCs in response to deoxygenation [D'Alessandro et al., 2013], a phenomenon that in vivo occurs to promote vasodilation in hypoxic districts [Sprague et al., 2001]. Therefore, in the present study, slower glycolytic rates albeit higher ATP and DPG levels might be likely explained by the lower cAMP levels in supplemented units (**Figure 19**), in comparison to complemented counterparts, which would in turn decrease cAMP-mediated ATP release from RBCs.

The observed decrease in cAMP levels is also relevant in the light of the role of this molecule in modulating second messenger cascades, such as the activation of cAMP-dependent kinases, which in turn affect regulation and post-translational modifications (i.e. phosphorylations) of erythrocyte membrane and membrane-skeletal proteins [Cohen and Gascard, 1992].

Glycolytic fluxes were not redirected towards the pentose phosphate pathway

On the basis of the aforementioned evidences, we wondered whether the observed lower levels of lactate were to be attributed to a slower rate of glucose consumption via the Embden-Meyerhof pathway or they rather hid a metabolic divertion toward the PPP, a pathway devoted to RBC protection from oxidative stress [Fico et al., 2004], in likewise fashion to control RBCs upon the second week of storage, as previously reported [Gevi et al., 2012; D'Alessandro et al., 2012].

In **Figure 20** we report the result for flux analyses of RBCs PPP intermediate metabolites, including 6-phosphogluconolactone, 6-phosphogluconate, erythrose 4-phosphate (E4P), ribulose 5-phosphate (RU5P), sedueptulose 7-phosphate and the byproduct NADPH. For all the tested metabolites we could observe lower relative levels of each compound in comparison to untreated controls, except for sedueptulose 7-phosphate and NADPH, where the levels were similar to untreated counterparts.

For NADPH, in particular, we could observe a 4-fold increase after 7 days of storage in supplemented units, while later on the detected levels were similar to those detected in

untreated counterparts. Since NADPH is an essential coenzyme in antioxidant reactions, including GSSG reduction to GSH, the observed result could be due to a reduced consumption of NADPH, promoted by decreased oxidative stress levels in supplemented units (also confirmed by lower accumulation of malondialdehyde – **Figure 20.D**), rather than to an actual increased production of this metabolite.

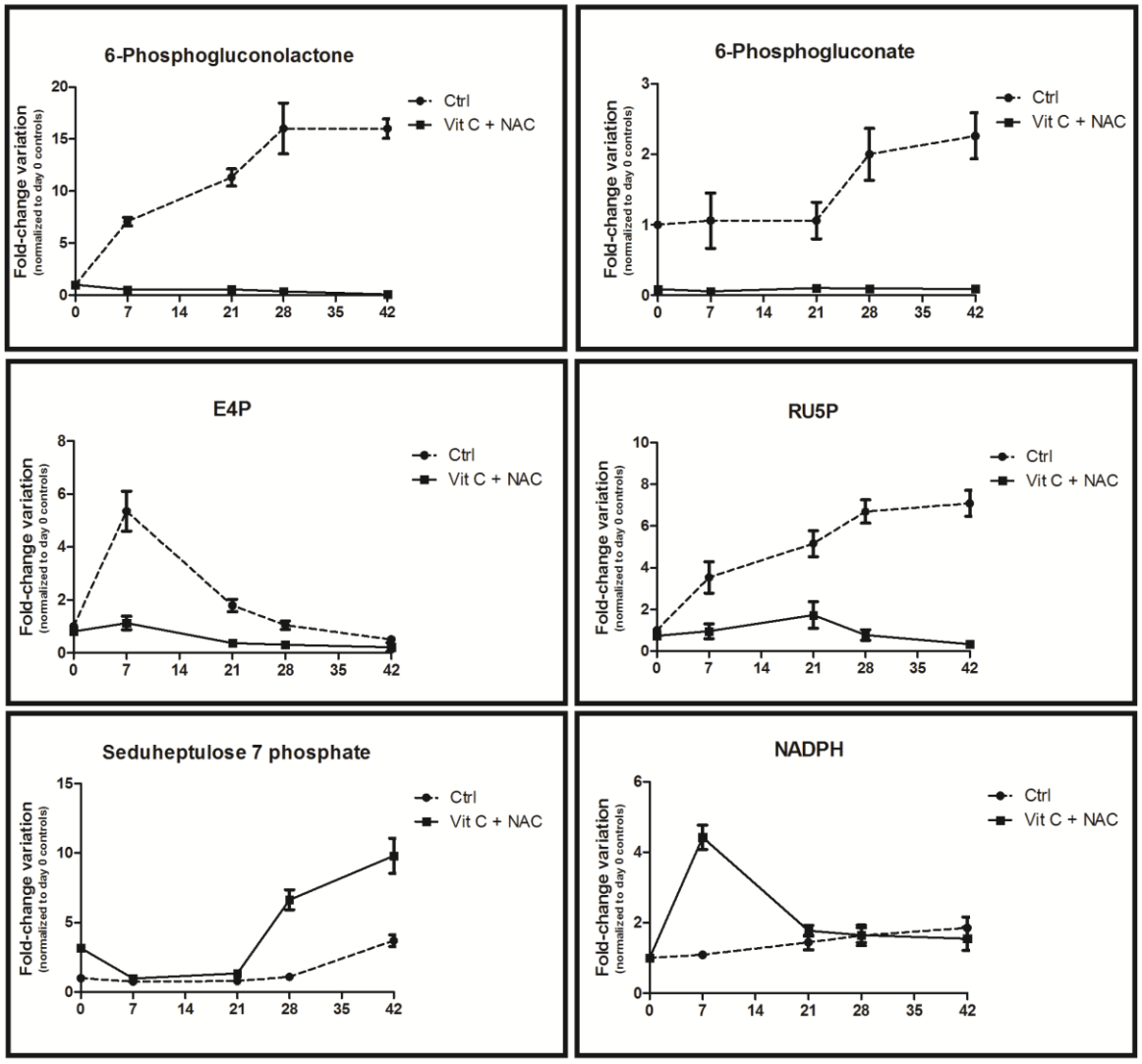

Figure 20. Time course metabolomic analysis of the pentose phosphate pathway in RBCs stored under control conditions (gaped line) or in CPD-SAGM supplemented with vitamin C and NAC (continuous line) at 4°C for up to 42 days. Results are plotted on a weekly basis (storage day 0, 7, 21, 28 and 42), as fold-change variations (means ± SD) upon normalization against day 0 controls.
Abbreviations: E4P: erythrose 4-phosphate; RU5P: ribulose 5-phosphate.

Increased relative levels of sedueptulose 7-phosphate in vitamin C + NAC supplemented units might result from a regular carbon flux from the oxidative to the non-oxidative phase of the PPP, that results in metabolic fluxes re-entering glycolysis, while in control RBCs prolonged storage results in the progressive flux towards the purine salvage pathway (PSP), as previously reported [Gevi et al., 2012].

Additives promoted anti-oxidant responses related to the glutathione system and homeostasis

Vitamin C and NAC were carefully selected for their expected potential benefits on the anti-oxidant defense systems, including glutathione homeostasis [Dawson et al., 1980a; Dawson et al., 1980b; Dawson et al., 1981; Mazor et al., 1996; Dumaswala et al., 2000; Nur et al., 2012].

In **Figure 21** we report the results for the main metabolites involved in the maintenance of glutathione homeostasis and biosynthesis [Lu, 2009], including GSH, GSSG, glutamic acid, γ-glutamyl cysteine, acetyl-cysteine, cysteine, cysteine-glycine, methionine, ascorbate and dehydroascorbate.

First of all, it is worthwhile to recall that day 0 levels of GSH, acetyl-cysteine, ascorbate and dehydroascorbate were different between controls and supplemented units (**Figure 21**). Also, it should be considered that results in **Figure 21** are plotted as fold change variations against day 0 control values, which further stresses the significance of the observed trends towards increase (GSH, acetyl-cysteine, ascorbate) and decrease (dehydroascorbate – the oxidized form of ascorbic acid) of the graphed metabolites in supplemented units. Furthermore, cysteine (one key aminoacid precursor of the tripeptide GSH) and thiol metabolism was up-regulated (cysteine, cysteine-glycine, methionine) in supplemented units (**Figure 21**). These results are indicative that vitamin C and NAC supplementation are more effective than anaerobic storage in protecting RBCs from oxidative stress. Indeed, while anaerobiosis results in deoxy-hemoglobin-dependent blockade of metabolic divertion towards the PPP [D'Alessandro et al., 2013; Rogers et al., 2009], it also impairs RBC capacity to cope with oxidative stress by negatively affecting glutathione homeostasis [D'Alessandro et al., 2013], which is instead boosted by vitamin C and NAC supplementation, as hereby observed (**Figure 21**).

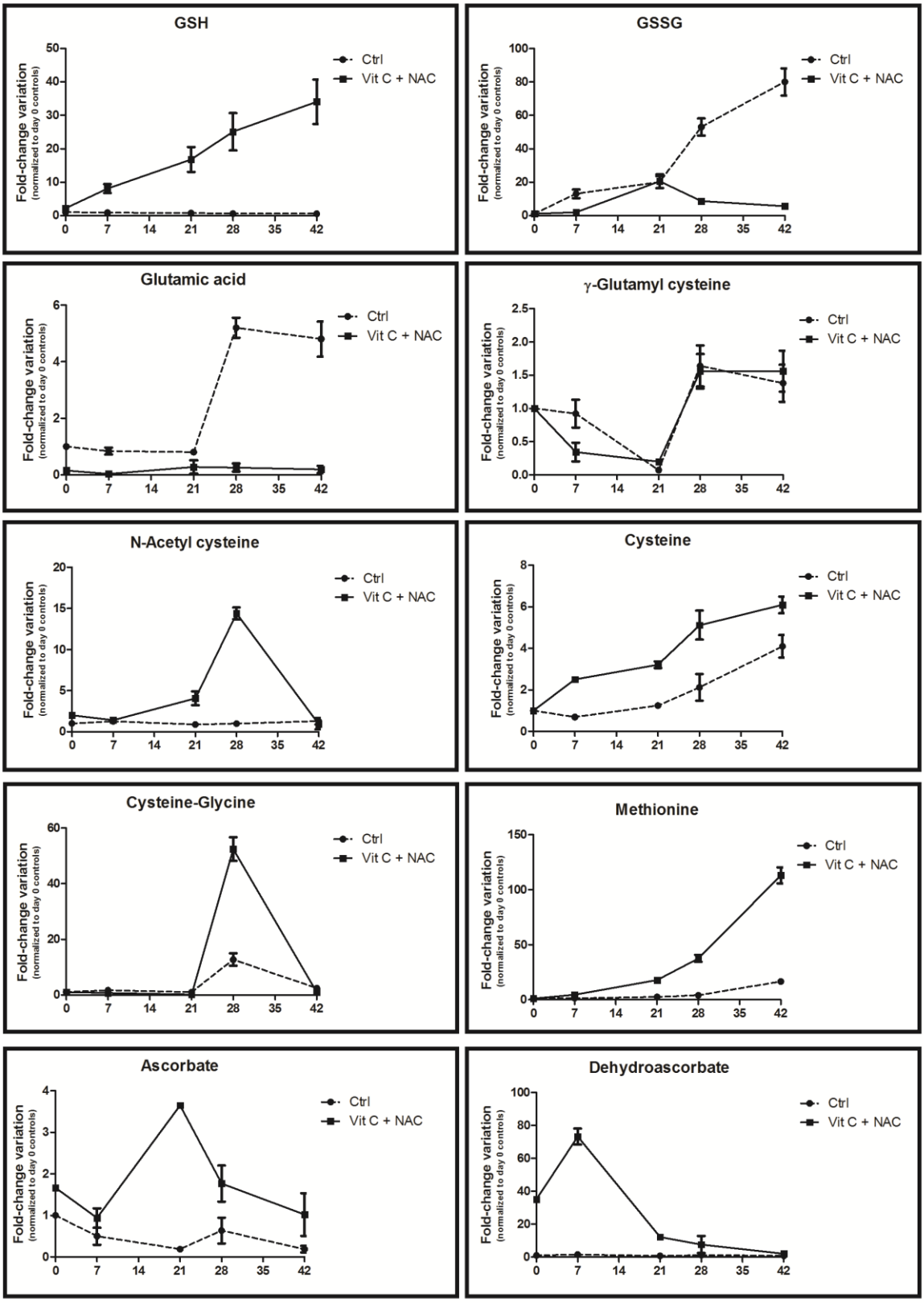

Figure 21. Time course metabolomic analysis of glutathione homeostasis-related metabolites in RBCs stored under control conditions (gaped line) or in CPD-SAGM supplemented with vitamin C and NAC (continuous line) at 4°C for up to 42 days. Results are plotted on a weekly basis (storage day 0, 7, 21, 28 and 42), as fold-change variations (means ± SD) upon normalization against day 0 controls.
Abbreviations: GSH: reduced glutathione; GSSG: oxidized glutathione.

It should be also noted that preservation of thiol groups by improved glutathione homeostasis should also affect the activity of several key metabolic enzymes that rely upon thiol groups in functional active sites, such as glyceraldehyde 3-phosphate dehydrogenase (glycolysis) [Li et al., 1991] and peroxiredoxin 2 (antioxidant defenses) [Rinalducci et al., 2011], the latter becoming oxidized and progressively migrating to the membrane over storage duration under blood bank conditions [D'Alessandro et al., 2012; Rinalducci et al., 2011].

The beneficial effects of vitamin C + NAC supplementation are evident at the glutathione homeostasis level, but also when focusing on lipid oxidation. In the light of malondialdehyde decrease in supplemented units (**Figure 17.D**), we further focused on prostaglandin metabolism (**Figure 22**), in particular on prostaglandin B1, D1, F1α and F2α (8-isoprostane). The latter metabolite, in particular, is a widely accepted marker of lipid peroxidation [Tsikas et al., 2012], and has been demonstrated to accumulate (especially in the supernatant) over storage duration [Hess, 2010; D'Alessandro et al., 2010; Lion et al., 2010; Karon et al., 2012; Gevi et al., 2012]. Concordingly we the tested hypothesis, supplemented units displayed lower levels of prostaglandins throughout the whole 42 days tested time span.

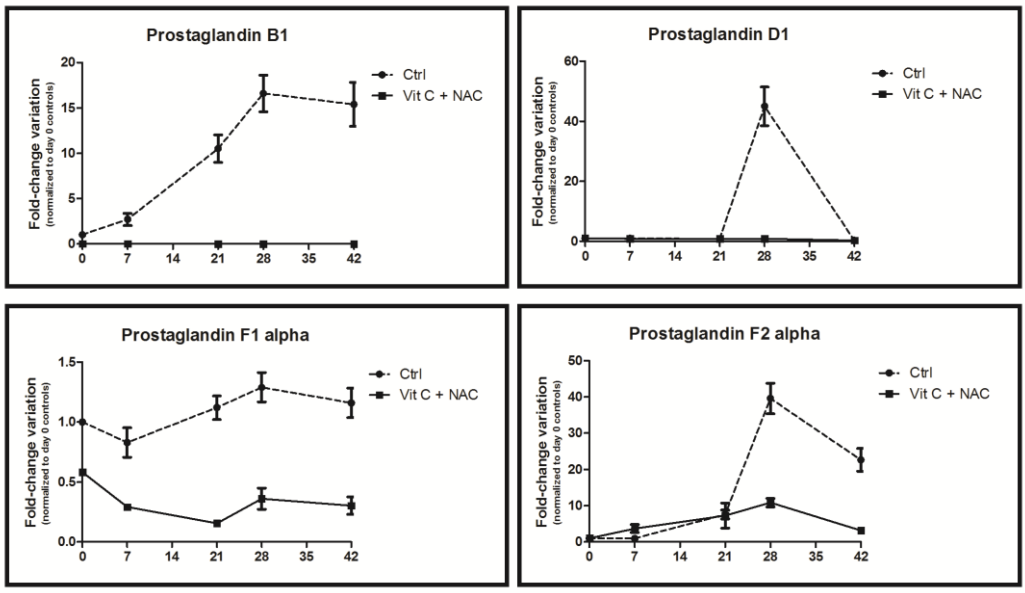

Figure 22. Time course metabolomic analysis of prostaglandins in RBCs stored under control conditions (gaped line) or in CPD-SAGM supplemented with vitamin C and NAC (continuous line) at 4°C for up to 42 days. Results are plotted on a weekly basis (storage day 0, 7, 21, 28 and 42), as fold-change variations (means ± SD) upon normalization against day 0 controls.

Supplementation of vitamin C and NAC promoted the purine salvage pathway (in analogy to untreated controls)

RBCs cannot *de novo* synthesize 5-phosphoribosylamine and thus rely upon salvage reactions to replenish purine reservoirs which serve as substrates for high energy phosphate purine compounds (such as ATP and adenine nucleotides, accounting for 70-80% of cellular nucleotides) [Schuster and Kenanov, 2005]. Erythrocyte membranes allow adenine and adenosine transport via facilitated diffusion, which allowed introducing adenine in additive solutions (such as in SAGM) without any major technical caveat [Zolla et al., 1977].

In like fashion to standard [Gevi et al., 2012] and anaerobic [D'Alessandro et al., 2013] storage, storage of vitamin C and NAC supplemented RBCs resulted in the progressive accumulation of both adenine and adenosine (although the accumulation rate of the latter was, from day 21 onwards, lower than in untreated controls – **Figure 23**).

Inosine, a major substrates for salvage reactions [Zolla et al., 1977], increased significantly over storage duration (**Figure 23**), in analogy to standard [D'Alessandro et al., 2012] and anaerobic storage [D'Alessandro et al., 2013]. Inosine accumulation might stem from deamination of adenosine, a documented process within the framework of RBC storage [Hess, 2010]. Inosine has attracted a great deal of attention in the field of blood preservation, since it may further undergo phosphorolysis to form hypoxanthine (increasing both in controls and supplemented units – **Figure 23**) and ribose 1-phosphate (R1P), a reaction that enables the introduction of a phosphorylated sugar (through non-oxidative phase PPP intermediates) into the RBC without ATP consumption.

ADP levels were higher in supplemented units in comparison to untreated controls (**Figure 23**), almost paralleling relative quantitative trends observed for ATP.

While inosine monophosphate (IMP) accumulation has been reported for standard [Gevi et al., 2012; Strauss and de Verdier, 1980] and deoxygenated [D'Alessandro et al., 2013] erythrocyte concentrates over storage duration, vitamin C and NAC supplementation resulted in higher than controls levels until storage day 21, while they decreased back to control levels by storage day 28 and 42 (**Figure 23**). However, it is worthwhile to stress that optimum biopreservation strategies of RBCs should pursue the conservation of control like levels of IMP [Sidi et al., 1989], as we could observe hereby (control like levels of IMP were detected at the end of the shelf-life – **Figure 23**).

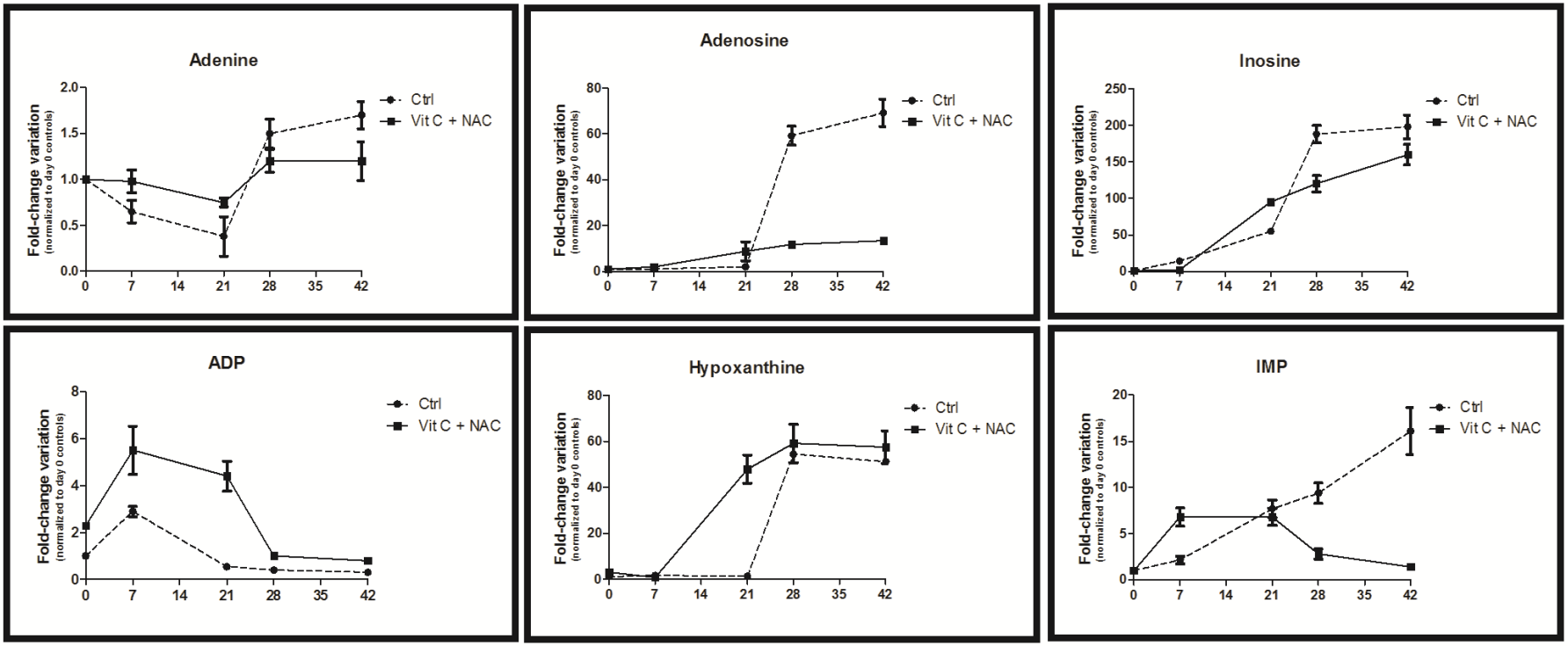

Figure 23. Time course metabolomic analysis of the purine metabolism in RBCs stored under control conditions (gaped line) or in CPD-SAGM supplemented with vitamin C and NAC (continuous line) at 4°C for up to 42 days. Results are plotted on a weekly basis (storage day 0, 7, 21, 28 and 42), as fold-change variations (means $\pm$ SD) upon normalization against day 0 controls.

Electron microscopy analyses evidenced substantial improvements about RBC morphology parameters only within the first 28 days of storage

Storage in the presence of vitamin C and NAC improved the morphology score within the first four weeks of storage (**Table 3**). However, supplementation of Vitamin C and NAC did not produce any significant improvement at the end of the storage period (**Table 3**). Indeed, at 42 days, the percentage of discocytes in supplemented units was not significantly higher than in untreated controls (24.2 $\pm$ 2.1 vs 21.8 $\pm$ 1.6% - **Table 3**), although the percentage of irreversibly altered RBCs (including spheroechinocytes, spherostomatocytes, spherocytes and degenerated shapes) was lower than controls (29.5% $\pm$ 3.6 vs 34.6 $\pm$ 3.2).

In **Figure 24,** we report a mosaic of SEM images, including control CPD-SAGM RBCs at day 0, 28 and 42 (**Figure 24.A, B** and **C**), and RBCs supplemented with vitamin C and NAC at day 0, 28 and 42 (**Figure 24.D, E** and **F**, respectively). While in supplemented units discocytes are still the majority at 28 days (51.8 $\pm$ 1.3 in **Table 3 - Figure 24.G**), unaltered discocytes represented a minoritarian percentage of the population and perfectly disc-shaped phenotypes are almost totally absent at the end of the storage period (**Figure 24.H**).

A direct comparison of these results against our recent short report on RBC morphology changes arising upon deoxygenation [Zolla and D'Alessandro, 2013] suggests that oxygen removal might preserve RBC morphology better than the hereby-discussed supplementation of anti-oxidants.

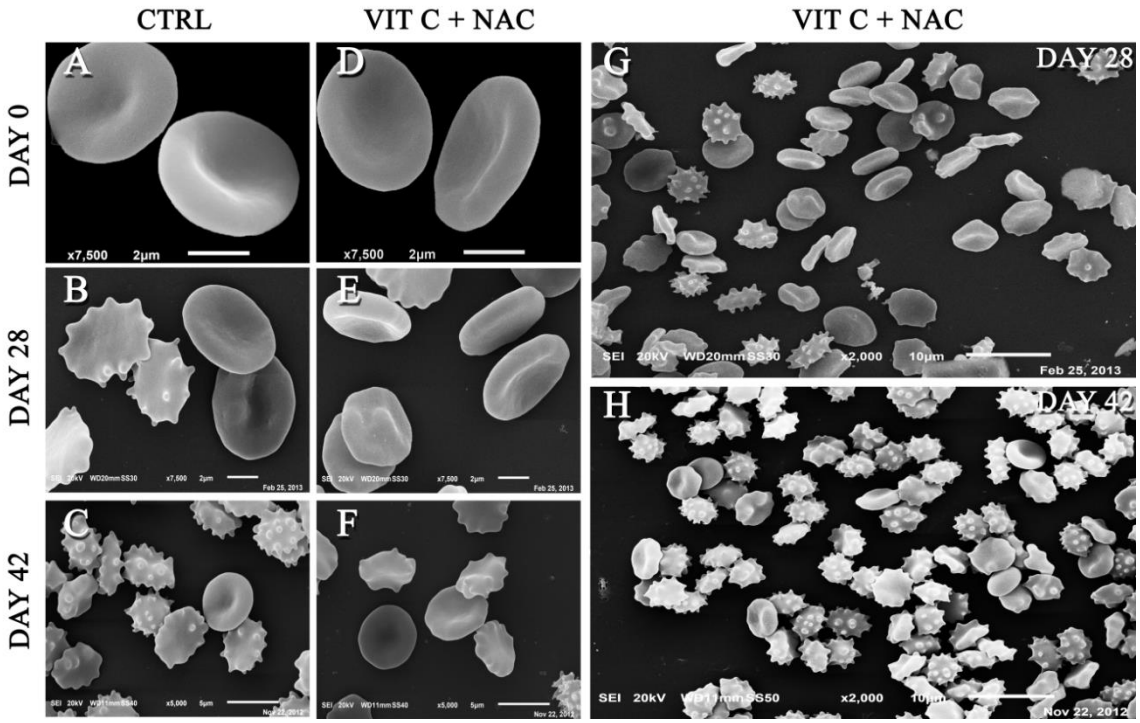

Figure 24. Scanning electron micrograph of control red blood cells (day 0 – **A**; day 28 – **B**; day 42 - **C**), and vitamin C + NAC-supplemented red blood cells (day 0 – **D**; day 28 – **E**; day 42 - **F**). In **E** and **F**, a x2,000 magnification of 28 and 42 days vitamin C + NAC-supplemented red blood cells, respectively. Scale bars and magnification values are reported in each panel. Panels were assembled with Photoshop CS 5.1 (Adobe Systems, Mountain View, CA, USA).

Table 3 – SEM erythrocyte shape classification

Storage Day	**Discocyte (%)**	**Reversibly* changed RBC (%)** **(echinocyte and stomatocyte shape)**	**Irreversibly* changed RBC (%)** **(spheroechinocyte, spherostomatocyte, spherocyte, ovalocyte, and degenerated shapes)**
0	77.3 ± 2.9	18.4 ± 4.6	4.3 ± 3.1
28 Control	46.1 ± 3.8	36.2 ± 1.4	17.7 ± 2.6
28 Vit C + NAC	51.8 ± 1.3**	32.6 ± 2.9**	15.5 ± 1.8
42 Control	21.8 ± 1.6	43.6 ± 2.7	34.6 ± 3.2
42 Vit C + NAC	24.2 ± 2.1	46.3 ± 1.9	29.5 ± 3.6

* Reversible and irreversible changes were classified based on classification criteria, as previously reported [Blasi et al., 2012]

** Statistically significant (*p-value* < 0.05 ANOVA in comparison to untreated controls at the same storage time point)

2.2.3 Conclusion

Recent strides in the field of MS-based metabolomics have prompted a thorough update and integration to decades of accurate biochemical observations with spectrophotometry and NMR. In particular, it is rapidly emerging a role for MS-based metabolomics in the fields of RBC research, transfusion medicine and clinical biochemistry [D'Alessandro et al., 2012b; Sparrow, 2012; Cluitmans et al., 2012].

In the present study, we could apply a validated HPLC-MS-metabolomics workflow to determine the effects of vitamin C and NAC supplementation (antioxidants) to CPD-SAGM erythrocyte concentrates stored under blood bank conditions.

As a result, we could observe decreased energy metabolism fluxes (glycolysis and PPP), depressed by the diminished uptake of glucose and increased internalization of ascorbate. On the other hand, anti-oxidant defenses were boosted, above all glutathione homeostasis, resulting in decreased haemolysis, lower accumulation of malondialdehyde and oxidation byproduct metabolites (including GSSG and prostaglandins).

However, replenishing the RBC antioxidant battery through vitamin C and NAC did not help preserving RBC morphology, as gleaned through SEM analyses, thus confirming a central role for energy metabolism, rather than oxidative stress, in the accumulation of the most evident RBC storage lesions (such as those targeting RBC phenotype).

Although metabolomics provides an exhaustive description of the biochemical scenario arising upon vitamin C and NAC supplementation, further clues will be soon collected through the application on this topic of other Omics disciplines, above all proteomics.

References

Bessis M. Red cell shapes. An illustrated classification and its rationale. Nouv. Rev. Fr. Hematol. (1972);12(6): 721–745.

Blasi B, D'Alessandro A, Ramundo N, Zolla L. Red blood cell storage and cell morphology. Transfus Med. (2012); 22(2):90-6.

Bosch FH, Were JM, Roerdinkholder-Stoelwinder B et al. Characteristics of red blood cell populations fractionated with a combination of counterflow centrifugation and Percoll separation. Blood (1992);79(1):254-260.

Cluitmans JC, Hardeman MR, Dinkla S, Brock R, Bosman GJ. Red blood cell deformability during storage: towards functional proteomics and metabolomics in the Blood Bank. Blood Transfus. 2012;10 Suppl 2:s12-8.

Cohen C. M., Gascard P. Regulation and post-translational modification of erythrocyte membrane and membrane-skeletal proteins. Semin. Hematol. (1992); 29:244–292.

Dawson RB, Dabezies M, Hershey RT, Myers CS, Miller RM. Blood preservation. XLIII. Studies on the ascorbate mechanisms of maintaining red cell 2,3-DPG. Transfusion. (1980)a;20(3):316-20.

Dawson RB, Hershey RT, Myers CS, Eaton JW. Blood preservation XLIV. 2,3-DPG maintenance by dehydroascorbate better than D-ascorbic acid. Transfusion. (1980)b;20(3):321-3.

Dawson RB, Hershey RT, Myers CS, Miller RM. Blood preservation 35. Red cell 2,3-DPG and ATP maintained by DHA-ascorbate-phosphate. Transfusion. (1981);21(2):219-23.

Dumaswala UJ, Wilson MJ, Wu YL, Wykle J, Zhuo L, Douglass LM, Daleke DL. Glutathione loading prevents free radical injury in red blood cells after storage. Free Radic Res. 2000 Nov;33(5):517-29.

D'Alessandro A, Liumbruno G, Grazzini G, Zolla L. Red blood cell storage: the story so far. Blood Transfus. 2010;8(2):82-8.

D'Alessandro A, Gevi F, Zolla L. A robust high resolution reversed-phase HPLC strategy to investigate various metabolic species in different biological models. Mol. Biosyst. (2011);7(4):1024–1032.

D'Alessandro A, D'Amici GM, Vaglio S et al. Time-course investigation of SAGM-stored leukocyte-filtered erythrocyte concentrates:from metabolism to proteomics. Haematologica (2012)a; 97(1):107-115.

D'Alessandro A, Giardina B, Gevi F, Timperio AM, Zolla L. Clinical metabolomics: the next stage of clinical biochemistry. Blood Transfus. (2012)b;10 Suppl 2:s19-24.

D'Alessandro A, Gevi F, Zolla L. Red blood cell metabolism under prolonged anaerobic storage. Molecular Biosystems 2013; 9(6):1196-209.

European Directorate for the Quality of Medicine & Heklathcare. Guide to the Preparation, Use and Quality Assurance of Blood Components. Reccomendation No.R (95) 15.16th edition. Council of Europe 2011, 2011

Farnum M, and Zukoski C. Effect of glycerol on the interactions and solubility of bovine pancreatic trypsin inhibitor. Biophys. J. (1999);76(5):2716–2726.

Fico A, Paglialunga F, Cigliano L, Abrescia P, Verde P, Martini G, Iaccarino I, Filosa S. Glucose-6-phosphate dehydrogenase plays a crucial role in protection from redox-stress-induced apoptosis. Cell Death Differ. 2004;11(8):823-31.

Gevi F, D'Alessandro A, Rinalducci S, Zolla L. Alterations of red blood cell metabolome during cold liquid storage of erythrocyte concentrates in CPD-SAGM. J Proteomics. 2012; 76:10-27.

Gyongyossy-Issa MI, Weiss SL, Sowemimo-Coker SO et al. Prestorage leukoreduction and lowtemperature filtration reduce hemolysis of stored red cell concentrates. Transfusion (2005); 45:90-96.

Harboe M. A method for determination of hemoglobin in plasma by near-ultraviolet spectrophotometry. Scand. J. Clin. Lab. Invest. (1959);11(1):66–70.

Henkelman S, Lagerberg JW, Graaf R et al. The effects of cryopreservation on red blood cell rheologic properties. Transfusion (2010);50(11):2393-2401.

Hess JR. Red cell changes during storage. Transfus Apher Sci. 2010;43(1):51-9.

Holovati JL, Wong KA, Webster JM, et al. The effects of cryopreservation on red blood cell microvesciculation, phosphatidylserine externalkization, and CD47 expression. Transfusion (2008);48:1658-1668.

Iordachescu M and Imai R. Trehalose biosynthesis in response to abiotic stresses. J. Integr. Plant Biol. (2008);50(10):1223–1229.

Kanehisa M and Goto S. KEGG: kyoto encyclopedia of genes and genomes. Nucleic Acids Res. 2000; 28(1):27-30.

Karon BS, Van Buskirk CM, Jaben EA, Hoyer JD, Thomas DD. Temporal sequence of major biochemical events during Blood Bank storage of packed red blood cells. Blood Transfus. 2012; 28:1-9.

Kofanova OA, Zemlyanskikh NG, Ivanova I, et al. Changes in the intracellular Ca^{2+} content in humanred blood cells in the presence of glycerol. Bioelectrochemistry (2008); 73(2):151-154.

Lagerberg JW, Truijens-de Lange R, de Korte D et al. Altered processing of thawed red cells to improve the in vitro quality during postthaw storage at 4 degrees C. Transfusion (2007);47:2242–2249.

Li YK, Boggaram J, Byers LD. Alkylation of glyceraldehyde-3-phosphate dehydrogenase with haloacetylphosphonates. An unusual pH-dependence. Biochem J. 1991;275 (Pt 3):767-73.

Lion N, Crettaz D, Rubin O, Tissot JD. Stored red blood cells: a changing universe waiting for its map(s). J Proteomics. 2010;73(3):374-85.

Lovelock JE. Het mechanism of the protective action of glycerol against hemolysis by freezing and thawing. Biochim. Biophys. Acta (1953);11:28–36.

Lu SC. Regulation of glutathione synthesis. Mol. Aspects. Med. 2009; 30:42-59.

May JM. Ascorbate function and metabolism in the human erythrocyte. Front Biosci. 1998;3:d1-10.

May JM, Qu ZC, Mendiratta S. Protection and recycling of alpha-tocopherol in human erythrocytes by intracellular ascorbic acid. Arch Biochem Biophys. 1998;349(2):281-9.

Mazor D, Golan E, Philip V, Katz M, Jafe A, Ben-Zvi Z, Meyerstein N. Red blood cell permeability to thiol compounds following oxidative stress. Eur J Haematol. 1996 Sep;57(3):241-6.

Melamud E and Vastag, JD. Rabinowitz. Metabolomic analysis and visualization engine for LC-MS data. Anal Chem. 2010;82(23):9818-9826.

Meryman HT, Hornblower M. A method for freezing and washing red blood cells using a high glycerol concentration. Transfusion (1972);12:145–156.

Nur E, Brandjes DP, Teerlink T, Otten HM, Oude Elferink RP, Muskiet F, Evers LM, ten Cate H, Biemond BJ, Duits AJ, Schnog JJ; CURAMA study group. N-acetylcysteine reduces oxidative stress in sickle cell patients. Ann Hematol. 2012;91(7):1097-105.

Pegg DE. Principles of cryopreservation. Methods Mol. Biol. (2007);368:39–57.

Pierpont ME, Judd DB, Tukey DP et al. Erythrocyte carnitine: a study of erythrocyte fractions isolated by discontinuous density gradient centrifugation. Biochem. Med. Metab. Biol. (1988):40(3):237-246.

Rinalducci S, D'Amici GM, Blasi B, Vaglio S, Grazzini G, Zolla L. Peroxiredoxin-2 as a candidate biomarker to test oxidative stress levels of stored red blood cells under blood bank conditions. Transfusion. 2011;51(7):1439-49.

Rogers SC, Said A, Corcuera D, McLaughlin D, Kell P, Doctor A. Hypoxia limits antioxidant capacity in red blood cells by altering glycolytic pathway dominance FASEB J. 2009; 23: 3159-3170.

Rowe AW, Eyster E, Kellner A. Liquid nitrogen preservation of red blood cells for transfusion: a low glycerol–rapid freeze procedure. Cryobiology (1968);5:119–128.

Schuster S, Kenanov D. Adenine and adenosine salvage pathways in erythrocytes and the role of S-adenosylhomocysteine hydrolase. A theoretical study using elementary flux modes. FEBS J. 2005, 272:5278-5290.

Sedgwick H, Cameron JE, Poon WC et al. Protwin phase behavior and crystallization: effect of glycerol. J Chem Phys (2007);127(12):125102.

Sidi Y, Gelvan I, Brosh S, Pinkhas J, Sperling O. Guanine ribonucleotide metabolism in human red blood cells: evidence for a high rate of GMP dephosphorylation. Biochem Med Metab Biol. 1989 Apr;41(2):149-54.

Sparrow RL. Time to revisit red blood cell additive solutions and storage conditions: a role for "omics" analyses. Blood Transfus. 2012;10 Suppl 2:s7-11.

Sprague RS, Ellsworth ML, Stephenson AH, Lonigro AJ. Participation of cAMP in a signal-transduction pathway relating erythrocyte deformation to ATP release. Am J Physiol Cell Physiol. 2001;281(4):C1158-64.

Stocks J, Dormandy TL. The autoxidation of human red cell lipids induced by hydrogen peroxide. Br J Haematol. 1971;20(1):95-111.

Strauss D, de Verdier CD. Preservation of red blood cells with purines and nucleosides. III. Synthesis of adenine, guanine, and hypoxanthine nucleotides. Folia Haematol Int Mag Klin Morphol Blutforsch. 1980;107(3):434-53.

Takahashi T, Hirsh A, Erbe E et al. Mechanism of cryoprotection by extracellular polymeric solutes. Biophys. J. (1988); 54(3):509–518.

Tsikas D, Suchy MT, Niemann J, Tossios P, Schneider Y, Rothmann S, Gutzki FM, Frölich JC, Stichtenoth DO. Glutathione promotes prostaglandin H synthase (cyclooxygenase)-dependent formation of malondialdehyde and 15(S)-8-iso-prostaglandin F(2α). FEBS Lett. 2012; 586: 3723-3730.

Wang Y, Schulten K, Tajkhorshid E. What makes an aquaporin a glycerol channel? A comparative study of AqpZ and GlpF. Structure (2005);13(8):1107–1118.

Yoshida T, AuBuchon JP, Tryzelaar L, Foster KY, Bitensky MW. Extended storage of red blood cells under anaerobic conditions. Vox Sang. 2007; 92:22-31.

Zan T, Tao J, Tang RC, Liu YC, Liu Y, Huang B, Zhou JY, Wu MH, Liu HL. [Effect of vitamin C antioxidative protection on human red blood cells]. Zhongguo Shi Yan Xue Ye Xue Za Zhi. 2005;13(6):1106-8.

Zolla L, Ioppolo C, Amiconi G, Benaglia A, Antonini E. Changes in rate of methemoglobin reduction and oxygen affinity of erythrocytes incubated with inosine, pyruvate and phosphate. Experientia. 1977; 33:1524-1526.

Zolla L, D'Alessandro A. An efficient apparatus for rapid deoxygenation of erythrocyte concentrates for alternative banking strategies. J Blood Transfus. 2013;2013:896537

Chapter 3

A new method to evaluate Red Blood Cell storage quality

3.1 Native protein complexes in the cytoplasm of red blood cells

Despite decades of advancements, the investigation of the red blood cell (RBC) cytosolic proteome still represents a challenging task because of the overwhelming abundance of hemoglobin. Besides, the separation method is one of the main limiting factors when investigating protein complexes.

In this study, we performed for the first time a 2D-clear native(CN)-SDS-PAGE followed by mass spectrometry-based identification to screen multi-protein complexes (MCPs) in the cytosol of human RBCs. Upstream to 2D-CN-SDS-PAGE, we applied a recently developed native pre-enrichment strategy that allows discriminating and separately collecting three distinct fractions, one of which being highly enriched for hemoglobin. Such pre-fractionation strategy is conservative, in that it makes soluble native-complex analyses amenable without loss of biological information. Owing to the resolution of native gel electrophoresis techniques we could observe and describe fifty-five potential hetero-oligomeric MPCs from the RBC native cytosolic proteome, among which ultra-tetrameric hemoglobin. The detected protein complexes were characterized by proteins mainly involved in oxygen transport, anti-oxidant responses, metabolism and protein degradation cascades, in agreement with recent *in silico* models. Metabolic enzyme oligomers also interacted with complexes of proteins involved in oxidative stress-responses, thus suggesting a functional relationship between metabolic modulation and anti-oxidant defenses.

3.1.1 Materials and methods

Sample collection

Red blood cell units were drawn from six healthy donor volunteers according to the policy of the Italian National Blood Centre ("Blood Transfusion Service for donated blood") and upon informed consent in accordance with the declaration of Helsinki. We studied RBC samples obtained from 6 healthy male donor volunteers [age 32.2±4.5 (mean±S.D.)] upon

centrifugation of whole blood and leukofiltration, as previously reported [D'alessandro et al., 2012b].

Lysis of RBCs and protein extraction were performed based on the method proposed by Olivieri et al. [2001] with some modifications. The leukofiltered (log-4) packed erythrocytes [D'Alessandro et al., 2012b] were isolated by centrifuging twice at 1000xg for 10 min at 4°C. Packed red blood cells (PRBCs) were washed three times in 5mM phosphate buffer pH 8.0, containing 0.9% w/v NaCl. Then, they were centrifuged at 3000xg for 10 min, at 4°C. PRBCs were lysed with 9 vol of cold 5 mM phosphate buffer pH 8.0 containing 1 mM EDTA and 1 mM PMSF. After 30 min of incubation in ice, cytosol was collected through centrifugation at 17000xg for 20 min at 4°C.

Fraction separation via Electro-Eluter cell

RBC cytosolic protein fractions were separated through a preparative native-gel electrophoresis performed in a modified Electro-Eluter cell (model 422; BioRad). The hereby proposed method has been already validated and thoroughly described in two recent publications from our laboratory [D'Amici et al., 2011a; D'Amici et al., 2011b]. Six vertical glass tubes (length: 60 mm; internal diameter: 10 mm) were filled with a polyacrylamide gel at two different concentrations. The stacking gel had an acrylamide concentration of 4% w/v and was 8 mm long. The acrylamide concentration of the cylindrical separation gel was 6.5 % w/v and the gel was about 40mm long. The negative electrode is at the top, while positive electrode is located at the bottom of the tube, where a membrane cap was located. The cap was endowed with a dialysis membrane (with a MW limit of 3500 Da). One hundred and fifty microgram of total proteins in 1 mL of PBS 5mM, pH 8.0, were mixed with 100 µL of sample buffer (0.1M Bis-Tris HCl, pH 7, 0.5M6-aminocaproic acid, 30% w/v sucrose and 0.001% w/v Ponceau red), while only 1 mL was loaded onto the stacking gel. The run was carried out at 4°C (in a cold chamber with controlled temperature) and at increasing voltages starting from 60 to 150 V for a total of 4 h. Fractions started to be collected from the gel in the membrane cap after the Ponceau red front reached the lower end of the gel. Three fractions of about 200 µL each were collected and were separately dialyzed in PBS 5 mM ph 8.0 for 10 h at 4°C.

Clear Native PAGE and CN/SDS-PAGE

For each fraction, protein concentrations were estimated by the 2D-Quant Kit (GE Healthcare). Proteins from each fraction were then run either on 1D CN-PAGE or 2D CN-SDS-PAGE.

The 1D and 2D experiments were performed in three technical replicates per each fraction per each donor. Which means a total of 6 (donors) x 3 (fractions) x 3 (technical replicates) = 54 total 1D and 2D gels.

1D CN-PAGE was performed according to Schägger et al. [1994]. RBC cytosolic fractions were loaded onto a 0.75-mm-thick 8-12% (F1) or 5–12.5% (F2 and 3) w/v acrylamide gradient gels (Protean II xi cell, BioRad). 130 (F1) or 150 µg (F2 and 3) of total proteins were loaded onto each lane after solubilization with clear native sample buffer (0.1 M BisTris-HCl pH 7.0, 0.5 M 6-aminocaproic acid, 30% w/v sucrose and 0.001% w/v Ponceau red). HMW native protein mixture (66-669kDa) (GE Healthcare) was taken as molecular weight marker. The run was carried out at 4°C starting from 50 to 200 V. Lanes from the 1D native electrophoresis were cut and equilibrated for 30 min in agitation in presence of 50 mM TrisHCl pH 8.8, 4% SDS, 30% glycerol and 6 M urea upon incubation with 3% DTT (for 15min) followed by 15min of incubation with 12% iodacetamide (reducing conditions). For the second dimension, lanes were loaded on a 11% (F1) or 12.5% (F2 and 3) acrylamide SDS gel and covered with cathode buffer with 0.5% agarose. The molecular weight of the proteins was determined by the Wide Range SigmaMarker^{TM} protein standard (Sigma Aldrich, St. Louis, MO, USA).

Proteins from fraction 1 were also run on 2D CN-CN-PAGE, native in both dimensions. 2D native gel was obtained by the combination of a classical 1D CN-PAGE with a second modified CN-PAGE [Witting and Schägger, 2009**]**. Lanes from the first native dimension were cut and equilibrated for 30 min in agitation in presence of 0.05 M tricine, 0.015 M Bis-Tris, 30% glycerol and 0.02% dodecylmaltoside (DDM), pH 7. The second native dimension was performed by adding detergent (0.02% DDM) to the cathode buffer.

Mass spectrometry identification of protein spots

Spots excised from the second dimension gels and subjected to in gel trypsin digestion according to Shevchenko et al. [1996], with minor modifications. The gel pieces were swollen in a digestion buffer containing 50 mM NH_4HCO_3 and 12.5 ng/mL trypsin (modified porcine trypsin, sequencing grade, Promega, Madison, WI) in an ice bath. After 30 min, the supernatant was removed and discarded; then 20 µL of 50 mM NH_4HCO_3 was added to the

gel pieces, and digestion was allowed to proceed overnight at 37 °C. The supernatant containing tryptic peptides was dried by vacuum centrifugation prior to MALDI-TOF/TOF [Suckau et al., 2003] and nano-LC-ESI-IT MS/MS identification [Baldwin, 2004].

MALDI-based identifications were performed through an Autoflex II MALDI-TOF/TOF mass spectrometer with the LIFT module (Bruker Daltonics) was used for mass analysis of peptide mixtures. Twenty microliters of the tryptic protein digests was loaded onto activated (0.1% TFA in acetonitrile) ZipTip columns and washed three times with 10 µL of 0.1% TFA in DD-H_2O. The peptides were eluted with 1 µL of matrix solution (0.7 mg/mL α-cyano-4-hydroxy-trans-cinnamic acid (Fluka, Germany) in 85% acetonitrile, 0.1% TFA and 1 mM $NH_4H_2PO_4$) and spotted directly on the MALDI-TOF target plate for automatic identifications (PAC384 pre-spotted anchor chip) Proteins were identified by PMF using the database search program MASCOT (http://www.matrixscience.com/) upon removal of background ion peaks. Accuracy was set within 50 ppm, while the enzyme chosen was trypsin and only 1 missed cleavage was allowed; fixed carbamidomethyl Cys and variable Met-oxidation, was used as optional search criterion. For those proteins for which PMF-based identification was not successful, most abundant peptides were further analysed with MALDI-TOF/TOF-based LIFT mode MS/MS analyses of precursor ions and repeated MASCOT-based database searches. Runs were performed automatically through FlexControl setting and Biotools processing of MS data (PMF) and, when PMF protein identification was unsuccesfull, automatic determination of the three most abundant peaks and identifications through MS/MS (LIFT analysis) on the three most intense ion peaks. A peptide mixture (Peptide calibration standard I, Bruker Daltonics) was used for external calibration.

Nano-LC-ESI-IT MS/MS identifications were performed on those proteins that could not be successfully identified either through PMF or LIFT (MS/MS) MALDI TOF/TOF analyses. Nano-LC-ESI-IT MS/MS analyses were performed through a split-free nano-flow chromatography separation system (EASY-nLC II, Proxeon, Odense, Denmark) coupled to a 3D-ion trap (model AmaZon ETD, Bruker Daltonik, Germany) equipped with an online ESI nano-sprayer (the spray capillary was a fused silica capillary, 0.090 mm o.d., 0.020 mm i.d.). For all experiments, a sample volume of 15 µL was loaded by the autosampler onto a homemade 2 cm fused silica precolumn (100 µm I.D.; 375 µm O.D.; Reprosil C18-AQ, 5 µm, Dr. Maisch GmbH, AmmerbuchEntringen, Germany). Sequential elution of peptides was accomplished using a flow rate of 300 nL/min and a linear gradient from Solution A (2% acetonitrile; 0.1% formic acid) to 50% of Solution B (98% acetonitrile; 0.1% formic acid) in 40 min over the precolumn in-line with a homemade 15 cm resolving column (75 µm I.D.;

375 µm O.D.; Reprosil C18-AQ, 3 µm, Dr. Maisch GmbH, Ammerbuch-Entringen, Germany). The acquisition parameters for the instrument were as follows: dry gas temperature, 220 °C; dry gas, 4.0 L/min; nebulizer gas, 10 psi; electrospray voltage, 4000 V; high-voltage end-plate offset, −200 V; capillary exit, 140 V; trap drive: 63.2; funnel 1 in, 100 V out 35 V and funnel 2 in, 12 V out 10 V; ICC target, 200 000; maximum accumulation time, 50 ms. The sample was measured with the "Enhanced Resolution Mode" at 8100 m/z per second (which allows mono isotopic resolution up to four charge stages) polarity positive, scan range from m/z 300 to 1500, 5 spectra averaged, and rolling average of 1. The "Smart Decomposition" was set to "auto".

Acquired spectra were processed in DataAnalysis 4.0, and deconvoluted spectra were further analyzed with BioTools 3.2 software and submitted to Mascot search program (in-house version 2.2, Matrix Science, London, UK). The following parameters were adopted for database searches: NCBInr database (release date 21/01/2012; 243 775 sequences); taxonomy = *Homo sapiens*; peptide and fragment mass tolerance of ± 0.3 Da; enzyme specificity (trypsin) with 2 missed cleavages considered; fixed modifications: carbamidomethyl (C); variable modifications: oxidation (M). For positive identification, the score of the result of (-10 x Log(P)) had to be over the significance threshold level ($P < 0.05$) and only peptides with Mascot scores $\geq$ 30 were considered. Peptide fragmentation spectra were also manually verified. In this manual verification, the mass error, the presence of fragment ion series, and the expected prevalence of C-terminus containing (y-type ions) in the high mass range, were all taken into account. All spots required a minimum of two verified peptides to be identified. Moreover, replicate measurements (n = 3) have confirmed the identity of these protein hits.

3.1.2 Results

Three fractions were collected upon preparative CN-PAGE through Electro Eluter cells: (i) F1, containing MPCs with a MW lower than the Hb/CA1 complex (< approximately 500kDa); (ii) F2, containing Hb (α and β chains), CA1 and other complexes with MW similar to the Hb/CA1 heterocomplex (≈500kDa); (iii) F3, containing MPCs with a MW higher than the Hb/CA-1 complex ($\geq$ 500kDa). Each fraction then underwent CN-PAGE first dimension separation of protein complexes and subsequent second dimension separation of the proteins from each complex through SDS-PAGE, as schematized in the workflow in **Figure 25.**

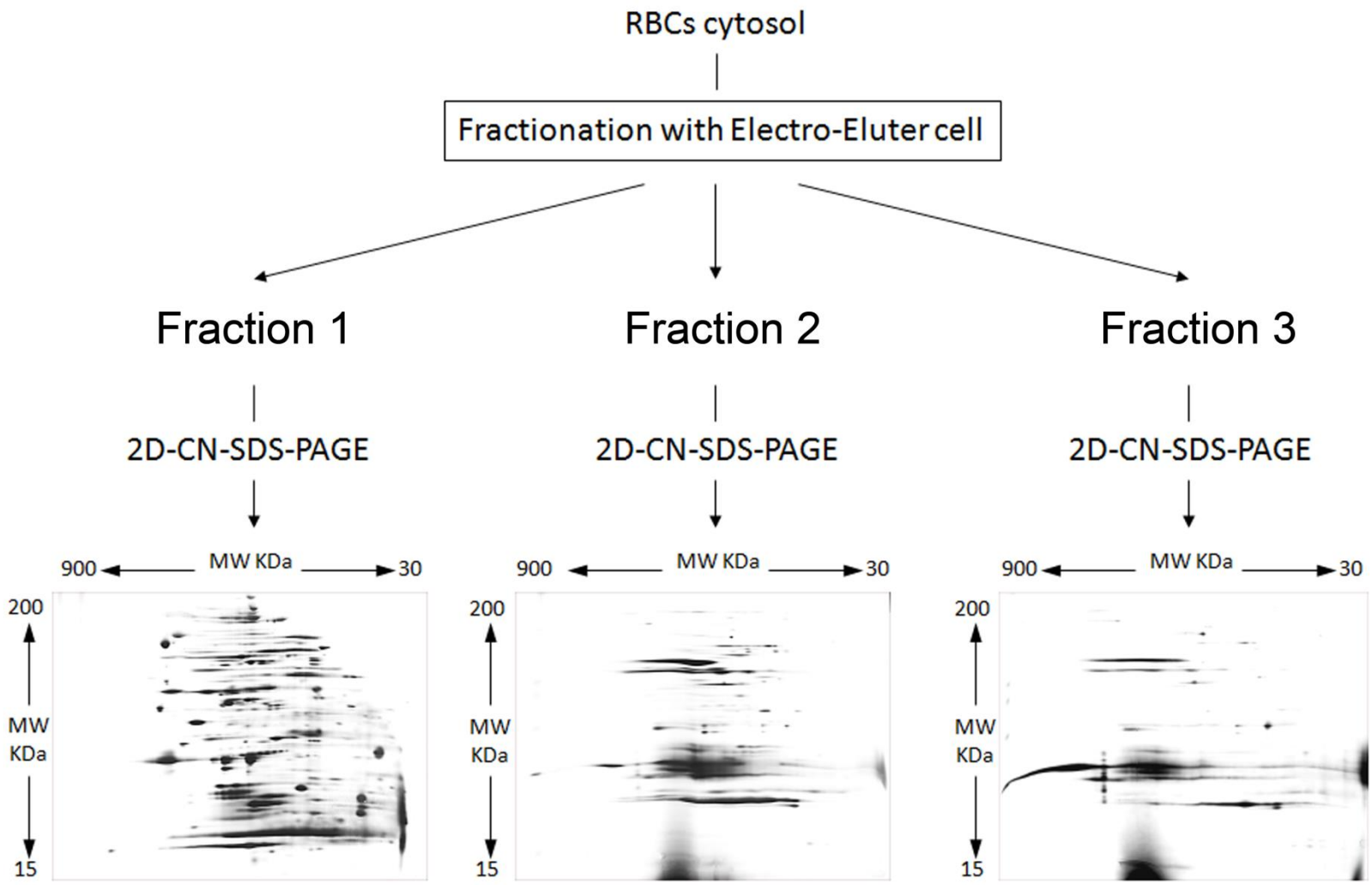

Figure 25. A brief overview of the analytical workflow. Red blood cell cytosolic protein extract underwent separation through electro-eluter cell fractionation, which allowed separation and recovery of three fractions on the basis of their molecular weight and electrophoretic mobility of native complexes. Each fraction then was further analysed with 1D-clear native PAGE (separating the cytosolic native complexes), followed by a second SDS-PAGE electrophoretic separation (orthogonally separating the proteins within each distinct complex).

Overall, first dimension CN-PAGE yielded the separation of 55 unique bands accounting for distinct protein complexes (**Figure 26**). Hb and CA1 were mainly present in F2 [Silverman et al., 1972] although also F3 contained traces of Hb contamination (**Figure 26**). Fractions 1–3 were further analyzed by second-dimensional SDS-PAGE gels (**Figure 27-29**) and a total of 238 distinct protein spots were detected. Protein spots were excised from the gels, trypsin digested and analyzed through mass spectrometry to pursue the identification of the separated spots. Results are reported in **Table 4-6**, along with the spot number (referred to those attributed in **Figures 27-29**), the extended protein name and indications about the theoretical molecular weight and Uniprot name of each entry, gene identifiers, and identification details (number of peptides and MASCOT scores).

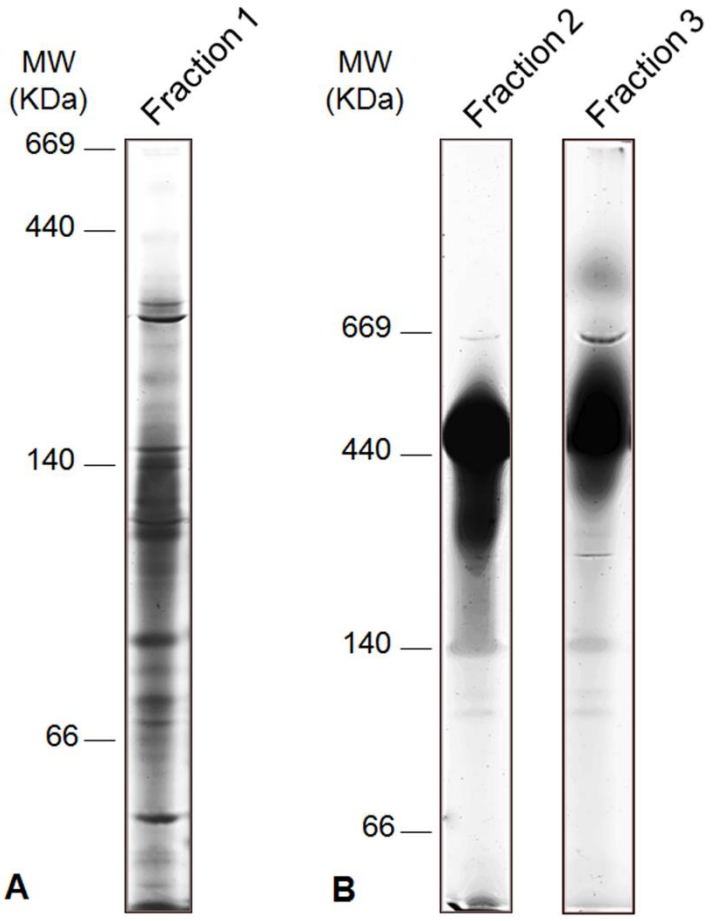

Figure 26. A detail of first dimension clear native (CN)-PAGE of fractions 1 to 3. The most abundant complex was the one containing hemoglobin and carbonic anhydrase in fraction 2 (and, in part, also contaminating fraction 3) at approximately 500kDa.

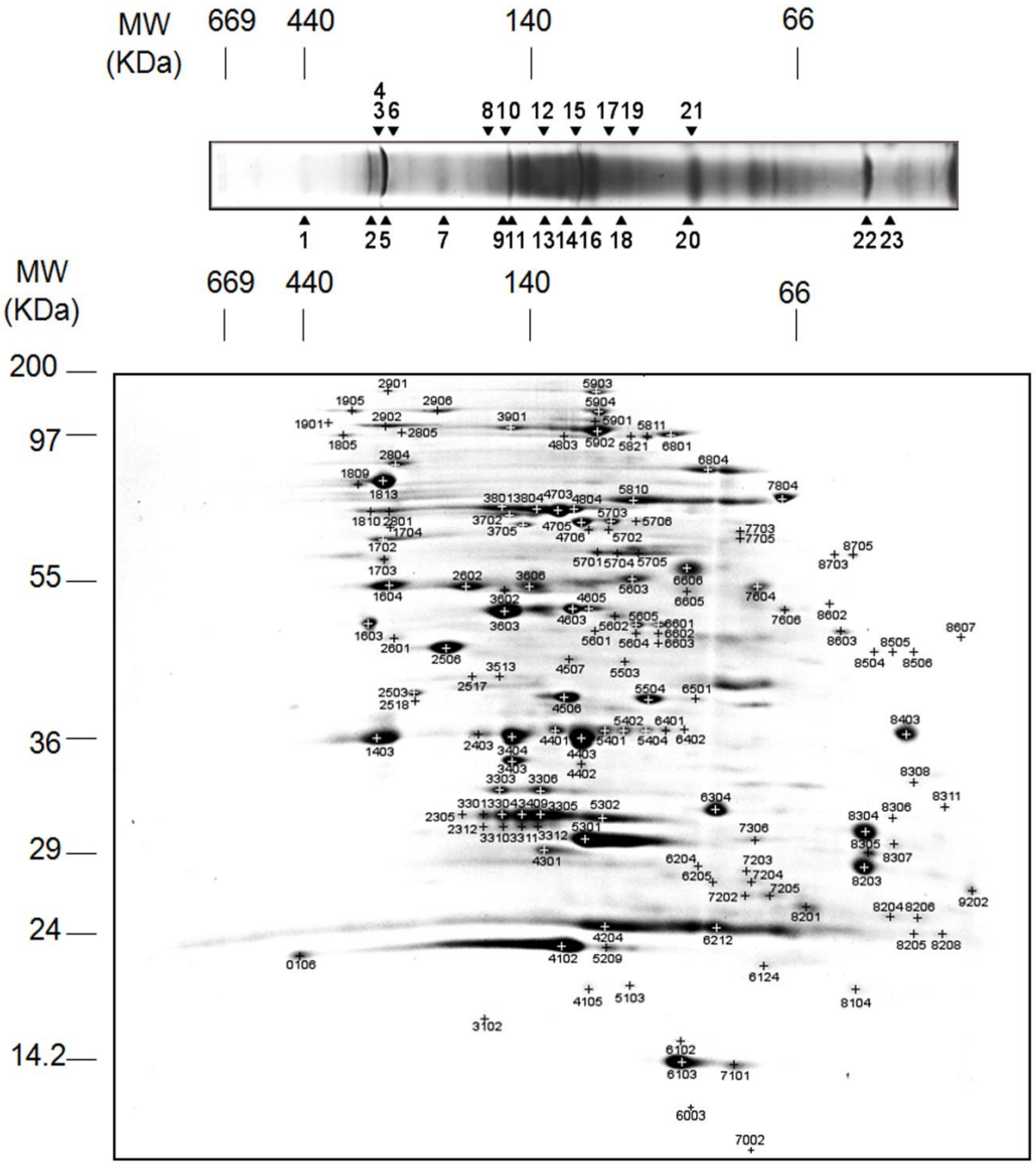

Figure 27. The resulting gel upon 2D-clear native (CN)-SDS-PAGE separation of proteins from fraction 1. Protein spots were identified with mass spectrometry and results are reported in Table 1 (fraction 1 section). The first CN-PAGE dimension is allineated on top, in order to highlight the separated bands each one consisting of at least a multi-protein complex, as detailed in Table 2 (fraction 1).

Table 4 – Protein identification upon 2D-CN-SDS-PAGE of Fraction 1

N° Spot	MW, Da	N° of peptides identified	Mascot Score	Gene name	NCBI Accession Number	Protein ID [Homo sapiens]
0106	21795	5 MALDI	73	*PRDX2*	gi|9955007	**Chain A, Thioredoxin Peroxidase B From Red Blood Cells**
1403	36301	12 MALDI	107	*ALAD*	gi|248839	**Delta-aminolevulinate dehydratase**
1603	52242	11 MALDI	81	*BLMH*	gi|7245509	**Chain A, Human Bleomycin Hydrolase**
1604	54800	11 MALDI	86	*ALDH1*	gi|2183299	**Aldehyde dehydrogenase 1**
1702	64425	9 MALDI	100	*PURH*	gi|1263196	**AICAR formyltransferase/IMP cyclohydrolase Bifunctional enzyme**
1703	82170	13	559	*APEH*	gi|7144648	**Oxidized protein hydrolase**
1704	68521	2	116	*APEH*	gi|181630	**DNF1552 protein**
1805	125186	3	105	*XPO7*	gi|21315062	**Exportin 7**
1809	87554 82529 82210	7 5 2	219 175 85	*CUL2* *CAPN1* *APEH*	gi|19482174 gi|189054948 gi|556514	**Cullin-2 isoform c** **Calpain-1 catalytic subunit** **Acylamino acid-releasing enzyme**
1810	71082 70755 71440	6 4 2	229 136 137	*HSPA8* *HSP70-HOM* *HSPA6*	gi|5729877 gi|188492 gi|34419635	**Heat shock cognate 71 KDa protein isoform 1** **Heat shock induced protein** **Heat shock 70 KDa protein 6**
1813	81173	14 MALDI	108	*APEH*	gi|23510451	**Acylamino-acid-releasing enzyme**
1901						**NOT IDENTIFIED**
1905	137999	10	304	*CAND1*	gi|21361794	**Cullin-associated NEDD8-dissociated protein 1 (CAND1)**
2305						**NOT IDENTIFIED**
2312						**NOT IDENTIFIED**
2403	36900 36950	3 3	118 112	*LDHB* *LDHA*	gi|4557032 gi|5031857	**L-lactate dehydrogenase B chain** **L-lactate dehydrogenase A chain isoform 1**
2503						**NOT IDENTIFIED**
2506	44630	14 MALDI	105	*AHCY*	gi|239937451	**Adenosylhomocysteinase isoform 2**
2517	46219	5 MALDI	64	*GOT1*	gi|4504067	**Aspartate aminotransferase, cytoplasmic**
2518	39265	4	142	*NIF3L1*	gi|10197632	**MDS015**
2601	45538	11	333	*UBAC1*	gi|55770884	**Ubiquitin-associated domain-containing protein 1**
2602	52358	11 MALDI	86	*SELENBP1*	gi|16306550	**Selenium-binding protein 1**
2801	70855	7 MALDI	82	*HSPA8*	gi|62897129	**Heat shock 70kDa protein 8 isoform 1 variant**
2804	68329	11 MALDI	116	*HSP90AA1*	gi|83318444	**HSP90AA1 protein**
2805	95096	5	175	*HSPA4*	gi|4579909	**Apg-2 (Heat shock 70KDa protein 4)**
2901						**NOT IDENTIFIED**
2902						**NOT IDENTIFIED**
2906	137999	10	299	*CAND1*	gi|38678112	**Cullin-associated NEDD8-dissociated protein 1**
3102	19641	4 MALDI	77	*NME1*	gi|38045913	**Nucleoside diphosphate kinase A isoform a**
3301	32097	17	573	*PNP*	gi|157168362	**Purine nucleoside phosphorylase**
3303	34181	10	338	*ESD*	gi|1882265	**Esterase D**
3304	32325 28909	23 3	735 95	*PNP* *CA1*	gi|157168362 gi|4502517	**Purine nucleoside phosphorylase** **Carbonic anhydrase 1**
3305	32097	18 MALDI	111	*PNP*	gi|157168362	**Purine nucleoside phosphorylase**
3306	34181	12	485	*ESD*	gi|182265	**Esterase D**

	32077	5	207	*PDXP*	gi|10092677	**Pyridoxal phosphate phosphatase**
3310	32382 28909	7 3	261 117	*PNP* *CA1*	gi|387033 gi|4502517	**Purine nucleoside phosphorylase** **Carbonic anhydrase 1**
3311	32382	7	267	*PNP*	gi|387033	**Purine nucleoside phosphorylase**
3312	32325	19	639	*PNP*	gi|157168362	**Purine nucleoside phosphorylase**
3403	36666	7 MALDI	86	*LDHA*	gi|62897717	**Lactate dehydrogenase A variant**
3404	36900 36950 36758 37688	21 10 8 8	830 343 278 261	*LDHB* *LDHA* *ALAD* *TALDO1*	gi|4557032 gi|5031857 gi|248839 gi|5803187	**L-lactate dehydrogenase B chain** **L-lactate dehydrogenase A chain** **Delta aminolevulinate dehydratase** **Transaldolase**
3409	32097	12 MALDI	103	*PNP*	gi|157168362	**Purine nucleoside phosphorylase**
3513	46447	8	296	*GOT1*	gi|4504067	**Aspartate aminotransferase, cytoplasmatic**
3602	53161 52928	11 6	365 277	*CPGL* *SELENBP1*	gi|15620780 gi16306550	**Glutamate carboxypeptidase** **Selenium-binding protein 1**
3603	41477	10	421	*HIP*	gi|19923193	**Hsc 70-interacting protein**
3606	52358	7 MALDI	95	*SELENBP1*	gi|16306550	**Selenium-binding protein 1**
3702	69995	6 MALDI	79	*HSPA1*	gi|4529893	**HSP70 1**
3705	66138	9 MALDI	94	*WDR1*	gi|12652891	**WD repeat domain 1**
3801	70855	10 MALDI	113	*HSPA8*	gi|62897129	**Heat shock 70kDa protein 8 isoform 1 variant**
3804	70854	7 MALDI	103	*HSPA8*	gi|5729877	**Heat shock cognate 71 kDa protein isoform**
3901	124447 118858 118745	9 2 2	333 113 73	*XPO1* *UBA1* *IDE*	gi|4507943 gi|23510338 gi|184556	**Exportin-1** **Ubiquitin like modifier activating enzyme 1** **Insulin-degrading enzyme**
4102	21795	12 MALDI	136	*PRDX2*	gi|9955007	**Chain A, Thioredoxin Peroxidase B From Red Blood Cells**
4105	19766 22048	7 6	242 239	*APRT* *PRDX2*	gi|4502171 gi|440308	**Adenine phosphoribosyltransferase isoform a** **Enhancer protein**
4204	22105	5 MALDI	72	*BLVRB*	gi|4502419	**Flavin reductase (NADPH)**
4301						**NOT IDENTIFIED**
4401	37688 37024 36758	15 6 3	463 233 177	*TALDO1* *AFAR* *ALAD*	gi|5803187 gi|2736256 gi|248839	**Transaldolase** **Aflatoxin aldehyde reductase AFAR** **Delta aminolevulinate dehydratase**
4402	36900	15	679	*LDHB*	gi|4557032	**L-lactate dehydrogenase B chain**
4403	36615	12 MALDI	135	*LDHB*	gi|4557032	**L-lactate dehydrogenase B chain**
4506	36892 36900 35481	8 4 2	250 162 87	*ALDR1* *LDHB* *AKR1CL2*	gi|5174391 gi|4557032 gi|12804019	**Alcool dehydrogenase NADP+** **L-lactate dehydrogenase B chain** **1,5-anhydro-D-fructose-reductase**
4507	39506 52523	2 2	116 87	*HMBS* *GSS*	gi|224510663 gi|4504169	**Chain A, the crystal structure of human Porphobilinogen deaminase** **Glutathione synthetase**
4603	52352	7 MALDI	89	*GSS*	gi|4504169	**Gutathione synthetase**
4605						**NOT IDENTIFIED**
4703	70855	8 MALDI	100	*HSPA8*	gi|62897129	**Heat shock 70kDa protein 8 isoform 1 variant**
4705	69109	16 MALDI	130	*LTA4H*	gi|29726225	**Chain A, Structure Of Leukotriene A4 Hydrolase D375n Mutant**
4706						**NOT IDENTIFIED**
4803						**NOT IDENTIFIED**
4804	70855	5 MALDI	73	*HSPA8*	gi|62897129	**Heat shock 70kDa protein 8 isoform 1 variant**
5103	19766	3	90	*APRT*	gi|4502171	**Adenine phosphoribosyltransferase isoform a**
5209	18315	4 MALDI (MS/MS)	67	*PRDX2*	gi|1617118	**TSA**

5301	29987	12 MALDI	133	*BPGM*	gi|4502445	**Bisphosphoglycerate mutase**
5302	27548	2 MALDI (MS/MS)	79	*GSTO1*	gi|4758484	**Glutathione S-transferase omega-1 isoform 1**
5401	37688 37024 36900	14 8 9	504 488 276	*TALDO1* *AFAR* *LDHB*	gi|5803187 gi|2736256 gi|4557032	**Transaldolase** **Aflatoxin aldehyde reductase AFAR** **L-lactate dehydrogenase B-chain**
5402	37385	9 MALDI	84	*TALDO1*	gi|48257056	**TALDO1 protein**
5404	37688	4	170	*TALDO1*	gi|5803187	**Transaldolase**
5503	39533	2	62	*HMBS*	gi|35309	**Porphobilinogen deaminase**
5504	37037	8	255	*PPP2R4*	gi|29725611	**Serine/threonine-protein phosphatase 2A activator isoform b**
5601	51635	2	76	*RNH1*	gi|3892027	**Chain A ribonuclease inhibitor-angiogenin complex**
5602	47055 52523	14 2	443 81	*DDI2* *GSS*	gi|33186798 gi|4504169	**DNA-damage inducible protein 2** **Glutathione synthetase**
5603	54560	7 MALDI	89	*PEPD*	gi|112491419	**Chain A, Crystal Structure Of Human Prolidase**
5604	51766 47421	8 9	365 274	*RNH1* *ENO1*	gi|21361547 gi|693933	**Ribonuclease inhibitor** **2-phosphopyruvate-hydratase alpha-enolase**
5605	47421	5	248	*ENO1*	gi|693933	**2-phosphopyruvate-hydratase alpha-enolase**
5701	56489	11	301	*USP14*	gi|4827050	**Ubiquitin carboxyl-terminal hydrolase 14 isoform a**
5702						**NOT IDENTIFIED**
5704	56489 60655	10 3	357 104	*USP14* *NAE1*	gi|4827050 gi|4502169	**Ubiquitin carboxyl-terminal hydrolase 14 isoform a** **NEDD8-activating enzyme E1 regulatory subunit isoform a**
5705						**NOT IDENTIFIED**
5706						**NOT IDENTIFIED**
5810	72719	8 MALDI	78	*GCLC*	gi|4557625	**Glutamate-cystein ligase catalytic subunit isoform a**
5811	96596	10	315	*USP5*	gi|1122278	**De-ubiquitinase**
5821	96596	3	102	*USP5*	gi|1122278	**De-ubiquitinase**
5901	117715	2 MALDI (MS/MS)	64	*UBA1*	gi|35830	**Ubiquitin activating enzyme E1**
5902	117774	10 MALDI	74	*UBA1*	gi|23510338	**Ubiquitin-like modifier-activating enzyme 1**
5903	144573	10 MALDI	79	*PFAS*	gi|148922280	**Phosphoribosylformylglycinamidine synthase**
5904	99695	6 MALDI	70	*DDB1*	gi|119594343	**Damage-specific DNA binding protein 1, 127kDa, isoform CRA_e**
6003						**NOT IDENTIFIED**
6102	15749	2	64	*SOD1*	gi|305677635	**Chain A, monomeric human Cu/Zn superoxide dismutase without Cu ligands**
6103	16096	2	66	*SOD1*	gi|1237406	**Cu/Zn-superoxide dismutase**
6124	20035 21674 21601	7 6 3	215 187 132	*CDC42/ ITSN1* *CDC42/PAK6* *hCG393694*	gi|374977519 gi|126031529 gi|119613210	**Chain A, Structure Of Designed Orthogonal Interaction Between Cdc42 And Nucleotide Exchange Domains Of Intersectin** **Chain A, The Crystal Structure Of Human Cdc42 In Complex With The Crib Domain Of Human P21-Activated Kinase 6** **hCG393694 isoform CRA_a**
6204						**NOT IDENTIFIED**
6205	25729	3	184	*GSTM2*	gi|494186	**Chain A, crystal structure of human class Mu Glutathione transferase Gstm2-2**
6212	22105	6 MALDI	67	*BLVRB*	gi|4502419	**Flavin reductase (NADPH)**
6304	25931	2	94	*LXN*	gi|119599089	**Latexin isoform CRA_a**
6401	37688	14	439	*TALDO1*	gi|5803187	**Transaldolase**

6402						**NOT IDENTIFIED**
6501	37037	9	273	*PPP2R4*	gi|29725611	**Serine/threonine-protein phosphatase 2A activator isoform b**
6601	47581 47421	13 11	515 363	*ENO2* *ENO1*	gi|5803011 gi|693933	**Gamma enolase** **2-phosphopyruvate-hydratase alpha-enolase**
6602	51635	3	106	*RNH1*	gi|3892017	**Chain A ribonuclease inhibitor-angiogenin complex**
6603	37922	2	72	*HMBS*	gi|292385	**Hydroxymethylbilane synthase**
6605	52928	2	62	*SELENBP1*	gi|16306550	**Selenium binding prtein 1**
6606	51766	2	72	*RNH1*	gi| 21361547	**Ribonuclease inhibitor**
6801	98441	16 MALDI	199	*NPEPPS*	gi|4210726	**Puromycin sensitive aminopeptidase**
6804	78420	17	821	*TGM2*	gi|39777597	**Protein-glutamine gamma-glutamyltransferase 2 isoform a**
7002	12904	4	137	*TBCA*	gi|4759212	**Tubulin-specific chaperone A**
7101	16096	2	66	*SOD1*	gi|1237406	**Cu/Zn-superoxide dismutase**
7202						**NOT IDENTIFIED**
7203	30333	5	157	*DCUN1D1*	gi|36030883	**DCN1-like protein 1**
7204	25837 27127	7 2	211 60	*PAFAH1B3* *GSTM3*	gi|4505587 gi|306820	**Platelet-activating factor acetylhydrolase IB subunit Gamma** **Glutathione transferase M3**
7205	38632	2	68	*ARFIP1*	gi|7657210	**Arfaptin 1 isoform 2**
7306						**NOT IDENTIFIED**
7604						**NOT IDENTIFIED**
7606	50461	6	180	*ARHGAP1*	gi|4757766	**RhoGTPase-activating protein 1**
7703	68484	14	432	*ALB*	gi|332356380	**Albumin**
7705	68484	3	102	*ALB*	gi|332356380	**Albumin**
7804	82538	9 MALDI	110	*DPP3*	gi|18491024	**Dpeptidyl peptidase 3**
8104	19211 21222	6 7	362 255	*RCL* *GGCT*	gi|5454002 gi|13129018	**Deoxyribonucleoside 5'-monophosphate N-glycosidase isoform 1** **Gamma-glutamylcyclotransferase isoform 1**
8201	22219 23031	5 4	186 145	*BLVRB* *ARHGDIB*	gi|4502419 gi|56676393	**Flavin reductase (NADPH)** **Rho GDP-dissociation inhibitor 2**
8203	7952	2 MALDI (MS/MS)	78	*1433/PA24A*	gi|4262000	**14-3-3 protein/cytosolic phospholipase A2**
8204	24697 36202	6 2	208 89	*PSMD10* *GAPDH*	gi|4506217 gi|31645	**26S proteasome non-ATPase regulatory subunit 10 isoform 1** **Glyceraldehyde-3-phosphate dehydrogenase**
8205	22446 22219	4 3	141 99	*ABHD14B* *BLVRB*	gi|14249382 gi|4502419	**Abhydrolase domain-containing protein 14B** **Flavin reductase (NADPH)**
8206	24697 22219	2 2	67 64	*PSMD10* *BLVRB*	gi|4506217 gi|4502419	**26S proteasome non-ATPase regulatory subunit 10 isoform 1** **Flavin reductase (NADPH)**
8208	21966 22446	3 2	98 68	*BLVRB* *ABHD14B*	gi|21361547 gi|14249382	**Biliverdin-IX beta reductase isozyme I** **Abhydrolase domain-containing protein 14B**
8304	29155	2 MALDI (MS/MS)	67	*YWHAE*	gi|5803225	**14-3-3 protein epsilon**
8305	28032 28528 27815 27871 29326	8 7 6 4 2	245 237 189 123 83	*YWHAQ* *YWHAG* *PGLS* *SFN* *YWHAE*	gi|5803227 gi|5726310 gi|6912586 gi|5454052 gi|5803225	**14-3-3 protein theta** **14-3-3 protein gamma** **6-phosphogluconolactonase** **14-3-3 protein sigma** **14-3-3 protein epsilon**
8306	27177	9	271	*CLIC*	gi|4588526	**Chloride ion channel intracellular**
8307						**NOT IDENTIFIED**
8308						**NOT IDENTIFIED**
8311						**NOT IDENTIFIED**
8403						**NOT IDENTIFIED**
8504	41653	15	486	*PPP1R7*	gi|4506013	**Protein phosphatase 1 regulatory subunit 7**
8505	41653	2	84	*PPP1R7*	gi|4506013	**Protein phosphatase 1 regulatory subunit 7**

8506	41653	6	181	*PPP1R7*	gi|4506013	**Protein phosphatase 1 regulatory subunit 7**
8602						**NOT IDENTIFIED**
8603						**NOT IDENTIFIED**
8607						**NOT IDENTIFIED**
8703						**NOT IDENTIFIED**
8705	51177	7	238	*GDI1*	gi|4503971	**Rab GDP dissociation inhibitor alpha**
9202	26337	8	343	*UCHL3*	gi|5174741	**Ubiquitin carboxyl-terminal hydrolase isozyme L3**

Protein identification was performed through nanoHPLC-ESI-MS/MS, unless where specified otherwise;
MALDI = protein identified through MALDI PMF
MALDI (MS/MS) = protein identified through LIFT mode analysis of selected peptides through MALDI TOF/TOF

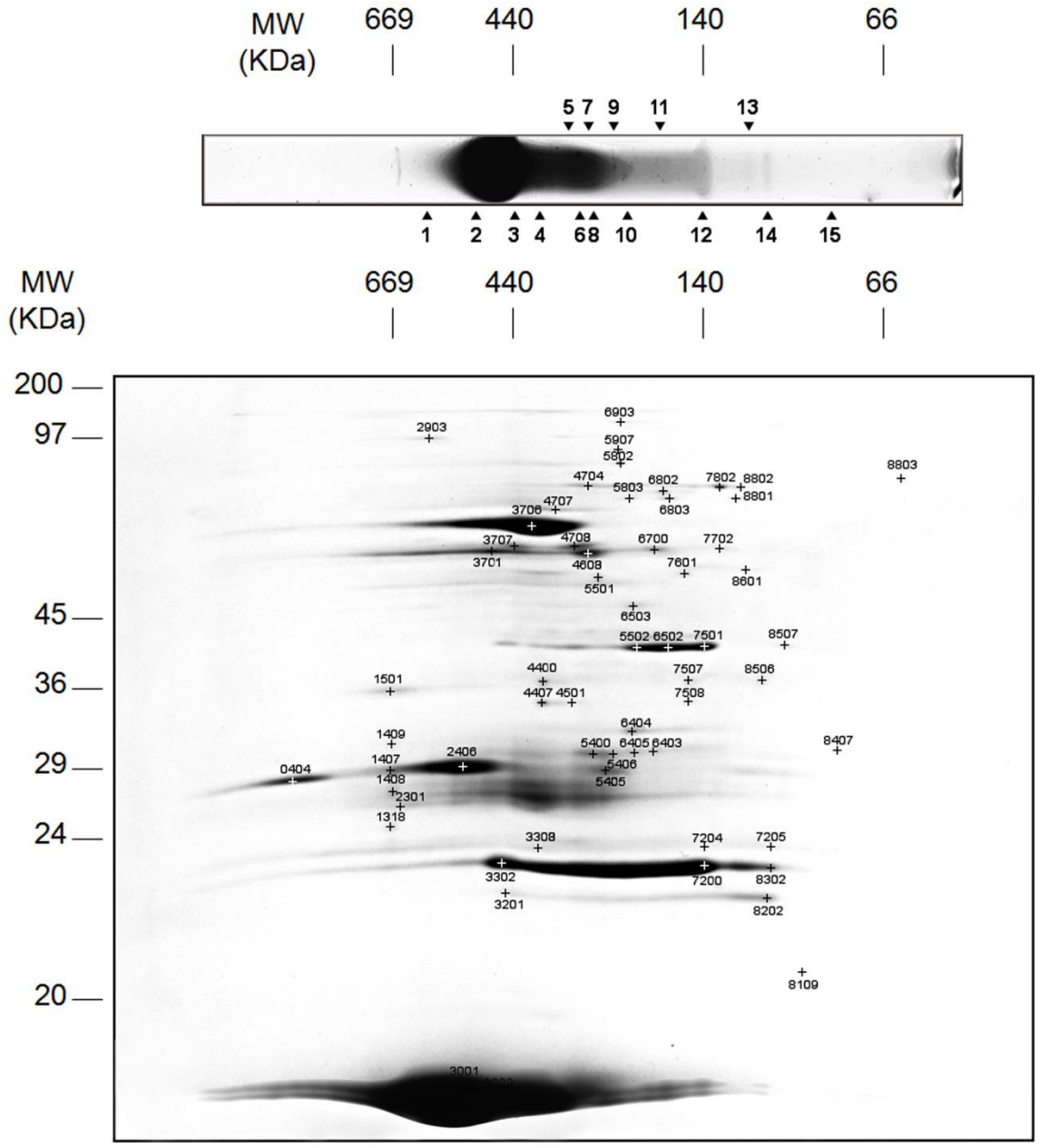

Figure 28. The resulting gel upon 2D-clear native (CN)-SDS-PAGE separation of proteins from fraction 2. Protein spots were identified with mass spectrometry and results are reported in Table 1 (fraction 2 section). The first CN-PAGE dimension is allineated on top, in order to highlight the separated bands each one consisting of at least a multi-protein complex, as detailed in Table 2 (fraction 2).

Table 5 – Protein identification upon 2D-CN-SDS-PAGE of Fraction 2

N° Spot	MW, Da	N° of peptides identified	Mascot Score	Gene name	NCBI Accession Number	Protein ID [Homo sapiens]
0404	28797	10	462	*CA1*	gi|14719797	**Chain A, Solution Structure Of The Cai Michigan 1 Variant, Carbonic anhydrase**
1318	25996	6	220	*PSMA2*	gi|4506181	Proteasome subunit alpha type-2
1407	28909	7	369	*CA1*	gi|4502517	Carbonic anhydrase 1
1408	28238	5	159	*PSMA7*	gi|12314029	Proteasome subunit, alpha type, 7
1409						**NOT IDENTIFIED**
1501	36631	8	340	*MDH1*	gi|5174539	**Malate dehydrogenase, cytoplasmic isoform 2**
2301	26938	15	570	*TPI1*	gi|4507645	**Triosephosphate isomerase isoform 1**
2406	28797 28408	16 16	908 888	*CA1* *CA1*	gi|14719797 gi|158428858	**Chain A, Solution Structure Of The Cai Michigan 1 Variant** **Chain A, X Ray Structure Of The Complex Between Carbonic Anhydrase I And The Phosphonate Antiviral Drug Foscarnet**
2903	89950	16	642	*VCP*	gi|6005942	Transitional endoplasmic reticulum ATPase
3001	16101 16163	20 8	1442 570	*HBB* *HBD*	gi|71727231 gi|73762521	**Beta globin** **Delta-globin Troodos variant**
3002	15257	9	611	*HBA*	gi| 57013850	**Hemoglobin subunit alpha**
3201	22048	3	149	*PRDX2*	gi|440308	**Enhancer protein**
3302	21909	15	595	*PRDX2*	gi|9955007	**Chain A, Thioredoxin Peroxidase B From Red Blood Cells**
3308	24903	4	223	*PRDX6*	gi|31657160	**Peroxiredoxin-6**
3701	52928	19	749	*SELENBP1*	gi|16306550	**Selenium-binding protein 1**
3706	59947	39	2025	*CAT*	gi|4557014	**Catalase**
3707	55454 52928	17 8	520 279	*ALDH1A1* *SELENBP1*	gi|21361176 gi|16306550	**Retinal dehydrogenase 1** **Selenium-binding protein 1**
4400	36900 36758 36950 36630	13 8 3 4	464 243 219 204	*LDHB* *ALAD* *LDHA* *LDHC*	gi|4557032 gi|248839 gi|5031857 gi|4504973	**L-lactate dehydrogenase B chain** **Delta-aminolevulinate dehydratase** **L-lactate dehydrogenase A chain isoform 1** **L-lactate dehydrogenase C chain**
4407	36950	6	224	*LDHA*	gi|5031857	**L-lactate dehydrogenase A chain isoform 1**
4501	36950	9	396	*LDHA*	gi|5031857	**L-lactate dehydrogenase A chain isoform 1**
4608	52928	26	901	*SELENBP1*	gi|16306550	**Selenium-binding protein 1**
4704	71082 68812 71440	12 10 4	361 315 126	*HSPA8* *PGM2* *HSPA6*	gi|5729877 gi|14603253 gi|34419635	Heat shock cognate 71 kDa protein isoform 1 Phosphoglucomutase 2 Heat shock 70 kDa protein 6
4707	65089	16	649	*PURH*	gi|20127454	**Bifunctional purine biosynthesis protein PURH**
4708	55427 52928	20 7	791 248	*ALDH1* *SELENBP1*	gi|2183299 gi|16306550	**Aldehyde dehydrogenase 1** **Selenium-binding protein 1**
5400	28909 32382	4 6	239 210	*CA1* *PNP*	gi|4502517 gi|387033	**Carbonic anhydrase 1** Purine nucleoside phosphorylase
5405	28909	10	387	*CA1*	gi|4502517	**Carbonic anhydrase 1**
5406	28909 32382	6 5	185 157	*CA1* *PNP*	gi|4502517 gi|387033	**Carbonic anhydrase 1** Purine nucleoside phosphorylase
5501	52928 53155	2 2	77 64	*SELENBP1* *BLMH*	gi|16306550 gi|4557367	**Selenium-binding protein 1** **Bleomycin hydrolase**
5502	22049	15	721	*PRDX2*	gi|32189392	**Peroxiredoxin-2 isoform a**
5802	82170	17	715	*APEX*	gi|7144648	**Oxidized protein hydrolase**
5803	66822	6	201	*WDR1*	gi|12652891	**WD repeat domain 1**
5907	98652 83584	13 6	398 341	*HSP90AA1*	gi|83699649 gi|306891	**Heat shock 90kDa protein 1, alpha** **90kDa heat shock protein**
6404	31956 23123	9 4	306 137	*ESD* *LHPP*	gi|33413400 gi|55960000	S-formylglutathione hydrolase **Phospholysine phosphohistidine inorganic pyrophosphate phosphatase**
6405	32382	9	405	*PNP*	gi|387033	Purine nucleoside phosphorylase

6403	32382	4	153	*PNP*	gi|387033	Purine nucleoside phosphorylase
6502	22049	12	530	*PRDX2*	gi|32189392	**Peroxiredoxin-2 isoform a**
6503	48254	10	317	*AHCY*	gi|178277	S-adenosylhomocysteine hydrolase
6700	52928	15	480	*SELENBP1*	gi|16306550	**Selenium-binding protein 1**
6802	70110 70792 71440	7 6 4	231 184 132	*HSPA1L* *HSPA1L* *HSPA6*	gi|386785 gi|3461866 gi|34419635	Heat shock protein Heat shock protein 70 testis variant Heat shock 70 kDa protein 6
6803	66822	10	314	*WDR1*	gi|12652891	**WD repeat domain 1**
6903	95127	7	226	*HSPA4*	gi|38327039	**Heat shock 70 kDa protein 4**
7200	21909	12 MALDI	119	*PRDX2*	gi|9955007	**Chain A, Thioredoxin Peroxidase B From Red Blood Cells**
7204	24903	3	224	*PRDX6*	gi|31657160	**Peroxiredoxin-6**
7205	24903	4	256	*PRDX6*	gi|31657160	**Peroxiredoxin-6**
7501	21909	8 MALDI	120	*PRDX2*	gi|9955007	**Chain A, Thioredoxin Peroxidase B From Red Blood Cells**
7507	36900 36950 36758	10 5 2	314 154 137	*LDHB* *LDHA* *ALAD*	gi|4557032 gi|5031857 gi|248839	L-lactate dehydrogenase B chain L-lactate dehydrogenase A chain isoform 1 Delta-aminolevulinate dehydratase
7508	36950	13	390	*LDHA*	gi|5031857	L-lactate dehydrogenase A chain isoform 1
7601	41477	3	205	*HIP*	gi|19923193	**Hsc70-interacting protein**
7702	52928	7	272	*SELENBP1*	gi|16306550	**Selenium binding protein 1**
7802	71082	23	981	*HSPA8*	gi|5729877	**Heat shock cognate 71 kDa protein isoform 1**
8109						**NOT IDENTIFIED**
8202	21909	11	374	*PRDX2*	gi|9955007	Chain A, Thioredoxin Peroxidase B From Red Blood Cells
8302	21909	12	530	*PRDX2*	gi|9955007	**Chain A, Thioredoxin Peroxidase B From Red Blood Cells**
8407	25848	4	128	*LXN*	gi|194473714	**Latexin**
8506	36900 36758	10 3	410 128	*LDHB* *ALAD*	gi|4557032 gi|248839	**L-lactate dehydrogenase B chain** **Delta-aminolevulinate dehydratase**
8507	37037	9	338	*PPP2R4*	gi|29725611	**Serine/threonine-protein phosphatase 2A activator isoform b**
8601	52523	15	527	*GSS*	gi|4504169	**Glutathione synthetase**
8801	69868	16	493	*LTA4H*	gi|4505029	Leukotriene A-4 hydrolase isoform 1
8802	71082 70237 71440	9 3 3	299 104 94	*HSPA8* *HSPA2* *HSPA6*	gi|5729877 gi|4204880 gi|34419635	Heat shock cognate 71 kDa protein isoform 1 Heat shock 70 KDa Protein 2 Heat shock 70 kDa protein 6
8803						**NOT IDENTIFIED**

Protein identification was performed through nanoHPLC-ESI-MS/MS, unless where specified otherwise;
MALDI = protein identified through MALDI PMF
MALDI (MS/MS) = protein identified through LIFT mode analysis of selected peptides through MALDI TOF/TOF

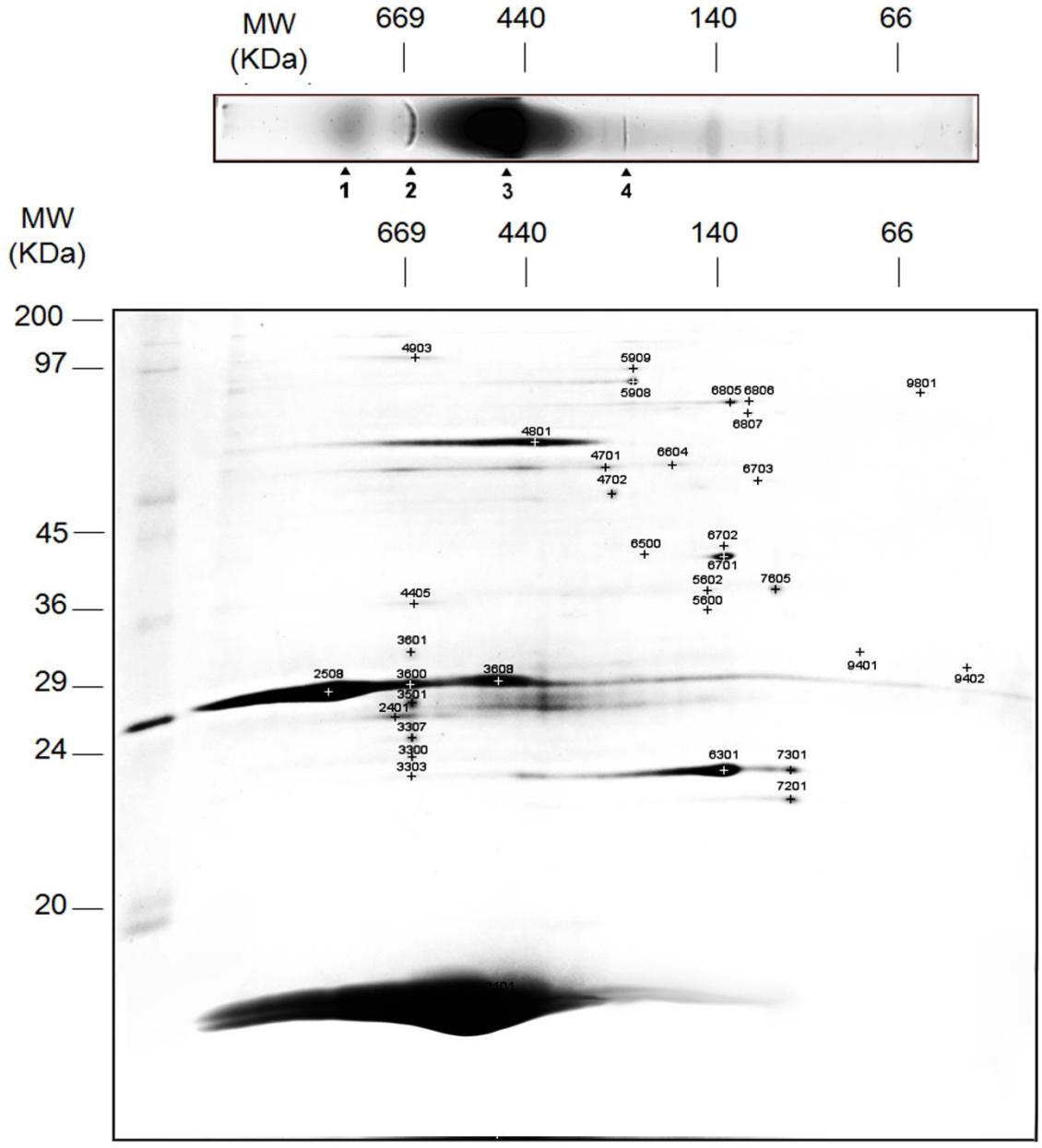

Figure 29. The resulting gel upon 2D-clear native (CN)-SDS-PAGE separation of proteins from fraction 3. Protein spots were identified with mass spectrometry and results are reported in Table 1 (fraction 3 section). The first CN-PAGE dimension is allineated on top, in order to highlight the separated bands each one consisting of at least a multi-protein complex, as detailed in Table 2 (fraction 3).

Table 6 – Protein identification upon 2D-CN-SDS-PAGE of Fraction 3						
N° Spot	**MW, Da**	**N° of peptides identified**	**Mascot Score**	**Gene name**	**NCBI Accession Number**	**Protein ID [Homo sapiens]**
2401	26894	12	570	*TPI1*	gi|136066	**Triosephosphate isomerase**
2508	28408	13	578	*CA1*	gi|158428858	**Chain A, X Ray Structure Of The Complex Between Carbonic Anhydrase I And The Phosphonate Antiviral Drug Foscarnet**
3101	16102	14	741	*HBB*	gi|4504349	**Hemoglobin subunit beta**
3300	23053	5	155	*PSMB5*	gi|558526	**Proteasome subunit X**
3303						**NOT IDENTIFIED**
3307	25996	5	166	*PSMA2*	gi|4506181	**Proteasome subunit alpha-type 2**
3501	20238	4	193	*PSMA7*	gi|12314029	**Proteasome subunit alpha-type 7**
3601	29822	7	216	*PSMA1*	gi|4506179	**Proteasome subunit alpha type-1 isoform 2**
3600						**NOT IDENTIFIED**
3608	28797	13	534	*CA1*	gi|14719797	**Chain A, Solution Structure Of The Cai Michigan 1 Variant; carbonic anhydrase**
4405	36631	5	158	*MDH1*	gi|5174539	**Malate dehydrogenase, cytoplasmic isoform 2**
4701	52928	13	482	*SELENBP1*	gi|16306550	**Selenium binding protein 1**
4702	53155	2	91	*BLMH*	gi|4557367	**Bleomycin hydrolase**
4801	59947	17	765	*CAT*	gi|4557014	**Catalase**
4903	89950	12	454	*VCP*	gi|6005942	**Transitional endoplasmic reticulum ATPase**
5600						**NOT IDENTIFIED**
5602	36709	4	147	*LDHB*	gi|229620	**Dehydrogenase H4,lactate**
5908	82210	14	559	*APEH*	gi|556514	**Acylamino acid-releasing enzyme**
5909						**NOT IDENTIFIED**
6301	21909	14	609	*PRDX2*	gi|9955007	**Chain A, Thioredoxin Peroxidase B From Red Blood Cells**
6500						**NOT IDENTIFIED**
6604	52928	4	136	*SELENBP1*	gi|16306550	**Selenium binding protein 1**
6701	21909	10	434	*PRDX2*	gi|9955007	**Chain A, Thioredoxin Peroxidase B From Red Blood Cells**
6702	21909	2	61	*PRDX2*	gi|9955007	**Chain A, Thioredoxin Peroxidase B From Red Blood Cells**
6703	52523	2	81	*GSS*	gi|4504169	**Glutathione synthetase**
6805	71082	24	979	*HSPA8*	gi|5729877	**Heat shock cognate 71 kDa protein isoform 1**
6806						**NOT IDENTIFIED**
6807						**NOT IDENTIFIED**
7201	21909	9	367	*PRDX2*	gi|9955007	**Chain A, Thioredoxin Peroxidase B From Red Blood Cells**
7301	21909	8	245	*PRDX2*	gi|9955007	**Chain A, Thioredoxin Peroxidase B From Red Blood Cells**
7605	36900	8	367	*LDHB*	gi|4557032	**L-lactate dehydrogenase B chain**
9401						**NOT IDENTIFIED**
9402	29326	8	336	*YWHAE*	gi|5803225	**14-3-3 protein epsilon**
9801	79600	9	267	*DPP3*	gi|375331941	**Dipeptidyl peptidase 3 isoform 2**

Protein identification was performed through nanoHPLC-ESI-MS/MS, unless where specified otherwise;
MALDI = protein identified through MALDI PMF
MALDI (MS/MS) = protein identified through LIFT mode analysis of selected peptides through MALDI TOF/TOF

Hereby described homo- and hetero- protein complexes derive from three main factors:

i) experimental observations (proteins that are components of the same complex are vertically aligned in the second dimension of the gel, while horizontal alignments were indicative of the likely presence of the same protein in distinct MPCs);

ii) the approximated stoichiometry of protein subunits in the multimers was predicted on the basis of the experimental molecular weight of the identified proteins (MWs of proteins detected in vertically aligned spots were summed up for each possible combination, and we excluded those combinations where the total of summed MWs was significantly higher or lower (≈ | 20kDa |) than the apparent MW of the complex from the first native gel dimension. Protein-protein interaction prediction tools (String, Ingenuity Pathway Analysis) and information available from the literature (UniProt, Ingenuity Knowledge Database, String Database) were exploited to confirm whether predicted interactions (or multimers – referenced in **Table 7**) had indeed been previously observed in other biological matrices or *in vitro* experiments.

MPCs included: (i) proteins involved in oxygen transport and transport metabolon (Hb-CA1); (ii) oxidative stress responses and molecular chaperones; (iii) enzymatic complexes; (iv) mixed metabolism/anti-oxidant/chaperone complexes; (v) protein degradation systems (ubiquitin and 20S core proteasome components).

Table 7– Multiprotein complexes identified in each Fraction
Fraction 1

Multiprotein complex	Band number	MW (KDa)	Protein subunit	Spot number	MW (KDa)	Subunit structure	First observed (Ref. n.)
Prdx2 homocomplex	1	~ 440	Peroxiredoxin-2	0106	21.8	Dimer of decamers	*(Low et al., 2008)*
CUL-CAND1 heterocomplex	2	313	Cullin	1809	87.5	Dimer	*(Bosu et al., 2008)*
			Cullin-associated NEDD8-dissociated protein 1	1905	138	Monomer	
ALAD homocomplex	3	290	Delta-aminolevulinate dehydratase	1403	36.3	Octamer (4 dimers)	*(Jaffe et al., 2001)*
ALAD-HSPA8 heterocomplex	4	287	Delta-aminolevulinate dehydratase	1403	36.3	Homohexamer (3 dimers)	*(Jaffe et al., 2001)*
			Heat shock 70 KDa protein 8	1810	70	Monomer	
APEH homo complex	5	324	Acylamino-acid-releasing enzyme	1813	81	Tetramer	*(Scaloni et al., 1999)*
ALDH1-HSPA8 heterocomplex	6	289	Aldehyde dehydrogenase 1	1604	54.8	Homotetramer	*(Agarwal et al., 1989)*
			Heat shock 70kDa protein 8	2801	70	Monomer	
HSP90AA1-HSPA8	6a	289	Heat shock 70kDa protein 8 isoform 1 variant	2801	70.8	Homodimer	
			HSP90AA1 protein	2804	68.3	Homodimer	*(Nemoto et al., 1995)*
AHCY homocomplex	7	178	Adenosylhomocysteinase	2506	44.6	Tetramer	*(Turner et al., 1998)*

			isoform 2				
NDPKA-PNP heterocomplex	8	155	Nucleoside diphosphate kinase A isoform a	3102	19.6	Homotrimer	*(Gilles et al., 1991)*
			Purine nucleoside phosphorylase	3301	32.3	Homotrimer	*(Ealick et al., 1990)*
ESD-GOT1 heterocomplex	9a	160	Esterase D	3303	34	Heterotetramer of homodimers	*(Young et al. 1988; Structural genomics consortium, 2009)*
			Aspartate aminotransferase. cytoplasmic	3513	46.4		
HIP homocomplex	9b	160	Hsc 70-interacting protein HSP70 1	3603 3702	41.4 70	Homotetramer	*(Uniprot P50502)*
PNP-HSPA8 heterocomplex	10	166	Purine nucleoside phosphorylase	3304	32.3	Homotrimer	*(Ealick et al., 1990)*
			Heat shock 70 KDa protein 8	3801	70	Monomer	
LDHB homocomplex	11	147	Lactate dehydrogenase B chain	3404	36.9	Tetramer	*(Holmes and Goldberg, 2009)*
LDHB-TALDO heterocomplex	11b	147	Lactate dehydrogenase B	3404	36.9	Homodimer	*(Holmes and Goldberg, 2009)*
			Transaldolase	3404	37.7	Homodimer	*(Thorell et al., 2000)*
ESD-HSPA8 heterocomplex	12	138	Esterase D	3306	34	Homodimer	*(Young et al., 1988)*
			Heat shock 70 KDa protein 8	3804	70	Monomer	
PNP-HSPA8 heterocomplex	13	134	Purine nucleoside phosphorylase	3305	32.3	Homodimer	*(Ealick et al., 1990)*

			Heat shock 70 KDa protein 8	3804	70	Monomer	
Prdx2-ALDR1 heterocomplex	14	139	Peroxiredoxin-2	4102	21.8	Homotrimer	*(Wang et al., 2010;Low et al., 2008;Li et al., 2005)*
			Alcohol dehydrogenase NADP+	4506	36.8	Homodimer	*(Sulzenbacher et al., 2004)*
GSS-HSPA8 heterocomplex	15	122	Glutathione synthetase	4603	52.3	Monomer	*(Polekhina et al., 1999)*
			Heat shock 70 KDa protein 8	4804	70	Monomer	
BPGM homocomplex	16	119	Bisphosphoglycerate mutase	5301	29.9	Tetramer (2 dimers)	*(Rosa et al., 1989)*
FLR-Prxd2 heterocomplex	17	110	Flavin reductase NADPH	4204	22	Monomer	*(Yamaguchi et al., 1994)*
			Peroxiredoxin-2	5209	21.8	Homotetramer	*(Wang et al., 2010;Low et al., 2008;Li et al., 2005)*
GSS-GSTO heterocomplex	17b	110	Glutathione S-transferase omega-1 isoform 1	5302	27.5	Homodimer	*(Board et al., 2000)*
			Glutathione synthetase	5602	52.5	Monomer	*(Polekhina et al., 1999)*
USP14-NEDD8 heterocomplex	18	112	Ubiquitin-carboxyl terminal hydrolase 14 isoform a	5704	56.4	Dimer	*(Hu et al., 2005)*
			NEDD8-activating enzyme E1 regulatory subunit isoform a	5704	60.6	Dimer	*(Walden et al., 2003)*
PEPD homocomplex	19	109	Human prolidase	5603	54.5	Dimer	*(Endo et al., 1989)*
SOD1-TALDO1 heterocomplex	19b	107	Cu/Zn SOD	6102/6103	16	Homodimer	*(Svensson et al., 2010)*
			Transaldolase	6402	37.6	Homodimer	*(Thorell et al., 2000)*

PP2A homocomplex	19c	≈110	Serine/threonine-protein phosphatase 2A activator isoform b	5504	37	Trimer	*(Jayadeva et al., 2010)*
HMBS homocomplex	19d	≈110	Hydroxymethylbilane synthase	6603	37.9	Trimer	*(Battersby et al., 1979)*
LDHB-GSS heterocomplex	19e	≈110	L-lactate dehydrogenase B	5401	36.9	Homodimer	*(Holmes and Goldberg, 2009)*
			Glutathione synthetase	5602	52.5	Monomer	*(Polekhina et al., 1999)*
ENO2 homocomplex	20a	95	Gamma enolase	6601	47.5	Homodimer	*(Chai et al., 2004)*
SOD1-RNH1 heterocomplex	21	83	Cu/Zn SOD	6102/6103	16	Homodimer	*(Svensson et al., 2010)*
			Ribonuclease inhibitor	6606	51.7	Monomer	
14-3-3 protein homocomplex/heterocomplex	22	58	14-3-3 protein epsilon	8203 8304	29 29	Homodimer Heterodimer	*(Uniprot P62258)*
			14-3-3 protein epsilon 14-3-3 protein gamma/sigma/theta	8305			
CLIC homocomplex	23	54	Chloride ion channel intracellular	8306	27	Dimer	*(Littler et al., 2004)*

Fraction 2

Multiprotein complex	Band number	MW (KDa)	Protein subunit	Spot number	MW (KDa)	Subunit structure	First observed (Ref. n.)
TER ATPase homocomplex	1	~550	Transitional endoplasmic reticulum ATPase	2903	89.9	Hexamer	*(Tang et al., 2010)*

CA1-Hb heterocomplex	2	~500	Carbonic anhydrase I	2406	28.8	?	
			Beta globin	3001	16.1		
Hb heterocomplex	2-8	500 -280	Beta globin	3001	16.1	Oligomers of heterodimers (α2β2 or α2δ2)	*(Fermi et al., 1984)*
			Delta globin	3001	16.1		
			Alpha globin	3002	15.2		
CAT-Prdx2 heterocomplex	3	440	Catalase	3706	60	Tetramer	*(Ko et al., 2000)*
			Peroxiredoxin-2	3302	22	Decamer (5 dimers)	*(Wang et al., 2010;Low et al., 2008;Li et al., 2005)*
CAT-LDHB heterocomplex	4	388	Catalase	3706	60	Homotetramer	*(Ko et al., 2000)*
			Lactate dehydrogenase B chain	4400	37	Homotetramer	*(Holmes and Goldberg, 2009)*
ALDH1-LDHB heterocomplex	5	368	Aldehyde dehydrogenase 1	4708	55	Homotetramer	*(Agarval et al., 1989)*
			Lactate dehydrogenase B chain	4501	37	Homotetramer	*(Holmes and Goldberg, 2009))*
PGM2-PNP heterocomplex	6	332	Phosphoglucomutase 2	4704	70	Homodimer	*(Mithieux et al., 1995)*
			Purine nucleoside phosphorylase	5400	32	Homohexamer (2 trimers)	*(Ealick et al., 1990)*
BMH homocomplex	7	313	Human bleomycin hydrolase	5501	52	Hexamer (3 dimers)	*(O'Farrell et al., 1999)*
SELENBP1-Prdx2 heterocomplex	8	~300	Selenium-binding protein 1	5501	53	Dimer	*(Jeong et al., 2009)*
			Peroxiredoxin 2	3302	22	Tetramer	*(Wang et al.,*

							2010;Low et al., 2008;Li et al., 2005)
Hydrolase-HSP heterocomplex	9	276	Oxidized protein hydrolase	5802	82	Monomer	*(Sandomenico et al., 2012)*
			Heat shock 90kDa protein 1, alpha	5907	99	Homodimer	*(Stebbius et al., 1997)*
			Heat shock 70 kDa protein 4	6903	95	Monomer	
ESD-AHCY heterocomplex	10	260	S-formylglutathione hydrolase	6503	34	Homodimer	*(Young et al., 1988)*
			S-adenosylhomocysteine hydrolase	6404	48	Homotetramer	*(Turner et al., 1998)*
LDHB homocomplex	11a	~148	Lactate dehydrogenase B-chain	7507	37	Homotetramer	*(Holmes and Goldberg, 2009)*
	11b	~148	Lactate dehydrogenase B Lactate dehydrogenase A	7507 7508	37 37	Tetramer of Heterodimers	*(Holmes and Goldberg, 2009)*
Prdx-2 homocomplex	12a	140	Peroxiredoxin-2	7501	22	Eptamer of non-reducible dimers	*(Wang et al., 2010;Low et al., 2008;Li et al., 2005)*
Prdx-2 homocomplex	12b	140	Peroxiredoxin-2	7200	22	Eptamer of dimers	
GSS homocomplex	13	104	Glutathione synthetase	8601	52	Dimer	*(Polekhina et al., 1999)*
Prdx2-Prdx6 heterocomplex	14	92	Peroxiredoxin-2	8302	22	Homodimer	*(Wang et al., 2010;Low et al., 2008;Li et al., 2005)*
			Peorxiredoxin-6	7205	24	Homodimer	*(Choi et al., 1998)*
LXN homocomplex	15	78	Latexin	8407	25.8	Homotrimer	*(Pallarès et al., 2005)*

Fraction 3							
Multiprotein complex	**Band number**	**Apparent MW (KDa)**	**Protein subunit**	**Spot number**	**MW (KDa)**	**Subunit structure**	**First observed (Ref. n.)**
CA1 homocomplex	1	~ 800	Carbonic anhydrase I	2508	28.8	28/30 subunits	*(Wang et al., 2010; D'Amici et al., 2011a; D'Amici et al., 2011b)*
20S proteasome (CP)	2	669	Proteaosme subunit beta-type 5	3300	23	28 subunits	*(Wang et al., 2010; Neelam et al., 2011)*
			Proteasome subunit alpha-type 2	3307	25.9		
			Proteasome subunit alpha-type 7	3501	28 (20.2)		
			Proteasome subunit alpha-type 1 isoform 2	3601	29.8		
MDH homocomplex	2b	~669	Malate dehydrogenase, cytoplasmic isoform 2	4405	36.6	Decamer of homodimers	*(Minarik et al., 2002)*
VCP-PSMA2 heterocomplex	2c	~669	Proteasome subunit alpha-type 2	3307	25.9	Homotetramer	*(Gorbea et al., 2000)*
			Transitional endoplasmic reticulum	4903	89.9	Homohexamer	*(Fermi et al., 1984)*

			ATPase (VCP)				
CA1 homocomplex	3	440	Carbonic anhydrase I	3608	28.8	15 monomers	*(Wang et al., 2010; D'Amici et al., 2011a; D'Amici et al., 2011b)*
APEH homocomplex	4	324	Acylamino acid releasing enzyme	5802	81	Tetramer	*(Sandomenico et al., 2012)*

Several proteins took part in distinct MPCs, though displaying the same apparent MW upon the second dimension SDS-PAGE separation (a particular of this phenomenon in F1, as highlighted in **Figure 30**). Some of these proteins are of high abundance in our sample, thus non-specific interactions cannot be fully excluded. However, due to the high resolution of 2D CN SDS-PAGE if compared to conventional gel filtration or sucrose gradient ultracentrifugation approaches [Li et al., 2009], we consider the results from this technique an excellent line of evidence for association. Although in the present study the first isoelectrofocusing dimension has been replaced with CN separation of MPCs, questions arise as to which biological process might end up influencing protein-protein interaction partners of a given protein without substantially altering the molecular weight. Our first guess was to test a subset of post-translational modifications, namely phosphorylations of serine/threonine or tyrosine residues. Indeed, phosphorylations are long known to modulate interactions in MPCs, especially in RBCs, whereas the thoroughly investigated model of the cytosolic domain of band 3 has revealed phosphorylation specific patterns of structural components interaction with the anion exchanger 1 protein at membrane level [Siciliano et al., 2010]. However, phosphopeptide enrichment through TiO_2 micro-columns of trypsin-digested protein spots (**Figure 30)** did not allow us to individuate phosphorylated peptides with confident MASCOT scores.

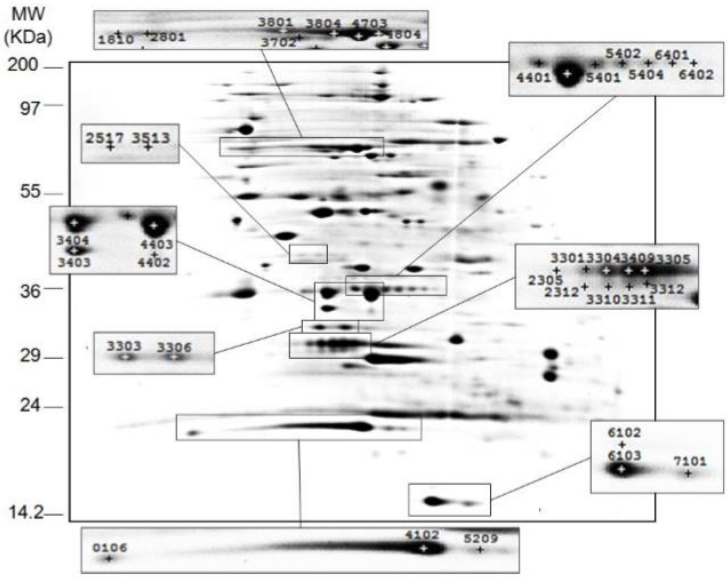

Figure 30. A detail of the second CN-SDS-PAGE dimension of fraction 1. A series of spots (eventually identified as the same protein –**Table 4**) are highlighted that show the same apparent molecular weight though belong to different protein complexes. The mechanisms that influence differential interaction/oligomerization of cytosolic proteins in RBCs seem to mainly involve mechanisms that do not substantially alter the apparent molecular weight, such as specific post translational modifications (e.g. phosphorylations). However, no definitive clue underpinning this assumption could be obtained from the present study.

3.1.3 Discussion

Since the present study focuses on protein complexes alone, it does not represent an explorative study of the RBC proteome. Hence, any direct comparison against existing literature on the overall number of the distinct entries individuated should be avoided. Indeed, despite decades of strides in the definition of the RBC proteome, the comprehensive assessment of the multi-protein organization of erythrocytes is still a virgin area of investigation. While *in silico* predictions have been purported with encouraging results [D'Alessandro et al., 2010; Goodman et al., 2007], it still remains undisclosed as to whether and to what extent bioinformatic models would live up to actual experimental observation. Indeed, persisting gaps in this research endeavour exist, since less than a handful of research articles have addressed the RBC membrane [van Gestel et al., 2010] and cytosol [Wang et al., 2010] native proteome, the latter mainly from a mere technical rather than a biological standpoint (only 6 complexes were individuated in the RBC cytosol, two of which accounting for Hbs). The present investigation has been designed as to bridge this gap, a goal that could be achieved through the auxilium of a sample preparation strategy that endows fractionation of the RBC cytosolic proteome and, in particular, of the vastly abundant Hb sub-fraction, while conserving native conformation of less abundant MPCs [D'Amici et al., 2011a; D'Amici et al., 2011b] without chemical cross-linking [Rappsilber et al., 2000].

In silico models of the RBC interactome agreed about the presence of a so called Repair or Destroy box [Goodman et al, 2007], also referred to as the Save or Sacrifice [D'Alessandro et al., 2010] sub-network, accounting for highly connected proteins (mainly Heat shock proteins – HSPs – and anti-oxidant enzymes) which are involved in the regulation of the redox poise. Indeed, RBC ageing *in vivo* and *in vitro* (blood bank conditions) is accompanied by the progressive accumulation of oxidative stress-triggered lesions utterly leading to RBC removal from the bloodstream [D'Alessandro et al., 2012a; Bosman et al., 2010]. It is thus small wonder that 20 out 55 individuate cytosolic MPCs in RBCs were characterized by proteins/enzymes involved in self-defensive mechanisms against oxidative stress. This is further highlighted by protein-protein interaction elaborations of proteins identified in each different fraction, as graphed in **Figures 31-33**. These results are consistent with existing interactomics elaborations by Goodman's [Rappsilberg et al., 2000] and our group [D'Alessandro et al., 2010], which pinpointed at a likely cross-talk/functional relationship between anti-oxidant defenses and metabolic enzymes (either by prevention of

generation of ROS or prevention of protein denaturation), through the probable direct interaction of specific proteins (especially HSP70 and HSP90, but also catalase, superoxide dismutases and peroxiredoxins) with metabolic enzymes (such as lactate dehydrogenase – LDH, glyceraldehyde 3-phosphate dehydrogenase - GAPDH –**Figures 31-33**). In the present investigation, we could confirm and expand these models by providing direct evidence of the co-participation of several metabolic enzymes with anti-oxidant/chaperone molecules in numerous MPCs (see for example the complex CAT-LDHB -**, Figure 33**), as detailed below.

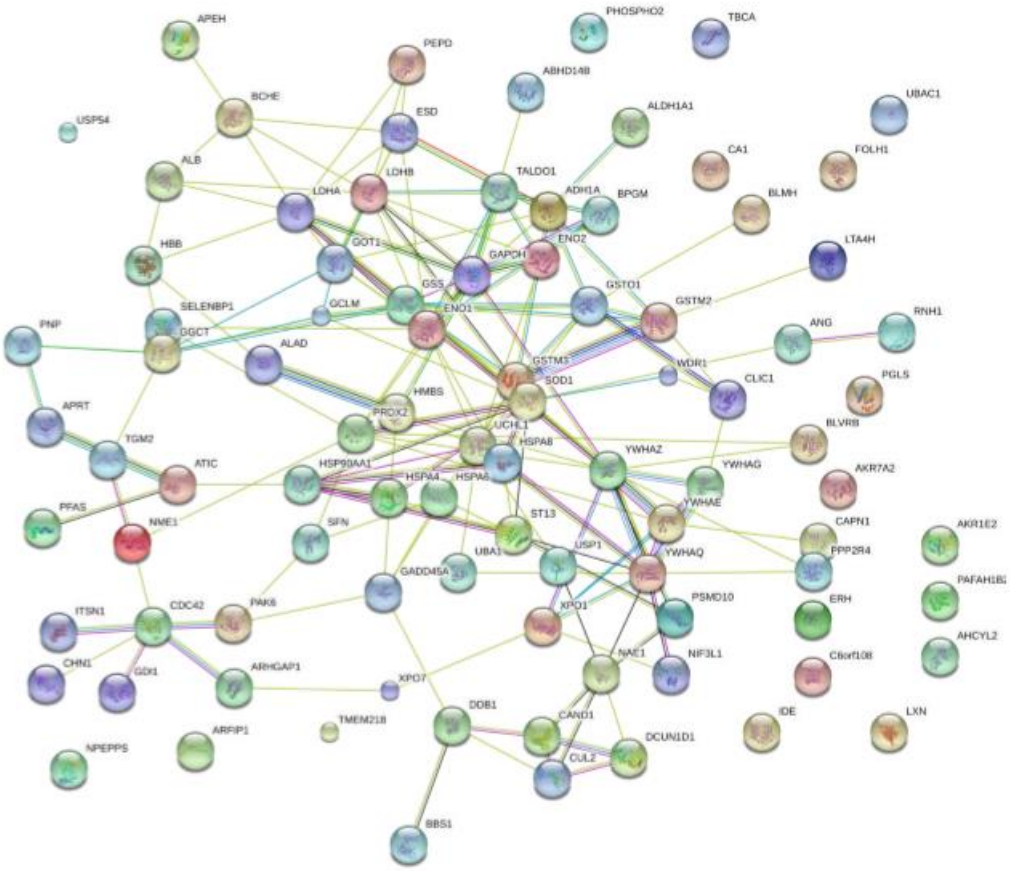

Figure 31. Protein-protein interaction in silico predictions of proteins identified in Fraction 1. Images have been obtained through String (http://string-db.org/) on the basis of experimental evidences on the Homo sapiens protein-protein interaction database (confidence score was set to high confidence = 0.7).

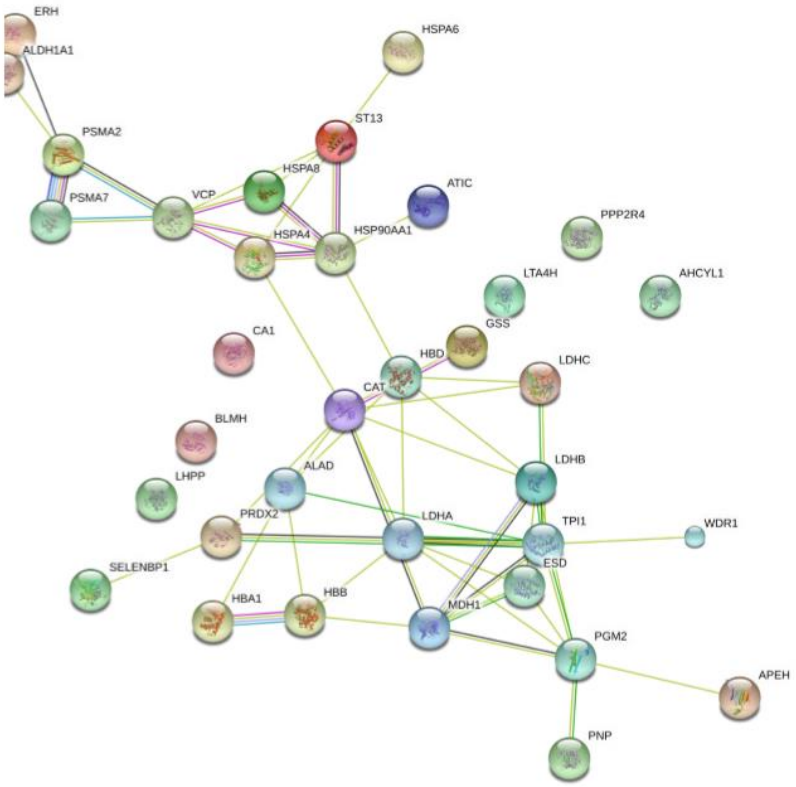

Figure 32. Protein-protein interaction in silico predictions of proteins identified in Fraction 2. Images have been obtained through String (http://string-db.org/) on the basis of experimental evidences on the Homo sapiens protein-protein interaction database (confidence score was set to high confidence = 0.7).

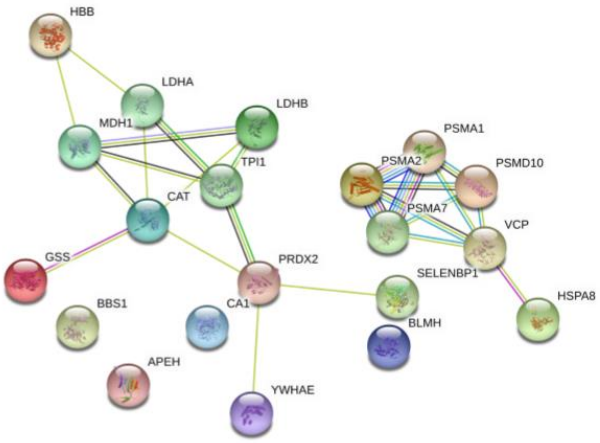

Figure 33. Protein-protein interaction in silico predictions of proteins identified in Fraction 3. Images have been obtained through String (http://string-db.org/) on the basis of experimental evidences on the Homo sapiens protein-protein interaction database (confidence score was set to high confidence = 0.7).

Hb-CA1 complex and Hb smear

The most abundant complex is a diffused band at approximately 500kDa in F2 and 3 (**Figure 26** and band 2 from **Figure 28**). This band corresponded to two main protein spots from F2 (2406 and 3001 – **Table 7** and **Figure 28**), accounting for CA1 and beta Hb, respectively. Interaction between those two proteins has been previously demonstrated [D'Amici et al., 2011a; D'Amici et al., 2011b; Silverman et al., 1979]. However, being aware that CA1 and Hb represent the most prevalent proteins in RBC cytosol, this result might be rather attributable to technical artifacts resulting from the overwhelming abundance of Hb in F2. In order to test this hypothesis, we performed 1D and 2D-native-SDS-PAGE gel experiments while loading half (75 µg), one third (50 µg) and one fifth (30 µg) of the original protein load amounts (150 µg) (data not show). Despite loading up to one fifth of the original proteins amounts, Hb and CA1 are still vertically aligned, thus suggesting that an actual biological phenomenon might underlie the observed Hb-CA1 co-localization/interaction. Indeed, this complex might affect gas transport to some extent, since Hb plays a role in the transport of carbon dioxide, while CA1 is responsible for the conversion of carbon dioxide into bicarbonate. However, it is not to be excluded that native gel bands at 440kDa might account for independent multimers of CA1 and Hbs. Indeed, multimerization of CA1 in ≈440kDa complexes (band 3 F3–**Figure 29**) had already been reported [Wang et al., 2010]. However, hereby we produce the first evidence about further dimerization of this high molecular weight complex at approximately ≈800kDa (band 1 from F3 – **Figure 29** and **Table 7**).

First dimension CN-PAGE of the most abundant fraction (band 2 to 8 in F2 – **Figure 26, Table 7**) also shows a smear from 440kDa down to ≈ 280kDa. In this molecular weight range, Hb is always present (**Figure 28**). As a mere suggestion, it is interesting to note that certain marine (among which *Oligobrachia mashikoi*) and terrestrial (such as *Lumbricus terrestris*) invertebrates do not host Hb within erythrocytes, while they rely for oxygen transport on giant respiratory extracellular proteins made up of globin chains of 3-3.6kDa, which are complexed in 350-440kDa multimers [Nakagawa et al., 2005].

Normal HbA molecules (tetramers of α2β2 globin chains) should weigh up to 64kDa. On the other hand, multimerization of human Hb is a phenomenon occurring in the frame of sickle cell anemia, whereas Hb S polymerizes in aqueous solution owing to the S alpha 2A beta 2(6)Glu →Val mutation [Rhoda et al., 1984]. However, it is worthwhile mentioning that Hb heterocomplexes (Hb α2β2 and α2δ2) had already been reported by Wang et al. at 180 or

237kDa the former and 352kDa the latter and suggested as an actual biological evidence of Hb tetramer multimerization [Wang et al., 2010]. Since our approach relied on a pre-enrichment strategy [D'Amici et al., 2011a; D'Amici et al., 2011b] where Hb was largely collected in F2 in order to unravel the otherwise hidden low abundance complexes in the other fractions, we could not discriminate as many Hb chain isoforms with different PTMs as in Wang et al. [2010].

Anti-oxidant enzymes and chaperones

Peroxiredoxin 2 (Prdx2) is the third most abundant cytosolic RBC protein, after Hb and CA1 [Low et al., 2008]. Eight homo- and heterocomplexes of Prdx2 have been identified in the present study (band 1, 14 and 17 from F1; 3, 8, 12a and 12b and 14 from F2 – **Table 2**). Multimeric conformation of Prdx2 has been reported to result from the oxidative stress-dependent oligomerization of dimers [Wang et al., 2010; Li et al., 2005] in decamers [Low et al., 2008] (further dimerized in band 1 in F1 – **Table 7, Figure 27**). Analogously, the ≈140kDa (bands 12a and 12b in F2 – **Table 7**) Prdx2 complex has been suggested to result from an eptameric organization [Rinalducci et al., 2011]. A ≈440kDa complex of decameric Prdx2 with tetrameric catalase (CAT) has been reported as well within the framework of RBC storage under blood bank conditions [Rinalducci et al., 2011] (band 3 in F2 – **Table 7, Figure 28**).

Interestingly, Prdx2 was found to be complexed with flavin reductase NADPH and alcohol dehydrogenase NADP+, both the enzymes catalyzing the reduction to NADPH (band 14 and 17, F1 – **Table 7, Figure 27**). Indeed, the oxidized Prdx2 is regenerated by thioredoxin reductase, with reducing equivalents derived from NADPH [Low et al., 2008].

Interaction between Prdx2 and selenium binding protein (SELENBP1 – band 8, F2 – **Table 7**) had been predicted, yet not assessed, through *in silico* models [D'Alessandro et al., 2010; Goodman et al., 2007] (**Figures 32 and 33**). Analogous considerations can be made for Prdx2 and Prdx6 (tetramer of homodimers, band 14, F2).

However, the anti-oxidant enzymatic system in RBCs is not only limited to Prdxs and catalase, since also Cu/Zn superoxide dismutase (SOD1) play a critical role in RBC physiology [D'Alessandro and Zolla, 2011].

While aberrant oligomerization of SOD1 dimers underlies the insurgence of familial amyotrophic lateral sclerosis [Svensson et al., 2010], we hereby describe the previously unreported association of SOD1 dimers with the monomer of the ribonuclease inhibitor protein (band 21, F1 – **Figure 27, Table 7**). On the other hand, the interaction of homo- or

heterocomplexes of 14-3-3 protein isoforms (epsilon, gamma, theta - band 22, F1) had already been reported in other cell types, including human epidermal keratinocytes [Liang et al., 2009].

Human glutathione synthetase (GSS) has a dimeric structure [Slavens et al., 2011], that we hereby confirm (band 13, F2 – **Table 7, Figure 28**). On the other hand, we also provide the first evidence of the interaction between HSPA8 and GSS in RBCs (band 15, F1).

The central role of HSPs in the interactome of RBCs had been previously hypothesized *in silico* [D'Alessandro et al., 2010; Goodman et al., 2007] and hereby confirmed with the presence of multiple heterocomplexes of HSPs with antioxidant and metabolic enzymes (bands 4, 6, 6a, 10, 12, 13, 15 in F1; band 9 in F2 - **Table 7, Figure 31**).

Acylamino acid-releasing enzyme/oxidized protein hydrolase is a homotetramer (hereby confirmed in band 5 from F1) displaying endopeptidase activity against oxidized and glycated proteins [Scaloni et al., 1992], both recurring phenomena in RBCs (e.g. Hb glycation).

Metabolic enzymes and functional relationship with antioxidant defenses

Since RBCs are devoid of any organelle, mitochondria included, they mainly rely on glycolysis to produce ATP and sustain their energy requirements. In the present study, we could not individuate multi-protein complexes including more than one glycolytic enzyme, thus suggesting that this kind of interactions might be absent, very labile or not amenable to the presence approach. Lactate dehydrogenase catalyzes the interconversion of pyruvate and lactate with concomitant interconversion of NADH and NAD+. Functional lactate dehydrogenase are homo or hetero tetramers composed of M and H protein subunits encoded by the LDHA and LDHB genes respectively [Holmes and Goldberg, 2009], hereby observed in band 11 of F1 and band 11 of F2 (**Table 7, Figures 31-33**). Aldehyde dehydrogenase 1 is organized in homotetramers [Agarwal et al., 1989] and requires NAD+ for its correct functioning. It is thus interesting to note its oligomerization with LDH tetramers (band 5, F2 – **Table 7**).

Human biphosphoglycerate mutase (BPGM) is dimeric, in contrast to yeast BPGM that displays a tetrameric structure [Fothergill-Gilmore and Watson, 1989]. However, we could observe that BPGM-positive band (no.16) at approximately ≈120kDa in F1 (spot no. 5301 - **Figure 27**), that might account for tetramers made up of two BPGM dimers. Dimeric structure of phosphoglucomutase 2 has been already reported in rabbit muscles and human RBCs [Lin et al., 1986] (band 6, F2).

In addition to the aforementioned oligomers, a wide series of metabolic enzyme complexes were observed for the first time in the RBC cytosol, especially in the Hb-depleted F1, though confirming consolidated *in vitro* evidences as it emerged from a rapid search in the UniProt database. Results included: hexamers of bleomicyin hydrolase, homo-octamers of delta-aminolevulinic acid dehydratase, dimers of gamma enolase, homotetramers of adenosylhomocysteinase isoform 2, hexamers (2 homotrimers) of purine nucleoside phosphorylase, trimers of nucleoside diphosphate kinase A, dimers of human prolidase, dimers of intracellular chloride ion channel, homohexamers of transitional endoplasmic reticulum ATPase, homodimers of esterase D and of cytoplasmic aspartate aminotransferase (**Table 7**).

It is also worthwhile to stress that these oligomers also further interacted to give rise to actual MPCs, and these interactions were not only limited to metabolic enzyme oligomers but also involved anti-oxidant enzymes, in a sort of a cross-talk between metabolic modulation and anti-oxidant defenses (see for example ALAD-HSPA8, SOD-TALDO and CAT-LDHB, and complexes in bands 4 and 19b of F1, band 4 of F2, respectively – **Table 7, Figures 31-33**) .

RBC proteasome

Recent evidences indicated the presence of functional 20S proteasome in leukocyte-depleted reticulocyte-depleted RBCs [Neelam et al., 2011]. A presence that might result in untoward burdens to those recipients transfused with longer stored packed RBC units, in the light of the progressive accumulation of 20S proteasomes in the supernatants of *in vitro* ageing RBCs [Geng et al., 2009]. Native assessment of RBC cytosol have previously evidenced the presence of a functional 20S proteasome complex weighing approximately 669kDa [Wang et al., 2010]. Our results agree with this observation, since 20S proteasome core particles represent the main contributors to oligomers found in F3 (band 2 in **Figure 29** and **Table 7**). The core particles interact to form a hollow cylindrical structure composed of 28 subunits arranged in four stacked rings (α7β7β7α7). Notably, we could discriminate at least four different α and β subunits (spots no. 3301, 3302, 3501, 3601 in F3 – **Table 6**).

Since the proteasome-dependent protein degradation process implies the cooperation with the ubiquitin system, it is of note the identification of ubiquitin-carboxyl terminal hydrolase 14 (USP14-spot no. 5704 from F1 – **Table 4**). USP14 is a proteasome-associated deubiquitinase which releases ubiquitin from the proteasome targeted ubiquitinated proteins. We could hereby assess for the first time in RBCs the presence of a complex characterized

by the interaction of USP14a and NEDD8 (band 18, F1 – **Table 7**). We expected that this complex should have included also cullin [Bosu and Kipreos, 2008], that was indeed identified (spots no.1809-**Table 4**) although it interacted with cullin-associated NEDD8-dissociated protein 1 (band 2 from F1-**Table 7, Figure 31**), whose role is to prevent NEDD8 association to cullin and thus justified our observations.

3.1.4 Conclusions

The RBC soluble proteome still represents a treasure trove of biological information. In the present investigation, the multiprotein complexes from RBC cytosol were screened by a pre-enrichment strategy for low abundance species, followed by 2D CN SDS-PAGE and identification by LC MS-MS. Fifty-five among known and potential novel MPCs were observed and described, mainly involved in oxygen transport, metabolism, anti-oxidant responses and protein degradation cascades. Although the presently adopted method provided an improved overview of the RBC cytosolic native proteome, the presence of co-migrating complexes suggests that further analytical efforts will be necessary to improve their separation in the future through alternative separative approaches downstream to our preparative native method. However, it is worth pointing out that the resolution of 2D native SDS-PAGE is recognized to be much higher than other conventional molecular weight-based separation methods (such as gel filtration chromatography or sucrose gradient ultracentrifugation). For this reason, if the sample has been well fractionated in order to reduce complexity, the 2D CN gel technique is considered a valuable tool to reveal biological protein associations [Li et al., 2009]. In the cases of co-migrating complexes, bioinformatics prediction tools and existing literature from human and non-human cellular models helped us to point out the presence in RBCs of those complexes that had been previously reported elsewhere.

When the composition of a complex is defined, the next key issue is the determination of its function. Thus future studies are mandatory to shed light on how these complexes end up influencing RBC ageing *in vivo* and *in vitro* and whether/to what extent alterations to the oligomeric configuration of cytosolic complexes is associated with specific pathologies (such as sickle cell anemia).

References

Agarwal, D.P., Cohn, P., Goedde, H.W., Hempel, J. Aldehyde dehydrogenase from human erythrocytes: structural relationship to the liver cytosolic isozyme. *Enzyme* 1989;42(1):47-52.

Baldwin, M.A. Protein identification by mass spectrometry: issues to be considered. *Mol. Cell. Proteomics* 2004; 3(1):1-9.

Battersby, A.R., Fookes, C.J.R., Matcham, G.W.J., McDonald, E., Gustafson-Potter, K.E. Biosynthesis of the natural porphyrins: experiments on the ring-closure steps and with the hydroxy-analogue of porphobilinogen. *J. Chem. Soc. Chem. Commun.* 1979;316-319.

Bosu, D.R.; Kipreos, E.T. Cullin-RING ubiquitin ligases: global regulation and activation cycles. *Cell. Div*. 2008;3,7.

C**hai, G., Brewer, J.M., Lovelace, L.L., Aoki, T., Minor, W., Lebioda, L.** Expression, purification and the 1.8 angstroms resolution crystal structure of human neuron specific enolase. *J. Mol. Biol.* 2004;341(4):1015-1021.

Choi, H.J., Kang, S.W., Yang, C.H., Rhee, S.G., Ryu, S.E. Crystal structure of a novel human peroxidase enzyme at 2.0 A resolution. *Nat. Struct. Biol.* 1998;5(5):400-406.

D'Alessandro, A.; Righetti, P.G.; Zolla, L. The red blood cell proteome and interactome: an update. *J. Proteome Res.* 2010;9(1):144-163.

D'Alessandro, A.; Zolla, L. The SODyssey: superoxide dismutases from biochemistry, through proteomics, to oxidative stress, aging and nutraceuticals. *Expert Rev. Proteomics* 2011;8(3):405-421.

D'Alessandro, A.; Blasi, B.; D'amici, G.M.; Marrocco, C.; Zolla, L. Red blood cell subpopulations in freshly drawn blood: application of proteomics and metabolomics to a decades-long biological issue. *Blood Transfus.* 2012; doi:10.2450/2012.0164-11. (a)

D'Alessandro, A.; D'Amici, G.M.; Vaglio, S.; Zolla, L. Time-course Investigation of SAGM-Stored Erythrocyte Concentrates: from Metabolism to Proteomics. *Hematologica* 2012, 97 (1), 107-115. (b)

D'Amici, G.M.; Rinalducci, S.; Zolla, L. An easy preparative gel electrophoretic method for targeted depletion of hemoglobin in erythrocyte cytosolic samples. *Electrophoresis* 2011;32(11):1319-1322.

D'Amici, G.M.; Rinalducci, S.; Zolla, L. Depletion of hemoglobin and carbonic anhydrase from erythrocyte cytosolic samples by preparative clear native electrophoresis. *Nat. Protoc*. 2011;7(1):36-44

Ealick, S.E., Rule, S.A., Carter, D.C., Greenhough, T.J., Babu, Y.S., Cook, W.J., Habash, J., Helliwell, J.R., Stoeckler, J.D., Parks, R.E. Jr, et al. Three-dimensional structure of human erythrocytic purine nucleoside phosphorylase at 3.2 A resolution. *J. Biol. Chem.* 1990;265(3):1812-20.

Endo, F., Tanoue, A., Nakai, H., Hata, A., Indo, Y., Titani, K., Matsuda, I. Primary structure and gene localization of human prolidase. *J. Biol. Chem.* 1989;264(8):4476-4481.

Fermi, G., Perutz, M.F., Shaanan, B., Fourme, R. The crystal structure of human deoxyhaemoglobin at 1.74 A resolution. *J. Mol. Biol.* 1984**;**175(2):159-74

Geng, Q.; Romero, J.; Saini, V.; Patel, M.B.; Majetschak, M. Extracellular 20S proteasomes accumulate in packed red blood cell units. *Vox. Sang*. 2009;97(3):273-274.

Gilles, A.M., Presecan, E., Vonica, A., Lascu, I. Nucleoside diphosphate kinase from human erythrocytes. Structural characterization of the two polypeptide chains responsible for heterogeneity of the hexameric enzyme. *J. Biol. Chem.* 1991;266(14):8784-8789.

Goodman, S.R.; Kurdia, A.; Ammann, L.; Kakhniashvili, D.; Daescu, O. The human red blood cell proteome and interactome. *Exp. Biol. Med.* (Maywood) 2007;232 (11):1391-1408.

Gorbea, C., Taillandier, D., Rechsteiner, M. Mapping subunit contacts in the regulatory complex of the 26 S proteasome. S2 and S5b form a tetramer with ATPase subunits S4 and S7. *J. Biol. Chem.* 2000;275(2):875–882.

Holmes, R.S.; Goldberg, E. Computational analyses of mammalian lactate dehydrogenases: human, mouse, opossum and platypus LDHs. *Comput. Biol. Chem*. 2009;33(5):379-385

Hu, M., Li, P., Song, L., Jeffrey, P.D., Chenova, T.A., Wilkinson, K.D., Cohen, R.E., Shi, Y. Structure and mechanisms of the proteasome-associated deubiquitinating enzyme USP14. *EMBO J*. 2005;24(21):3747-3756.

Jaffe, E.K., Martins, J., Li, J., Kervinen, J., Dunbrack, R.L. Jr. The molecular mechanism of lead inhibition of human porphobilinogen synthase. *J. Biol. Chem.* 2001;276(2):1531-1537.

Jayadeva, G., Kurimchak, A., Garriga, J., Sotillo, E., Davis, A.J., Haines, D.S., Mumby, M., Graña, X. B55alpha PP2A holoenzymes modulate the phosphorylation status of the retinoblastoma-related protein p107 and its activation. *J. Biol. Chem.* 2010;285(39):29863-29873.

Jeong, J.Y., Wang, Y., Sytkowski, A.J. Human selenium binding protein-1 (hSP56) interacts with VDU1 in a selenium-dependent manner. *Biochem. Biophys. Res. Commun.* 2009;379(2):583-588.

Ko, T.P., Safo, M.K., Musayev, F.N., Di Salvo, M.L., Wang, C., Wu, S.H., Abraham, D.J. Structure of human erythrocyte catalase. *Acta Crystallogr. D. Biol. Crystallogr.* 2000;56(Pt 2): 241-245.

Li, S.; Peterson, N.A.; Kim, M.Y.; Kim, C.Y.; Hung, L.W.; Yu, M.; Lekin, T.; Segelke, B.W.; Lott, J.S.; Baker, E.N. Crystal Structure of AhpE from Mycobacterium tuberculosis, a 1-Cys peroxiredoxin. *J. Mol. Biol*. 2005;346(4):1035-1046.

Li, X.; Xie, C.; Jin, Q.; Liu, M.; He, Q.; Cao, R.; Lin, Y.; Li, J.; Li, Y.; Chen, P.; Liang, S. Proteomic screen for multiprotein complexes in synaptic plasma membrane from rat hippocampus by blue native gel electrophoresis and tandem mass spectrometry. *J. Proteome Res.* 2009;8(7):3475-3486.

Liang, S.; Yu, Y.; Yang, P.; Gu, S.; Xue, Y.; Chen, X. Analysis of the protein complex associated with 14-3-3 epsilon by a deuterated-leucine labeling quantitative proteomics strategy. *J. Chromatogr. B Analyt. Technol. Biomed. Life Sci.* 2009;877(7):627-634.

Lin, Z.; Konno, M.; Abad-Zapatero, C.; Wierenga, R.; Murthy, M.R.; Ray, W.J. Jr; Rossman, M.G. The structure of rabbit muscle phosphoglucomutase at intermediate resolution. *J. Biol. Chem*. **1**986;261(1):264-274.

Littler, D.R., Harrop, S.J., Fairlie, W.D., Brown, L.J., Pankhurst, G.J., Pankhurst, S., DeMaere, M.Z., Campbell, T.J., Bauskin, A.R., Tonini, R., Mazzanti, M., Breit, S.N., Curmi, P.M. The intracellular chloride ion channel protein CLIC1 undergoes a redox-controlled structural transition. *J. Biol. Chem.* 2004**;**279(10):9298-9305.

Low, F.M.; Hampton, M.B.; Winterbourn, C.C. Peroxiredoxin 2 and peroxide metabolism in the erythrocyte, *Antioxid. Redox Signal*. 2008;10:1621 e 1629.

Minarik, P., Tomaskova, N., Kollarova, M., Antalik, M. Malate dehydrogenases – structure and function. *Gen. Physiol. Biophys*. 2002;21:257-265.

Mithieux, G., Ajzannay, A., Minassian, C. Identification of membrane-bound phosphoglucomutase and glucose-6 phosphatase by 32P-labeling of rat liver microsomal membrane proteins with 32P-glucose-6 phosphate. *J. Biochem.* 1995;117(4):908-914.

Nakagawa, T.; Onoda, S.; Kanemori, M.; Sasayama, Y.; Fukumori, Y. Purification, characterization and sequence analyses of the extracellular giant hemoglobin from Oligobrachia mashikoi. *Zoolog. Sci*. 2005;22(3):283-291.

Neelam, S.; Kakhniashvili, D.G.; Wilkens, S.; Levene, S.D.; Goodman, S.R. Functional 20S proteasomes in mature human red blood cells. *Exp. Biol. Med.* (Maywood) 2011;236(5):580-591.

Nemoto, T., Ohara-Nemoto, Y., Ota, M., Takagi, T., Yokoyama, K. Mechanism of dimer formation of the 90-kDa heat-shock protein. *Eur. J. Biochem.* 1995;233(1):1-8.

O'Farrell, P.A., Gonzalez, F., Zheng, W., Johnston, S.A., Joshua-Tor, L. Crystal structure of human bleomycin hydrolase, a self-compartmentalizing cysteine protease. *Structure*. **1**999;7(6):619-627.

Olivieri, E.; Herbert, B.; Righetti, P.G. The effect of protease inhibitors on the two-dimensional electrophoresis pattern of red blood cell membranes. *Electrophoresis* 2001;22(3):560-5.

Pallarès, I., Bonet, R., García-Castellanos, R., Ventura, S., Avilés, F.X., Vendrell, J., Gomis-Rüth, F.X. Structure of human carboxypeptidase A4 with its endogenous protein inhibitor, latexin. *Proc. Natl. Acad. Sci. U. S. A.* 2005;102(11):3978-3983.

Polekhina, G., Board, P.G., Gali, R.R., Rossjohn, J., Parker, M.W. Molecular basis of glutathione synthetase deficiency and a rare gene permutation event. *EMBO J.* 1999;18(12):3204-3213

Rappsilber, J.; Siniossoglou, S.; Hurt, E.C.; Mann, M. A generic strategy to analyze the spatial organization of MPCs by cross-linking and mass spectrometry. *Anal. Chem.* 2000;72 (2):267-275.

Rhoda, M.D.; Blouquit, Y.; Caburi-Martin, J.; Monplaisir, N.; Galacteros, F.; Garel, M.C.; Rosa, J. Effects of the alpha 20 mutation on the polymerization of Hb S. *Biochim. Biophys. Acta* 1984;786 (1-2):62-66

Rinalducci, S.; D'Amici, G.M.; Blasi, B.; Zolla, L. Oxidative stress-dependent oligomeric status of erythrocyte peroxiredoxin II (PrxII) during storage under standard blood banking conditions. *Biochimie* 2011;93(5):845-853.

Rosa, R., Blouquit, Y., Calvin, M.C., Prome, D., Prome, J.C., Rosa, J. Isolation, characterization, and structure of a mutant 89 Arg----Cys bisphosphoglycerate mutase. Implication of the active site in the mutation. *J. Biol. Chem.* 1989;264(14):7837-7843.

Sandomenico, A., Russo, A., Palmieri, G., Bergamo, P., Gogliettino, M., Falcigno, L., Ruvo, M. Small peptide inhibitors of acetyl-peptide hydrolase having an uncommon

mechanism of inhibition and a stable bent conformation. *J. Med. Chem.* 2012;55(5):2102-2111.

Scaloni, A.; Jones, W.M.; Barra, D.; Pospischil, M.; Sassa, S.; Popowicz, A.; Manning, L.R.; Schneewind, O.; Manning, J.M. Acylpeptide hydrolase: inhibitors and some active site residues of the human enzyme. *J. Biol. Chem*. 199**2**;267:3811–3818.

Scaloni, A., Ingallinella, P., Andolfo, A., Jones, W., Marino, G., Manning, J.M. Structural investigations on human erythrocyte acylpeptide hydrolase by mass spectrometric procedures. *J. Protein. Chem.* 1999;18(3):349-360.

Schägger, H.; Cramer, W.A.; van Jagow, G. Analysis of molecular masses and oligomeric states of protein complexes by blue native electrophoresis and isolation of membrane protein-protein complexes by two-dimensional native electrophoresis. *Ana.l Biochem.* 1994;217:220-230.

Shevchenko, A.; Wilm, M.; Vorm, O.; Mann, M. Mass spectrometric sequencing of proteins from silver-stained polyacrylamide gels. *Anal. Chem.* 1996;68:850–858.

Siciliano, A.; Turrini, F.; Bertoldi, M.; Matte, A.; Pantaleo, A.; Olivieri, O.; De Franceschi, L. Deoxygenation affects tyrosine phosphoproteome of red cell membrane from patients with sickle cell disease. *Blood Cells Mol. Dis*. 2010;44 (4):233-242

Silverman, D.N.; Backman, L.; Tu, C. Role of hemoglobin in proton transfer to the active site of carbonic anhydrase. *J. Biol. Chem*. 1979;254 (8):2588-2591.

Slavens, K.D.; Brown, T.R.; Barakat, K.A.; Cundari, T.R.; Anderson, M.E. Valine 44 and valine 45 of human glutathione synthetase are key for subunit stability and negative cooperativity. *Biochem. Biophys. Res. Commun.* 2011;410 (3):597-601.

Stebbins, C.E., Russo, A.A., Schneider, C., Rosen, N., Hartl, F.U., Pavletich, N.P. Crystal structure of an Hsp90-geldanamycin complex: targeting of a protein chaperone by an antitumor agent. *Cell.* 1997;89(2):239-250.

Structural genomics consortium (SGC). "Crystal structure of human glutamate oxaloacetate transaminase 1 (GOT1)." Submitted (AUG-2009) to the PDB data bank Cited for: X-RAY CRYSTALLOGRAPHY (2.05 ANGSTROMS) OF 14-412 IN COMPLEX WITH PYRIDOXAL PHOSPHATE AND TARTARIC ACID, SUBUNIT, PYRIDOXAL PHOSPHATE AT LYS-259.

Suckau, D.; Resemann, A.; Schuerenberg, M.; Hufnagel, P.; Franzen, J.; Holle, A. A novel MALDI LIFT-TOF/TOF mass spectrometer for proteomics. *Anal. Bioanal. Chem*. 2003;376,:952–965.

Sulzenbacher, G., Alvarez, K., Van Den Heuvel, R.H., Versluis, C., Spinelli, S., Campanacci, V., Valencia, C., Cambillau, C., Eklund, H., Tegoni, M. Crystal structure of E.coli alcohol dehydrogenase YqhD: evidence of a covalently modified NADP coenzyme. *J. Mol. Biol*. 2004;342(2):489-502.

Svensson, A.K.; Bilsel, O.; Kayatekin ,C.; Adefusika, J.A.; Zitzewitz, J.A.; Matthews, C.R. Metal-free ALS variants of dimeric human Cu,Zn-superoxide dismutase have enhanced populations of monomeric species. *PLoS One* 2010;5 (4):10064.

Tang, W.K., Li, D., Li, C.C., Esser, L., Dai, R., Guo, L., Xia, D. A novel ATP-dependent conformation in p97 N-D1 fragment revealed by crystal structures of disease-related mutants. *EMBO J*. 2010**;**29(13):2217-2229.

Thorell, S., Gergely, P. Jr, Banki, K., Perl, A., Schneider, G. The three-dimensional structure of human transaldolase. *FEBS Lett.* 2000;475(3):205-208.

T**urner, M.A., Yuan, C.S., Borchardt, R.T., Hershfield, M.S., Smith, G.D., Howell, P.L.** Structure determination of selenomethionyl S-adenosylhomocysteine hydrolase using data at a single wavelength. *Nat. Struct. Biol.* 1998;5(5):369-376.

van Gestel, R.A.; van Solinge, W.W.; van der Toorn, H.W.; Rijksen, G.; Heck, A.J.; van Wijk, R.; Slijper, M.. Quantitative erythrocyte membrane proteome analysis with Blue-native/SDS PAGE. *J. Proteomics* 2010**;**73 (3):456-465.

Walden, H., Podgorski, M.S., Schulman, B.A. Insights into the ubiquitin transfer cascade from the structure of the activating enzyme for NEDD8. *Nature*. 2003;422(6929):330-334

Wang, X.; Chen, G.; Liu, H.; Zhao, Z.; Li, Z. Four-dimensional orthogonal electrophoresis system for screening protein complexes and protein-protein interactions combined with mass spectrometry. *J. Proteome Res*. 2010**;**9 (10):5325-34

Witting, I.; Schägger, H. Native electrophoretic techniques to identify protein-protein interactions. *Proteomics* 2009;9:5214-5223

Yamaguchi, T., Komoda, Y., Nakajima, H. Biliverdin-IX alpha reductase and biliverdin-IX beta reductase from human liver. Purification and characterization. *J. Biol Chem.* 1994;269(39):24343-24348.

Young, L.J., Lee, E.Y., To, H.A., Bookstein, R., Shew, J.Y., Donoso, L.A., Sery, T., Giblin, M., Shields, J.A., Lee, W.H. Human esterase D gene: complete cDNA sequence, genomic structure, and application in the genetic diagnosis of human retinoblastoma. *Hum. Genet*. 1988;79(2):137-141.

Curriculum vitae of the candidate

GENERAL DATA:

Last name	Pallotta
First name	Valeria
Date of birth	23/10/1985
Place of birth	Viterbo
City	Viterbo
Street and number	Viale Fiume n°16
Postcode	01100
Phone	320-6375739
E-mail	pallotta@unitus.it valep23@hotmail.it
Nationality	Italian

EDUCATION:

Date (from-to)	March 1, 2011 – February 28, 2014
Educational Institution	University of Tuscia (Viterbo) PhD student in Genetic and Cell Biology Tutor: Prof. Lello Zolla, laboratory of proteomics and mass spectrometry
Subject area of study	Proteomics Thesis: **Proteomics and metabolomics in transfusion medicine: new technologies to improve red blood cell storage**
Expertise	Protein separation methods (SDS-PAGE, 2D IEF/SDS-PAGE), protein-protein interaction analysis (CN-PAGE, BN-PAGE, 2D CN/SDS-PAGE, 2D BN/SDS-PAGE), Western blot, alternative protein separation method (depletion of hemoglobin and carbonic anhydrase from erythrocyte cytosolic samples by preparative clear native electrophoresis).
Date (da-a)	September 2008 – July 2010

Educational Institution	University of Tuscia (Viterbo)
Educational qualification	Second degree (Master) in Cellular and Molecular Biology
Subject area of study	"HEL protein from *Arabidopsis thaliana* and its role in plant defence". Tutor: Prof.ssa Carla Caruso. Laboratory of biochemistry and molecular biolgy
Degree/grade	110/110 cum laude
Expertise	SDS-PAGE, agarose gel electrophoresis (DNA, RNA), enzymatic hydrolysis, molecular cloning techniques, bacterial transformation, protoplast transformation (*Arabidopsis t.)*, PCR, DNA and RNA extraction and purification, recombinant protein expression in *E.coli,* purification and rinaturation of recombinant proteins.
Date (from-to)	September 2005 – January 2008
Educational Institution	University of Tuscia (Viterbo)
Educational qualification	First degree (Bachelor) in Biological Sciences
Subject area of study	"Alzheimer's disease". Tutor: Prof. Giovanni Casini
Degree/grade	110/110
Date (from-to)	Academic year 1999/2000 – academic year 2003/2004
Secondary school	Classical Lyceum, Viterbo
Degree/grade	90/100

PROFESSIONAL EXPERIENCES:

Date (from-to)	November 2013 – January 2014
Working experience	Teaching for Molecular Biology laboratory
Educational Institution	University of Tuscia (Viterbo)
Date (from-to)	November 2012 – January 2013

Working experience	Teaching assistant for Molecular Biology laboratory
Educational Institution	University of Tuscia (Viterbo)
Date (from-to)	November 2011 –January 2012
Working experience	Teaching assistant for Molecular Biology laboratory
Educational Institution	University of Tuscia (Viterbo)
Date (from-to)	September 1, 2010 – February 28, 2011
Working experience	Stage
Educational Institution	Laboratory of proteomics and mass spectrometry, Prof. Lello Zolla (University of Tuscia).
Expertise	Clear Native-PAGE (CN-PAGE), Blue Native-PAGE (BN-PAGE), SDS-PAGE, Western Blot.
Date (from-to)	April 2009 – July 2010
Working experience	Stage
Educational Institution	Laboratory of biochemistry and molecular biology, Prof.ssa Carla Caruso (D.A.B.A.C., University of Tuscia)
Expertise	SDS-PAGE, agarose gel electrophoresis, enzymatic hydrolysis, molecular cloning techniques, bacterial transformation, protoplast transformation of *Arabidopsis t.*, PCR, DNA and RNA extraction and purification, recombinant protein expression in *E.coli,* purification and rinaturation of recombinant proteins.
Date (from-to)	January 2007 – June 2007
Working experience	Stage (150 hours)
Institute	Laboratory of clinical analysis “Casa di cura Salus” (Viterbo), Dott.ssa Patrizia Battaglia.
Expertise	Microbiology techinques, clinical chemistry, hematology, coagulation, enzyme immunoassays.

CONFERENCE AND SEMINARS:

December 12, 2012	"Protezione brevettuale delle nuove varietà vegetali e delle invenzioni biotecnologiche", Dott. Stefano Borrini, SIB (Italian Patent Society). University of Tuscia.
October 29, 2012 – October 31 2012	2D-DIGE Workshop, Enea Casaccia – Santa Maria di Galeria (Roma).
June 12, 2012 – June 15, 2012	VII connational conference ItPA (Italian Proteomic Association), Viterbo.
April 11, 2011 – April 15, 2011	XI proteomics and mass spectrometry course, Vitorchiano (Viterbo).

ABSTRACT E POSTER:

SIB Ferrara September 18-20, 2013:
The role of NBN protein in cell homeostasis: proteomic identification of the interactors of NBN and of its fragments arising from the pathological 657del5 founder mutation.
Domenica Cilli, Cristiana Mirasole, **Valeria Pallotta**, Angelo D'Alessandro, Lello Zolla, Paolo Ascenzi, Alessandra Di Masi

ItPA Padova June 18-21, 2013:
Native protein complexes in the cytoplasm of Red Blood Cells.
Valeria Pallotta, Sara Rinalducci, Cristina Marrocco, Valentina Longo, Lello Zolla

ItPA Padova June 12-15, 2012:
Red blood cell processing for cryopreservation: from fresh blood to deglycerolization.
Valeria Pallotta, Gian Maria D'Amici, Angelo D'Alessandro, Roberto Rossetti, Lello Zolla

SIMTI Rimini May 23-26, 2012:
Red blood cell processing for cryopreservation: from fresh blood to deglycerolization.
Valeria Pallotta, Gian Maria D'Amici, Angelo D'Alessandro, Roberto Rossetti, Giuliano Grazzini, Lello Zolla

LIST OF PUBLICATIONS:

Pallotta V, D'Alessandro A, Rinalducci S, Zolla L.
Native protein complexes in the cytoplasm of red blood cells. J Proteome Res. 2013 Jul 5;12(7):3529-46. doi: 10.1021/pr400431b. Epub 2013 Jun 19. PubMed PMID: 23781972.

Marrocco C, **Pallotta V**, D'alessandro A, Alves G, Zolla L.
Red blood cell populations and membrane levels of peroxiredoxin 2 as candidate biomarkers to reveal blood doping. Blood Transfus. 2012 May;10 Suppl 2:s71-7. doi: 10.2450/2012.011S. PubMed PMID: 22890272; PubMed Central PMCID: PMC3418622.

Pallotta V, D'Amici GM, D'Alessandro A, Rossetti R, Zolla L.
Red blood cell processing for cryopreservation: from fresh blood to deglycerolization. Blood Cells Mol Dis. 2012 Apr 15;48(4):226-32. doi: 10.1016/j.bcmd.2012.02.004. Epub 2012 Mar 15. PubMed PMID: 22424604.

Pallotta V*, Gevi F*, D'Alessandro A, Zolla L (* shared first authorship).
Red blood cell storage with vitamin C and N-acetylcysteine prevents oxidative stress-related lesions: a metabolomic overview. Blood Transfus. 2013; in press

Pallotta V, Naro F, D'Alessandro A, Zolla L.
Supplementation of anti-oxidants in leukofiltered erythrocyte concentrates: assessment of morphological changes through scanning electron microscopy. Blood Transfus. 2013, Brief communication; in press

Cilli D, Mirasole C, **Pallotta V**, D'Alessandro A, Zolla L, Antoccia A, Ascenzi P, Di Masi A.
Identification of the interactors of human nibrin (NBN) and of its 26 kDa and 70 kDa fragments arising from the NBN 657del5 founder mutation. PLOSE ONE, to be submitted